UNIVERSITY OF CALGARY

The r-process Code SiRop:

Applications to Nuclear Sensitivity Studies and High-energy Astrophysics

by

Zachary Shand

A THESIS

SUBMITTED TO THE FACULTY OF GRADUATE STUDIES

IN PARTIAL FULFILLMENT OF THE REQUIREMENTS FOR THE

DEGREE OF MASTER OF SCIENCE

GRADUATE PROGRAM IN PHYSICS AND ASTRONOMY

CALGARY, ALBERTA

September, 2016

Abstract

The r-process has long remained an unsolved puzzle in nuclear physics and astrophysics. The astrophysical sites of the r-process have eluded discovery despite much experimental and theoretical research. In order to better understand all aspects of the involved physics we have developed SiRop. SiRop is an r-process code which has been improved from a previous version (r-Java 2.0) to include enhanced utilities for running simulations and collecting advanced statistical data. Use of SiRop can assist in identifying key isotopes and help guide nuclear experiments. The code can also used to study high-energy astrophysical phenomena and opens up an avenue explaining high-energy phenomena, like fast radio bursts (FRB), which continue to challenge traditional models. A detailed analysis was performed on the statistical methods employed in current sensitivity studies and an improvement on existing techniques was developed.

Acknowledgements

I would like to thank my parents for all their love and support.

And I would like to thank my graduate advisor, Dr. Rachid Ouyed, for all his patience and guidance.

Table of Contents

List of Tables

List of Figures and Illustrations

List of Symbols, Abbreviations and Nomenclature

Symbol	Definition
BH	Black Hole
FRB	Fast Radio Burst
FRDM	Finite Range Droplet Model
GCD	Galactic Chemical Evolution
GUI	Graphical User Interface
HEW	High Entropy Wind
HFB	Hartree-Fock-Bogoliubov
NS	Neutron Star
NSE	Nuclear Statistical Equilibrium
NSM	Neutron Star Merger
ODE	Ordinary Differential Equation
PDE	Partial Differential Equation
QN	Quark Nova
SN	Supernova
WPA	Waiting Point Approximation

Chapter 1

Introduction

Understanding where all the elements came from is a fundamental question about the evolution of the universe and the Galaxy that we still don't completely understand to this day. The nuclear processes responsible and the models for stellar environments are immensely complex and require intensive study by a broad range of scientists across several sub-fields of physics. In particular, the elements produced by the r-process seem particularly difficult to explain. Theoretical models typically require the development of complex computer programs to assist in solving them. The work I undertook for my thesis was focused on creating more sophisticated code which will help advance the sophistication with which scientists can understand the nuclear reactions which occur during the generation of the heaviest elements through r-process nucleosynthesis.

The main focus of my work was in improving upon an existing r-process code called r-Java to create a new version named SiRop. The main contributions I made to the code were in introducing a new set of modules designed to run and assist in analysing the results of what are refereed to as sensitivity studies. In addition to this improvement to the code I applied the code to two problems. The first resulted in a published paper for a model for a newly discovered high-energy astrophysical phenomena known as FRBs. The second was an in-depth analysis of the statistical techniques currently used to interpret the results of sensitivity studies. In addition to being of interest scientifically, these also help to show the strengths of r-Java and SiRop and showcase its ability as a state-of-the-art research code.

This dissertation will be structured as follows. First we will go over some basics for the r-process, beginning in Sec. 1.1. After the basics have been covered, in Chapter 2 I will cover the details of our nucleosynthesis code SiRop and outline its capabilities and my contributions to the sensitivity module. These introductory sections will be followed by two papers submitted for

publication in scientific journals. The first (Chapter 3) is on the model I constructed for FRBs and fits to the observational data. The second paper (Chapter 4 is on the analysis on the statistics which have been used to analyse sensitivity studies where I demonstrate the potential biases in the currently used methods and present a new statistical metric and a procedure to improve the robustness of the methods for future use. Finally, we conclude with a short summary in Chapter 5.

1.1 Stellar Nucleosynthesis

The elements that exist today on Earth and in stars in our Galaxy were all produced by nuclear reactions. The bulk of these elements are fused in the cores of massive stars where the high temperatures from fusion processes support stars against gravitational collapse. This process ends once iron begins to fuse in a star's core as further fusion processes no longer generate thermal energy to counteract gravitational collapse leading to either a core-collapse supernova (SN) or conversion of the star into a black hole (BH). As a result, regular stellar burning is insufficient to explain the origin the bulk of elements heavier than iron up to and including uranium. Since these elements have high charge, charged particle interactions become unlikely candidates in the production of these elements. The only possible option then becomes neutron capture processes. Since the 1950s (Burbidge et al. (1957), Cameron (1957)), our understanding of the situation leads us to conclude that the rapid neutron capture (the r-process) and slow neutron capture (the s-process) are the main source of these heavy elements. The s-process proceeds at low neutron densities where neutron capture occurs much slower than the β-decays of the produced isotopes. The r-process is the opposite operating at much higher neutron number densities where the neutron captures occur far more rapidly than the β^--decay.

The ultimate goal of r-process simulations is to explain and reproduce the relative abundance distribution of isotopes. In Fig. 1.1 we show the solar abundances and the r-process residuals and what we hope to see from r-process simulations would be the a facsimile of the r-process residuals in blue. This is not what we are able to achieve in practice due to a combination of uncertainties

in both astrophysical models and nuclear models alike. On the astrophysics side of the equation, we do not currently have conclusive evidence for the site of the r-process. Some prospective sites include core-collapse SN, neutron star mergers, or quark novae (QN). Each site predicts very different densities and temperatures which can drastically affect the results of simulated r-process abundances (see for example Kostka et al. (2014b) for a comparison of these three sites). On the nuclear side many nuclei predicted to be in the r-process path have been unmeasured. In Fig. 1.2 we can see that although many unstable neutron rich nuclei have been measured there remain many isotopes out of reach of current experimental facilities. Due to the large number of isotopes which exist on the neutron rich side, we will not be able to measure all nuclei and properties, but we can theoretically help to isolate the most important ones. This is the purpose of nuclear sensitivity studies and the main focus for their development in SiRop which is a tool designed to identify key isotopes in the r-process.

1.1.1 S-Process and R-Process Residuals

The s-process is thought to mainly occur in asymptotic giant branch (AGB) stars and in massive stars. The CNO cycle in a star burns helium nuclei into heavier elements and while the neutron separation energy of most alpha particle nuclei is quite large ($\sim$16 MeV), isotopes from the CNO cycle have much lower separation energies. The main source of these neutrons is expected to be from $^{13}\mathrm{C}(\alpha,n)^{16}\mathrm{O}$ and $^{22}\mathrm{Ne}(\alpha,n)^{25}\mathrm{Mg}$. The former is naturally sourced by the continued CNO cycle in the hydrogen burning layer above the helium burning region in the star's core. The latter is expected to play a significant role only in more massive stars ($\sim$8 Msun).

Understanding the s-process is important in its own right as a nucleosynthetic process, but is also a necessary element in understanding the r-process abundances. The heavy metal abundance of our sun and solar-system is the best known set of isotopic abundances available. These abundances comprise a mixture of r- and s-process neutron capture elements and in order to determine what isotopes are produced by the r-process we first must calculate the yields from the s-process. The r-process residuals are computed using solar data and the yields from what is referred to as a

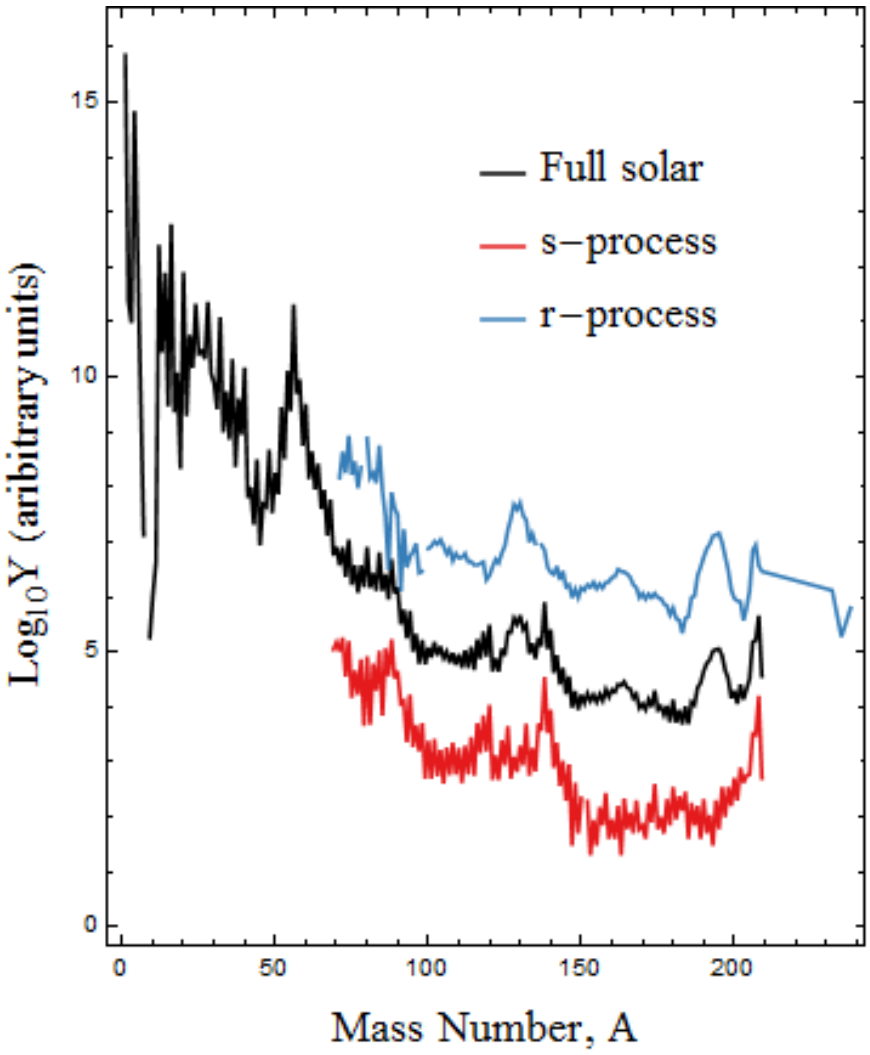

Figure 1.1: Solar observations of isotopic abundance as a function of isotope mass. The theoretical r-process contribution is determined by subtracting theoretically predicted s-process yields from the measured solar abundances. The data are from Lodders (2003) and Sneden et al. (2008).

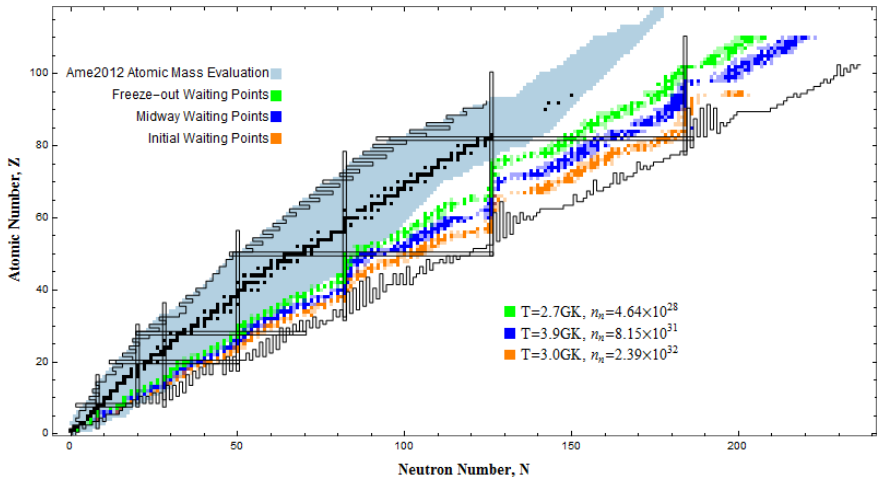

Figure 1.2: Here we show the measured nuclear masses according the the 2012 atomic mass evaluation (Audi et al. 2012). Overlaid in green are three theoretical r-process paths at different temperature and densities along with theoretical predictions for the neutron drip-line based on the HFB21 mass model.

canonical or site-independent s-process model (see e.g. Sneden et al. (2008)). These solar r-process residuals are the de facto method for calculating the r-process abundances which r-process theory attempts to explain.

1.2 Observational constraints

Detection of elemental abundances at the surfaces of stars is an important aspect of understanding the r-process and the robustness of its operation through the lifetime of the Galaxy. These measurements have never allowed for full coverage of the elements from iron to uranium due to a combination of spectral line strength, distance to the stellar object, and interference from stronger lines from more abundance metals (especially iron). Measurement of isotopic fractions in distant stellar objects are even more difficult to achieve: the element must have sufficient isotopic shift to be observable and it must be possible to achieve high resolution spectral measurements capable of resolving the hyper-fine splitting. The combination of these observational constraints make direct and detailed observation of stellar r-process abundances difficult and there are only a handful of astrophysical objects where these measurements can be made in large detail. About a half-dozen

metal poor r-process enriched stars have been identified where elemental abundances of several r-process elements was measureable and these objects have remarkable agreement with the scaled solar r-process residuals. Outside of these excellent observational objects, spectral identification of neutron capture elements has mainly focused on Ba and Eu as representative s- and r-process elements because each is mainly produced in only the r- or s- process and they both have favourable spectral lines (Aoki et al. (2003), Cescutti et al. (2005)) in addition to being r-only (Eu) and s-only (Ba) elements.

Single elemental abundance measurements cannot be used to directly constrain r-process codes which simulate abundances, but are crucial in understanding the role of r-process sites in the context of GCE. The existence of metal poor, r-rich stars in addition to high [Eu]/[Fe] measurements in stellar objects severely restricts the ability of astrophysical objects as r-process sites in the early Galaxy. The two traditional r-process sites, SN and neutron star mergers (NSM), must adopt extreme model parameters in order to successfully explain early Galactic enrichment of neutron capture elements. NSM are typically discounted from operating early on in the Galaxy's history due to rarity of double neutron star (NS) systems, the time required to produce such binaries, and the even longer in-spiral times of required for merger and ejection of the produced r-process elements. Supernovae do not suffer from the timing constraints of NS mergers, but are instead challenged by the large amount of r-process material they must eject into their environment to explain the high enrichment of r-process elements observed in certain stellar objects.

Chapter 2

SiRop: Simulation of Rapid neutron capture

2.1 R-process codes

SiRop is an r-process code which has been designed to be user friendly while simultaneously allowing scientists to take advantage of a highly optimized program for running simulations. Development of an r-process code is not a trivial task and requires significant coding and testing of numerical schemes and also requires a large set of data which is on its own difficult to compute. In general, a minimal r-process code requires nuclear masses (many of which are unmeasured), β-decay half lives and a (simple) model for the astrophysical environment's temperatures and densities. With these, the r-process can be modelled using the waiting point approximation (WPA). The waiting point approximation is an equilibrium solution which is used to calculate the relative number of isotopes of a given isotopes. This gives normalized population coefficients given by:

$$\frac{Y(Z,A+1)}{Y(Z,A)} = n_n \frac{G(Z,A+1)}{2G(Z,A)} \left[\frac{A+1}{A}\frac{2\pi\hbar^2}{m_u kT}\right]^{3/2} \exp(S_n/kT) \tag{2.1}$$

where $Y(Z,A)$ is the abundance of the isotope with atomic number Z and mass number A, n_n is the neutron number density, $G(Z,A)$ is the partition function of the isotope with atomic number Z and mass number A, m_u is the atomic mass unit, k is Boltzmann's constant, T is temperature, and S_n is the one neutron separation energy (or neutron binding energy) of the isotope with atomic number Z and mass number A. This equation is used to describe the abundances of an isotopic chain (i.e. all isotopes of one element) and is coupled to adjacent elements by an effective β-decay rate. A more general description for the r-process do not make use of the above Eq. 2.1 and instead explicitly list all nuclear reactions as rates of change in a set of coupled ordinary differential equations (ODE). This WPA is particularly attractive computationally because solutions to coupled ODE scale non-linearly with the number of equations (e.g. matrix inversion of dense matrices for

solution eigenvalues requires N^3 operations in general). Even in the WPA, numerical schemes must be implemented and checked for stability and correctness which is, for non-linear problems, problem specific and requires a large investment to produce a working code that is trustworthy.

More general r-process codes are possible only when rates of all relevant nuclear reactions are available either through theoretical or experimental tabulation. A more complete set of coupled ODEs can be written when all these rates are available and an r-process simulation can track and evolve all isotopic species explicitly. This is generally a much slower process even when specialized numerical techniques can be developed due to the order of magnitude of the increase in the number of species being tracked; however, it is thought that this approach is generally more trustworthy when compared to the equilibrium solutions which have unknown equilibration time-scales. An additional advantage of these more complex schemes is that they directly allow for the inclusion of more nuclear reaction types than the WPA. The equilibrium solution for the WPA (sometimes referred to as the nuclear Saha equation since it is a nuclear analogue to the Saha-Langmuir equation for elemental ionization states) assumes an equilibrium between the fast neutron capture and neutron photo-dissociation coupled by the much slower β-decay processes. While processes like fission can be added into the waiting point formalism as an added coupling between distant isotopes, many other processes are entirely incompatible including β-delayed neutron emission and charged-particle reactions (i.e. capture reactions of charged particles like protons or helium nuclei). In order to include the effects of all relevant nuclear processes in the r-process, the WPA must be replaced by the full set of rate equations. Additionally, a full network is the needed for accurate simulations at low temperatures (< 1 GK) where the number and energy of the thermally generated photons violate the equilibrium assumptions in the WPA.

Tabulated values for r-process calculations come from direct measurements and nuclear theories of varying complexity. A lack of neutron target for nuclear beams and the short lifetimes of these isotopes prevents the creation of many species in the lab. The measurements currently possible for accessible r-process relevant nuclei are mainly masses, β-decay half-lives and β-delayed

neutron emission probabilities. These measurements are only possible at radioactive beam facilities which are capable of producing and separating very neutron-rich rare-ion beams. The success of nuclear models is generally established by their ability to match measured nuclear masses which many are able to accomplish with global fits with rms errors around 0.6 MeV. Their ability to correctly predict masses of isotopes yet to be accessed by experiments is altogether another matter and models produce divergent predictions. Another avenue for testing these models is to compare them to the imprints of their properties left by nature in stellar abundances. The ability of a nuclear model to reproduce the r-process abundances can be used to test the validity of a nuclear model and potentially identify regimes where the model is insufficient and may require direct measurements of nuclear properties like half-lives or cross-sections to establish more accurate physical parameters than those provided by theory.

Alternatively, r-process simulations may be useful in determining key isotopes whose physical characteristic must be known accurately or with high precision in order to correctly predict isotopic or elemental yields from models of r-process environments. The extraordinarily large parameter space and uncertainties in both astrophysical and nuclear physics theory preclude many standard statistical methods like least-squares regression or Monte-Carlo methods from being applicable; however, targeted studies guided by r-process simulation results will hopefully yield assist theoreticians and experimentalists in determining the key nuclei to understand the r-process abundances. To this end, an r-process code must be capable of running simulations with variations in its physical parameters whose output can be analysed in order to estimate the strength of the impact they induced.

2.2 SiRop's Interface

SiRop and r-Java have always been intended to be user friendly applications. Many scientific codes built are remain as command-line driven applications which do not typically lend themselves to easy use by non-experts or someone new to the code. The r-process is a cross-disciplinary subject

Figure 2.1: Main screen after loading SiRop. All modules can be accessed from this home page.

.

which requires a dedicated code for simulating the nuclear reaction network. As such we wanted to establish a simple interface to a program that many different scientists could make effective use of. In particular, we needed to expand the interface to include a way to automate the running of many different simulations to generate statistics for sensitivity studies. The user's manual for SiRop is included in Appendix B; however, I will go over the basics of the program here.

The program loads and displays like a typical desktop application and from its main screen all other modules can be accessed (see Fig. 2.1). Much of the program's GUI is based on r-Java and includes a similar data table, page for creating graphs and charts, and window for presenting messages to the user. The largest change to the program, is as mentioned, the addition of modules specifically for sensitivity studies (see Fig. 2.2). This was the major contribution I made to SiRop in addition to the module for calculating and displaying the r-process path (see Fig. 2.3).

The sensitivity module was designed to allow for very general and arbitrary nuclear parameter variations in the hope of being flexible enough to meet almost any conceivable set of nuclear changes. A single so-called Operation (a set of changes for one queued simulation) can be com-

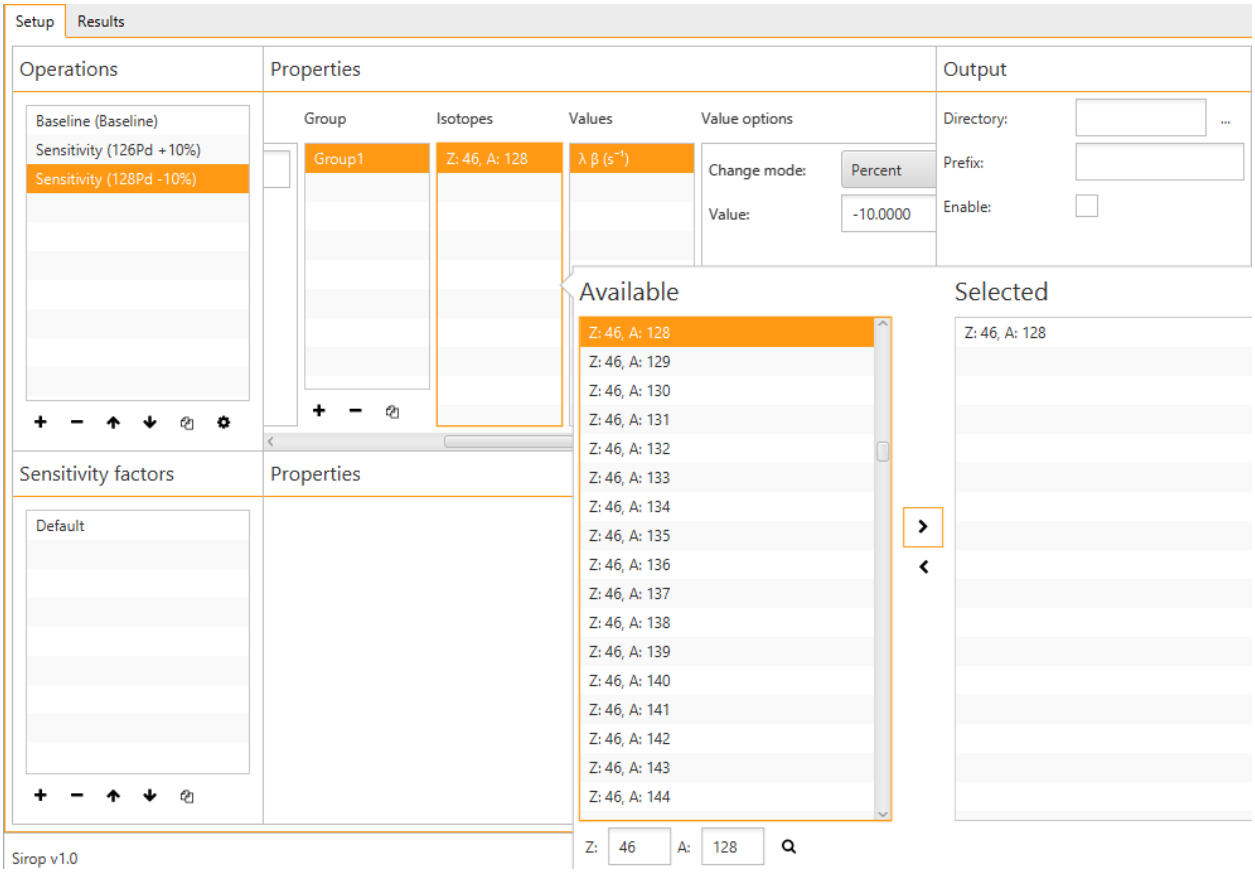

Figure 2.2: Sensitivity module new to SiRop from r-Java. This part of the program is used to setup different sensitivity studies and offers a graphical tool for picking isotopes and their nuclear properties to have varied during batch exectution of the code.

.

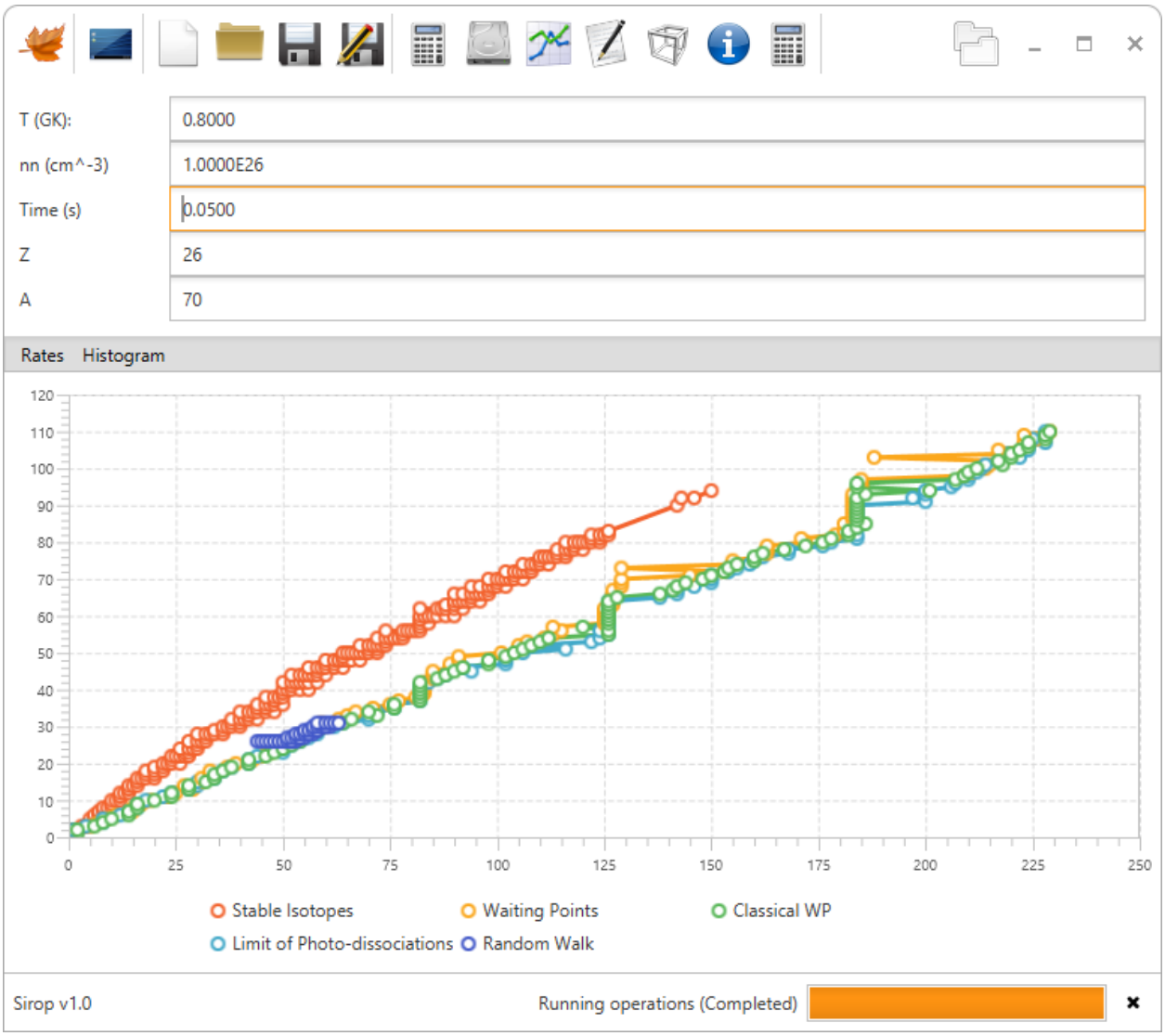

Figure 2.3: The new module for calculating the r-process path based on different modles. The module can be used to identify key isotopes without having to run a complete (and lengthy) r-process simulation.

.

posed of different groups of changes to the physical values for different isotopes including nuclear mass, β-decay rates, and cross-sections.

2.3 History of r-Java and SiRop

The current state of the r-process code, SiRop, is a result of the continued development of a nucleosynthesis code over several years of research conducted by many individuals. The original version of the code, r-Java, was limited to the simplest computations involving only equilibrium solutions (i.e. nuclear statistical equilibrium (NSE) and WPA). Advances in both nuclear theory and public availability of theoretical rates and cross sections allowed for expansion of the code to accommodate calculations using a full rate equation and led to the development and release of r-Java 2.0. This newest version of the code allowed for simulation of the r-process in regimes where the WPA is no longer valid and inclusion of more diverse reactions than allowed in the WPA (e.g. β-delayed neutron emission). Following the successful development of r-Java 2.0, the ability for automated computation and statistical analysis of the simulation results was identified as the next major expansion for the code. During development of the newest version of r-Java the decision was made to change the name of the code, effectively re-branding our program. The new name, SiRop, stands for Simulation of Rapid neutron capture and is a nod to the Canadian origin of the code and the French collaboration during the development the original r-Java code. The new name also also no longer emphasizes the implementing language[1] which was originally meant to highlight the cross-platform and GUI capabilities of the program but eventually became a distracting focus point when introducing the program. While the program is currently still implemented in the Java programming language that fact no longer needs to be brought to attention by its name.

The development of SiRop from r-Java has been a slow build-up from a simple static r-process code up to a fully dynamic code capable of solving the rate equation which includes basic neutron captures up to fission recycling. The evolution from its original to the most recent version has this

[1] Additionally, it prevents any possible confusion with the CRAN package rJava which is a low level R to Java interface.

history imprinted in aspects of the program. Some of these are obvious at the front end and the way users interact with the program, while others are hidden in the guts of the program and may be important for future development of the code itself. The most important design choice has always been to allow flexible use of input values for masses, half-lives, rates and cross sections. This seems like an obvious advantage however it does limit the ability for certain possible simplifying assumptions from being built into the program. At the lowest programming level, things like the size of the network and the isotopic membership cannot be known until the program is run and the nuclear inputs are imported. For a user, the total lack of restrictions is powerful, but requires knowledge nuclear physics and its role in the r-process to make best use of this freedom.

The transition form r-Java 2.0 to SiRop has mainly consisted of the addition of batch simulation capabilities and automated computation of relevant statistics for sensitivity studies. The addition of a module dedicated to sensitivity studies was designed and implemented in the code to assist setting up and running multiple r-process simulations. The module allows modification of any nuclear input parameter and is general enough to accommodate essentially any arbitrary variation desired for a nuclear sensitivity study. A graphical tool lists all isotopes and their parameters with the option to change each parameter by an absolute constant amount, a relative fraction or by percent. Several nuclear input parameters can be modified in one sensitivity study and it is even possible to vary multiple isotopic species simultaneously. Once the sensitivity study parameters have been input the code is programmed to automatically run the baseline followed by all queued variations. As each queued simulation is completed the sensitivity metrics are automatically calculated and the outputs are graphed and displayed in the program's interface.

In order to assist in setting up nuclear sensitivity studies and understanding their output, a new module for computing the r-process path has been added to SiRop. The module is rather self-contained and can be used to compute the r-process path given by some astrophysical parameters and outputs the result to the screen and graphs. The r-process path can be computed in two main ways: either through the WPA at high-temperatures (1-3 GK) or by equating the β-decay rates

with the neutron capture rates. A third method, however, can be used by calculating a random walk beginning with a test isotope. This is possible only with a full set of nuclear rates, but it is, in my opinion, rather helpful for both understanding the the r-process and for testing which isotopes are going to be of relevance during a particular simulation. The hope is ultimately to assist those interested in nuclear sensitivity studies by assisting in determining before-hand which isotopes will be of relevance before running a potentially long set of simulations. In practice, isotopes which do not fall within or near the computed r-process path are not worth including into a sensitivity study, especially in the testing or exploration stages of a research project.

In addition to the to sensitivity module, there has been one other major modification to the code. Faster execution of a code is always desirable and a method has been developed which successful increases the efficiency to the program. One of the largest costs in evaluating the time integration between time steps is the non-linear scaling of the matrix arithmetic. The change from the WPA to a full network of neutron capture reactions is an increase from about a hundred elements to several thousand isotopes. For completeness, all isotopes imported were previously included in the coupled ODEs; however, isotopes near the proton drip-line do not play a role in r-process environments. Even the stable isotopes may not participate until after exhaustion of neutrons in the system and the subsequent nuclear decay to stability. In r-Java 2.0, when these isotopes are imported they bloat up the matrix and waste evaluation time in instances where it can be determined that they cannot be produced between time steps. Although the program is equipped with sparse matrix algorithms the code execution time still scales worse than linearly with system size and these isotopes unnecessarily slow down the program.

The code was modified to be able to recompute the design of the rate matrix and equipped with a heuristic algorithm to detect which isotopes are not reachable between the current and next time step. At early times in the simulation, when the densities are highest and require the smallest time steps, the number of isotopes present is significantly smaller and so the code is allowed to spend less computational time during the most time restrictive portion of the simulation. The speed-up is

dependent on the number of isotopes present during the execution of the program and diminishes as the system evolves to contain a large array of isotopes. Nevertheless, the speed-up is a rather encouraging step especially since previous attempts at matrix computation speed-ups seemed to have reached a maximum during development of r-Java 2.0. More background on the numerical treatment and other possible prospects for improvements to the numerical schemes is presented in Appendix A.

2.4 Computational and Theoretical Limitations

At its heart, SiRop is a numerical ODE solver. During execution the code is solving a general differential equation for nuclear burning with several simplifying assumptions. The most important assumption is that only a subset of all possible nuclear reactions are included, which includes β-decay, α-decay, neutron capture, neutron photodissociation, β-delayed neutron emission, spontaneous fission, neutron induced fission, β-delayed fission and a restricted set of α capture reactions. For the r-process, these are the most important reactions. While most other nuclear reactions and decay processes are possible, in practice, most of them can be safely ignored due to the their low cross-sections (which are much smaller than the neutron capture cross sections). An important exception is the charged-particle key reactions in supernova theories for the r-process which are traditionally computed using an altogether separate code and then transferred to a specialized r-process code (see e.g. Woosley & Hoffman (1992), Meyer et al. (1992), or Farouqi et al. (2010)).

Other nuclear reactions or processes ignored through this approximation could play a yet-to-be understood role in the r-process. Neutrinos are not included in our model, but have been shown to play an important role in SN r-process scenarios and compact object (NS or BH) merger scenarios (e.g. Arcones & Bliss (2014), Perego et al. (2014)). Neutrinos may provide the required neutron excess (or electron fraction) in less traditional models like BH accretion disks (Caballero et al. 2012). Spallation reaction channels are also largely ignored, but have the potential to largely effect the r-process at temperatures greater than a few million degrees kelvin ((Goriely et al. 2008)) and,

at least to our knowledge, these have never been implemented into an r-process code. In addition to nuclear reactions, nuclear isomerism (which is the existence of a long-lived non-ground state isotope) has the potential to modify the predictions of r-process simulations. As the code evolves in the future an expanded set of nuclear processes may be possible.

The second major limitation to SiRop is its lack of nuclear or astrophysical modelling capabilities. This stems from the design philosophy of r-Java and SiRop which aims to be site independent. The code offers a small selection of parametrized astrophysical models, but makes no attempt at detailed solutions to general hydrodynamic partial differential equations (PDE). The degree with which these parametric astrophysical environments agree with models for astrophysical environments varies, but in many cases the expansion profiles generally follow smooth power-law dominated density trajectories (see e.g. Arcones & Thielemann (2013)). On the nuclear side, the story is a bit more complicated for an r-process code. The theoretical calculation of nuclear quantities requires a mass model from which all reaction rates must be calculated from in a self-consistent theory. Mass tables are easily available , but the respective decay rates are not. For this reason, even the defaults in SiRop are a mix of the finite range droplet model (FRDM)(Möller et al. 2003), Hartree-Fock-Bogoliubov (HFB) and mass model (Goriely et al. 2008, 2009). As a result, it is essentially impossible to require consistent nuclear inputs into SiRop and even if it was a reasonable expectation it would be near impossible to validate any user inputs.

When performing nuclear sensitivity studies, there are however, two theoretically accessible equations which allow us to make some simple correlations to mass variations in the underlying nuclear inputs. These are Fermi's Golden Rule and the principle of detailed balance. Since it is simpler, we will start with detailed balance, which is the following equation relating inverse reactions:

$$\lambda_{(\gamma,a)}(T) = \frac{(2I^0+1)(2j_a+1)}{(2I'^0+1)}\frac{G_I}{G_{I'}}\left(\frac{mk_BT}{2\pi\hbar^2}\right)^{3/2}\langle\sigma v\rangle_{(a,\gamma)}e^{-S_n/kT}, \tag{2.2}$$

where $\lambda_{(\gamma,a)}$ is the reaction rate for dissociation of a particle a , I^0 is the ground state nuclear spin, G is the nuclear partition function, $\langle\sigma v\rangle$ is the thermally averaged cross section of the forward

(capture) reaction, m is the nuclear mass, k_B is Boltzmann's constant and T is temperature (see e.g. Goriely et al. (2008)). If we have precomputed theoretical values for the cross section and its associated photodissociation then, assuming all other factors in the above equation are undisturbed by this change, an updated value for the new rate, $\lambda'_{(\gamma,a)}$, can be written as follows

$$\lambda'_{(\gamma,a)} = \lambda_{(\gamma,a)} \frac{e^{S_n/kT}}{e^{S'_n/kT}} = \lambda_{(\gamma,a)} e^{-\delta S_n/kT}, \tag{2.3}$$

where δS_n is the corresponding change to the neutron separation energy produced by changes in predicted nuclear masses. This equation, however, requires us to assume that the change in masses and separation energy have no effect on the cross-section.

For our second approximation, we begin by writing Fermi's Golden Rule:

$$\lambda_\beta = G_F^2 |M_{np}|^2 F(Z, Q_\beta) \frac{(Q_\beta - m_e c^2)^5}{60\pi^3 \hbar (\hbar c)^6}, \tag{2.4}$$

where G_F is Fermi's constant, $|M_{np}|$ is the so-called matrix element and $F(Z, Q_\beta)$ is the Fermi-function. This implies that a quintic dependence on the nuclear Q_β value and re-written as a second update formula gives an updated value for the β-decay rate known as Sargent's law

$$\lambda'_\beta = \lambda_\beta \left[1 + \frac{\delta Q_\beta}{Q_\beta - m_e c^2} \right]^5, \tag{2.5}$$

where δQ_β is the change in the reaction energy caused by changes in the masses. This relation is also not strictly correct as it assumes that the shape function and matrix elements are constant. Both assumptions may be violated, but may provide a crude estimate for updating the β-decay rates in lieu of a full recalculation of the model. These new relations have been added as optional automatic updates in the nuclear sensitivity module in order to provide some estimate of variations caused by changes in nuclear masses in full reaction network calculations which are normally insensitive to masses due to their direct use of nuclear rates and cross-sections.

In general, however, there are some order of magnitude estimates which can be suggested for use in sensitivity studies. For nuclear masses (and by extension the nuclear Q_β values as well) should not be changed by more than about 1 MeV since the error of mass models have

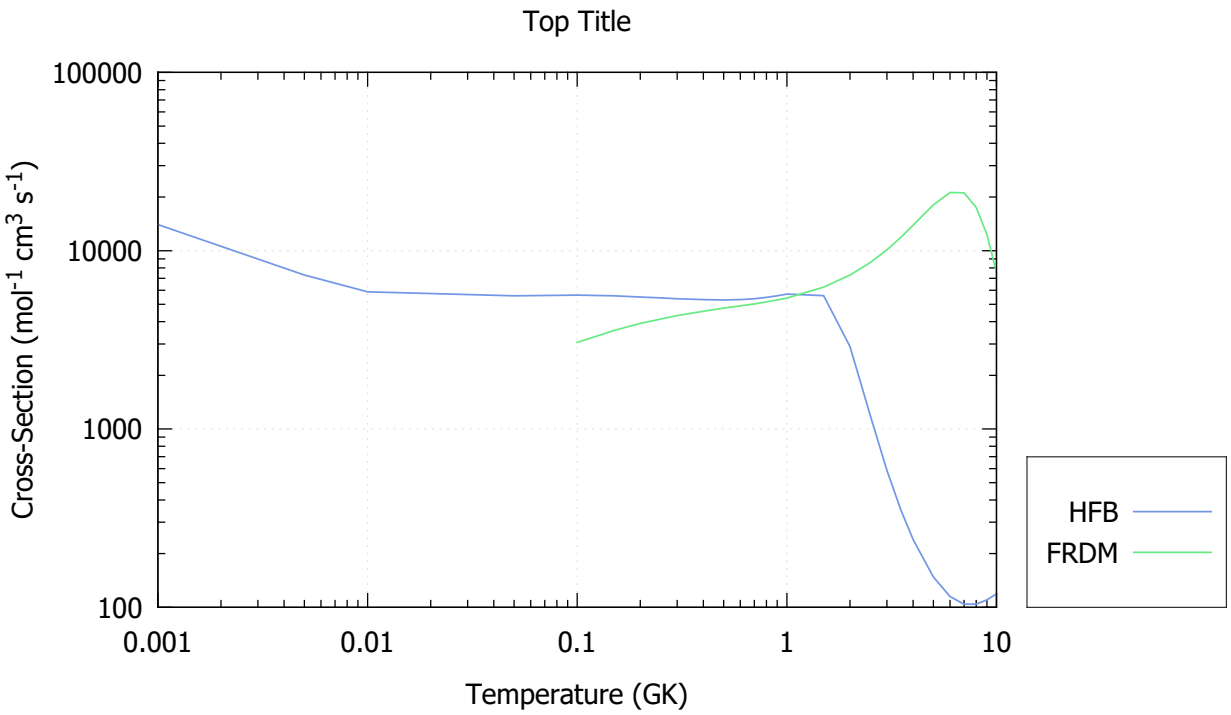

Figure 2.4: The cross-sections for an isotope (cadmium-130) as computed using the FRDM and HFB models. The data sources are from Goriely et al. (2008) and Rauscher & Thielemann (2001).

typical rms errors of about 0.6 MeV. For isotopes with measured masses, the changes should be within the experimentally available errors which are typically much smaller (< 100 keV in many cases). For β-decay rates, the changes can be guided by the above equation based on Eq. 2.5, but typically should not exceed a factor of 5-10. For the β-delayed neutron emission probabilities, the values must be normalized values, so increasing the value by more than 1 is meaningless. The program will automatically re-normalize the values internally, but care should be made to properly all relevant probabilities ($P_{0n}, P_{1n}, P_{2n}, and P_{3n}$) as desired. The cross-sections provide the largest possible range of allowable values and can be multiplied by factors up to 10^4. Models for neutron-capture cross-sections depend strongly on the theoretical model and different models can predict very different values and behaviour. The magnitude of this difference can be seen in Fig. 2.4 which shows two models based on not only different mass models, but also different theoretical frameworks for computing the reaction probabilities.

Chapter 3

Paper I: Quark Nova Model for Fast Radio Bursts

Forward to Paper I

The following manuscript was accepted for publication in Research and Astronomy (Shand et al. 2016). FRBs are the new "hot topic" in astronomy and were originally discovered in 2007 (the Lorimer burst) (Lorimer et al. 2007) and later re-confirmed as true astrophysical signals in 2013 (Thornton et al. 2013). In-between, there is a somewhat humorous history where the signals were thought to be from a seldom used microwave in a break room. While it was confirmed that this particular microwave produced almost identical signals in the radio dish at the Parkes observatory, further study and careful analysis of the signal has led to the conclusion that these signals are indeed truly astronomical in origin. Many possible explanations for the origin of these FRB signals were proposed; however, almost all models provide only rough estimates of the energetics and time scale.

The original idea for a quark nova (QN) FRB model came from Dr. Ouyed based on the radiation from the decaying free neutrons ejected from the NS surface; however, as the model evolved it became clear that the millisecond duration of the FRB pulse could be explained using the radioactivity of the r-process elements expected to be produced in the QN ejecta. In consultation with the authors listed in the publication, I took charge of constructing the model for FRBs based on the QN model. The equations describing the model, the figures and computed quantities were derived and compiled by myself. The co-authors were involved in establishing key model predictions and figures of relevance in addition to consultation during the models conception and assistance in final production of the manuscript.

The manuscript was prepared for an audience experienced in astronomy and astrophysics, so the following is some relevant background of relevance to the published paper. The observational

signatures were discovered in radio data using methods for extracting radio pulsar data. Pulsar signals are frequently too faint to measure directly in radio spectra; however, Fourier techniques can be used to pick up the very regular pulsations pulsars are named after. Once the period of a pulsar is identified the time series signal can be stacked or folded to enhance the signal. This process enhances the signal while the white noise tends to be reduced. The retrieved signal is not at a single frequency and there is a delay between the highest and lowest frequencies observed. This time delay is due to dispersion of the radio signal through the cold hydrogen gas of the interstellar medium (ISM) gives the following expression relating arrival time and the frequencies:

$$\Delta t \approx 4.15 \times 10^6 \,\text{ms} \times (f_{\text{lo}}^{-2} - f_{\text{hi}}^{-2}) \times \text{DM} \tag{3.1}$$

where Δt is the difference in arrival time (in seconds) of the signal across the frequency band given by the frequencies f_{hi} and f_{lo} (in MHz) and the dispersion measure (DM) ($\text{cm}^{-3}\,\text{pc}$) is typically solved for to provide an estimate of the distance. The DM measures the gas density (in cubic centimetres) and distance (in parsecs). (For more information on pulsar astronomy in general see Lorimer & Kramer (2012).) This value can be combined with with models for the Galaxy to provide distance measurements to the observed pulsar or object. The analysis of FRB data is done with almost the exact same methods as pulsars, except they are more difficult to locate in data due to their lack of repetition. Sophisticated data searching techniques based on de-dispersing the data to remove the effects of dispersion are used to search for such signals in the data to locate pulsar-like signals. While this allows us to locate the signals in source data it assumes a lot about the emission at the object's source. The assumption made with this analysis is then that the emission mechanism at the FRB source occurs simultaneously across all frequency bands. In our model using a QN, this assumption is invalidated and we find lower DM values than predicted using typical pulsar techniques and is what we refer to as an extended time spectrum.

The mechanism through which we achieve this time delay is realized due to emission at the NS light cylinder (LC). The strong magnetic field ($\sim 10^12\,\text{G}$) of the NS is forced to co-rotate; however, at some location this forced co-rotation exceeds the speed of light. This point is refereed to as

the LC of the NS and at this point electron-positron currents are generated to satisfy Maxwell's equations. The currents generated at the LC produce a "mono-polar" magnetic field, so called because the field strength falls off with a power law identical to an electric monopole field. The intersection of the spherical ejecta with this cylinder in space provides a sweeping mechanism which provides emission over a period of time much larger than that of a typical pulsar.

The model links together r-process nucleosynthesis with a particular astrophysical site and an observable emission mechanism that we have used to explain FRB. If the model can be verified through further observations and more detailed development of the model, it would be provide direct observational evidence for the r-process in QN. As a result it would prove the existence of quark stars and provide an way to observe unstable r-process nuclei decaying through the synchrotron emission of their emitted electrons.

In the Results section of the manuscript, we propose explanations to two observed astrophysical phenomena. The first is the so-called 511 keV lines. These strong emission lines are observed by telescopes with large clustering of the signals near the Galactic center. The energy of the emission corresponds exactly with the photons produced from electron-positron annihilation and an explanation for their origin has been lacking. The second phenomena is the observation of an apparent "death-line" in the traditional $P\dot{P}$ diagram. When plotting the periods (P)and the spin-down rate ($\dot{P}$) there is an apparent lack of neutron stars (observed as pulsars) which have high periods and low spin-down rates. The data seem to suggest a cut-off point called the death-line where no observations of a neutron star have been made suggesting that the pulsation mechanism is shut-off, or "dies." The graveyard can be seen in the bottom right of Fig. 3.1 which shows the various classifications of pulsars along with characteristic age and magnetic field for a neutron star along with the age tracks in color for a quark star. There are several theories based on neutron star population synthesis techniques, but a definitive physical reason for this apparent cut-off has yet to be accepted by the astrophysical community.

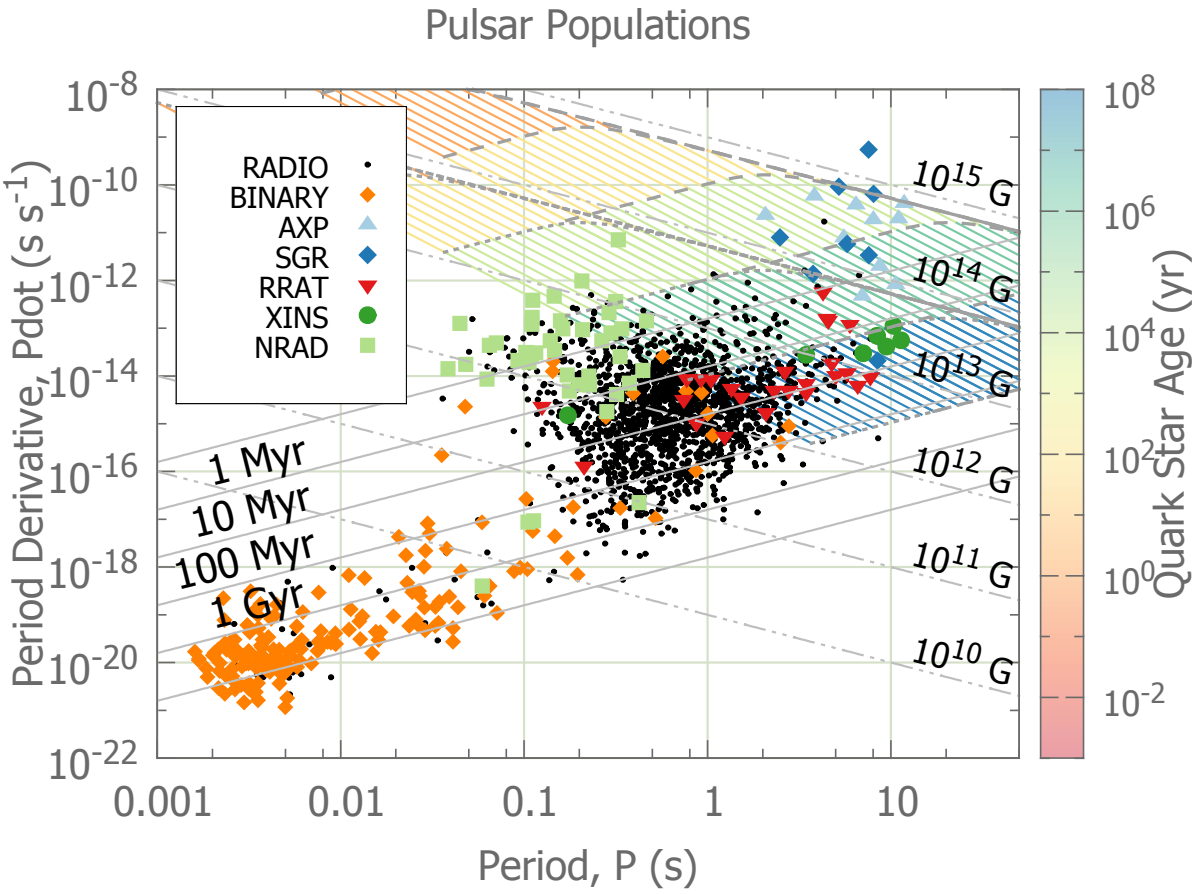

Figure 3.1: $P\dot{P}$ diagram of the observed pulsar populations. The bottom right corner of the graph is the region called the ”graveyard” and the creates a suggested cut-off below which no neutron stars/pulsars have been observed. The data plotted are from the Australian Telescpoe National Facility (ATNF) Pulsar Catalogue available at http://www.atnf.csiro.au/people/pulsar/psrcat/ (Manchester et al. 2005) in addition to the McGill Online Magnetar Catalogue available at http://www.physics.mcgill.ca/ pulsar/magnetar/main.html (Olausen & Kaspi 2014).

Quark Nova Model for Fast Radio Bursts

Zachary Shand, Amir Ouyed, Nico Koning and Rachid Ouyed

Department of Physics and Astronomy, University of Calgary, 2500 University Drive NW, Calgary AB T2N 1N4, Canada

Abstract: FRBs are puzzling, millisecond, energetic radio transients with no discernible source; observations show no counterparts in other frequency bands. The birth of a quark star from a parent neutron star experiencing a quark nova - previously thought undetectable when born in isolation - provides a natural explanation for the emission characteristics of FRBs. The generation of unstable r-process elements in the quark nova ejecta provides millisecond exponential injection of electrons into the surrounding strong magnetic field at the parent neutron star's light cylinder via β-decay. This radio synchrotron emission has a total duration of hundreds of milliseconds and matches the observed spectrum while reducing the inferred dispersion measure by approximately 200 cm^{-3} pc. The model allows indirect measurement of neutron star magnetic fields and periods in addition to providing astronomical measurements of β-decay chains of unstable neutron rich nuclei. Using this model, we can calculate expected FRB average energies ($\sim 10^{41}$ ergs) and spectral shapes, and provide a theoretical framework for determining distances.

Keywords: stars: neutron — nuclear reactions, nucleosynthesis, abundances — radiation mechanisms: general — radio continuum: general

3.1 Introduction

The observation of fast radio bursts (FRBs) has created an interesting puzzle for astronomers. Explaining the origin of these millisecond bursts has proven difficult because no progenitor has been discovered and there is no detectable emission in other wavelengths. Many possible explanations for these bursts have been put forward: blitzars (Falcke & Rezzolla 2014), neutron star mergers (Totani 2013), magnetars (Popov & Postnov 2007, 2013; Lyubarsky 2014; Pen & Connor 2015),

asteroid collisions with neutron stars (Geng & Huang 2015), and dark matter induced collapse of neutron stars (Fuller & Ott 2015), to name a few; however, none so far have been able to explain the many puzzling features of the emission: the signal dispersion, energetics, polarization, rate, emission frequency, and lack of (visible) companion/source object.

Direct observational evidence for quark stars is difficult to accrue due to some of their similarities to neutron stars (e.g. compactness, high magnetic field, low luminosity). In our model, FRBs signal the birth of a quark star and as more FRB observations become available, they may be able to provide evidence for the existence of quark stars. Other theoretical observational signatures of quark stars include: gravitational waves from quark star oscillation modes (Gondek-Rosińska et al. 2003; Flores & Lugones 2014); gravitational waves from a strange-quark planet and quark star binary system (Geng et al. 2015); equation of state constraints of the mass-radius relationship (Drago et al. 2015) and high-energy emission directly from the quark star in X-ray and gamma ray emission (Ouyed et al. 2011).

The quark nova (hereafter QN) model has many ingredients which prove useful when trying to explain FRBs. Firstly, the parent neutron star has a strong magnetic field which can generate radio synchrotron emission. Secondly, the neutron rich ejecta of the QN has a unique mechanism for producing these electrons via β-decay of nuclei following r-process nucleosynthesis in the QN ejecta (Jaikumar et al. 2007; Charignon et al. 2011; Kostka et al. 2014c). Our model makes use of the β-decay of nuclei in the ejecta of a QN to produce radio synchrotron emission. The exponential decay inherent to the nuclear decay explains the millisecond pulses observed in a way that no other model so far can.

As an isolated, old neutron star spins down the central density increases. Neutron star spin-down, which increases the core density leading to quark deconfinement, in conjunction with accretion and s-quark seeding can trigger an explosive phase transition (Ouyed et al. 2002; Staff et al. 2006; Ouyed et al. 2013). This explosion ejects a dense layer of neutrons which produce unstable heavy nuclei (Keränen et al. 2005; Ouyed & Leahy 2009). These unstable nuclei decay and

become observable at the light cylinder (hereafter LC) where they emit synchrotron emission due to the strong magnetic field. (For a 10 s period and 10^{12} G parent neutron star this corresponds to $B \sim 300$ G at the LC.) This generates a unique geometry and field configuration where our emission occurs at the intersection of a cylinder and sphere in space traced out by the ejecta as it passes through the LC.

We expect FRBs to be associated with old, isolated neutron stars and not young, rapidly rotating neutron stars. Neutron stars born with short periods quickly spin down and increase their central densities and, when these neutron stars are born with sufficient mass, deconfinement densities are reached very quickly (within days to weeks). Instead of emitting as an FRB, these QN will interact with the supernova ejecta leading to either a super-luminous supernova (Kostka et al. 2014a), or a double-humped supernova (Ouyed et al. 2013). This interaction with the surrounding material is expected to either disrupt the FRB emission, or bury the signal in the surrounding dense ejecta. The remaining neutron stars which are born massive and with high periods will take much longer (millions of years) to achieve the required critical core density. As such, we expect a continuum of FRB progenitors with a range of periods and magnetic fields to be emitting at various frequencies and luminosities.

Two important consequences of this scenario are: 1) an extended time spectrum as the sphere sweeps across higher and higher latitudes of the LC and 2) an exponential time profile with a millisecond duration from decay of β-decaying nuclei. As will be demonstrated, these qualities match observations of FRBs and allow us to provide testable predictions for distances, energies, rates and bandwidth of future FRB measurements which we can link to old, isolated neutron star populations and nuclear rates.

3.2 Model Overview

As a neutron star ages, spin-down increases its central density. For massive enough neutron stars, this can cause a phase transition that gives birth to a quark star. The exploding neutron star ejects -

at relativistic speeds - the outer layers of the neutron rich crust. The ejecta is converted to unstable r-process material in a fraction of a second and reaches a stationary r-process distribution which is maintained by the high-density of the ejecta and the latent emission of neutrons from fission (fission recycling). This distribution of unstable nuclei, which normally would decay within seconds, can continue to exist while the density is high and fissionable elements are able to release neutrons back into the system. This stationary distribution will be disrupted by decompression (or other disruption) of the QN ejecta as it passes through the LC of the surrounding parent neutron star magnetic field.

Once the ejecta is beyond the current sheets of the LC, the QN ejecta will no longer support a stationary r-process distribution and electromagnetic radiation from the ejecta will no longer be attenuated by the LC plasma, becoming visible [1]. The nuclei will decay via a rapid series of β-decays. These generated electrons are emitted with MeV energies in a strong magnetic field producing radio synchrotron emission. The frequency and power of this emission depends, of course, on the magnetic field strength at the LC where the QN ejecta crosses it. As a result, the emission spectrum is controlled by the geometry of the spherical intersection of the ejecta with the LC and allows inference of the progenitor neutron star's period and magnetic field.

A distinguishing detail in our model is the duration of the emission, which has a duration of seconds instead of milliseconds. The signal is a continuous series of synchrotron emissions from bunches of electrons generated from β-decay, which produce coherent, millisecond duration pulses at each frequency over several seconds (or hundreds of milliseconds for a bandwidth limited observation), as can be seen in Fig. 3.2. This is in apparent contrast with observations, which indicate a total emission duration of milliseconds. This discrepancy in the FRB duration stems from the de-dispersion process which stacks all frequency channels to a common initial time (as is done in pulsar de-dispersion and signal folding). As such, according to our model, the FRB emits a series of coherent, self-similar signals at different frequencies which have been erroneously stacked

[1] The current sheets at the LC produce a Faraday cage effect which shields the emission of β-decay occurring before the r-process material crosses the LC.

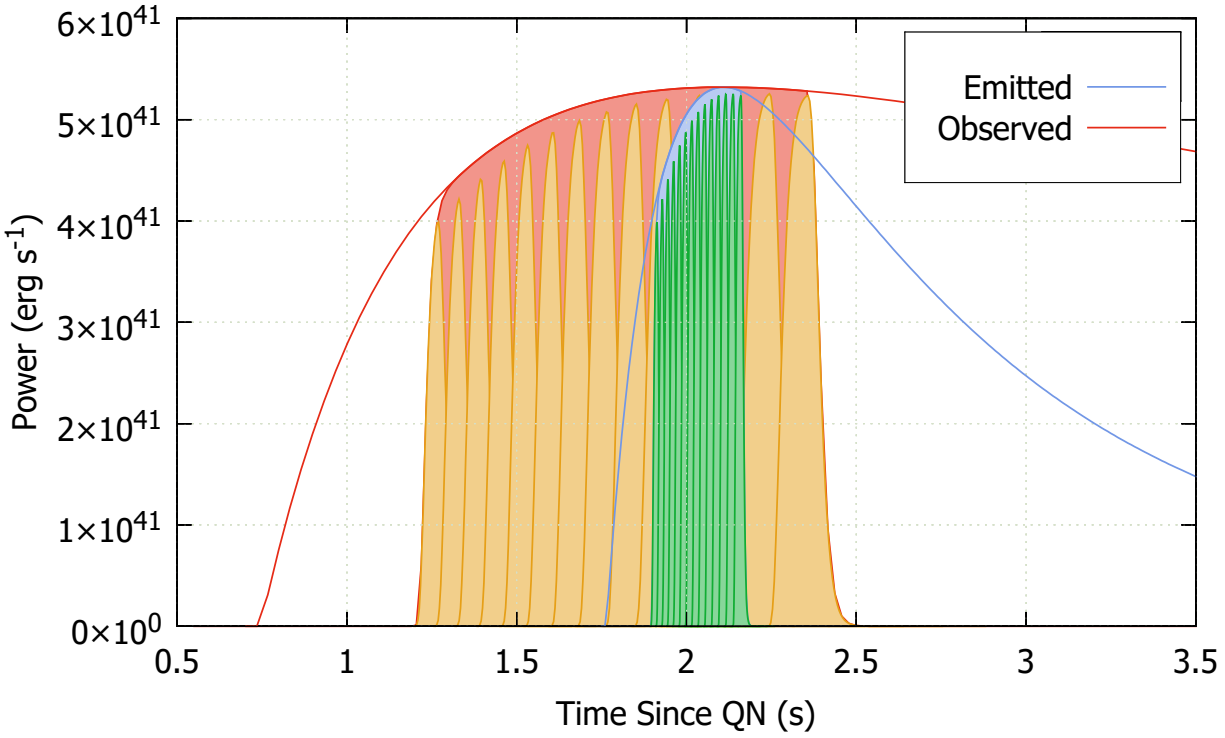

Figure 3.2: Light curve of the FRB emission at the source (blue) and the observed emission with dispersion smearing (red). The filled portion of the curves indicates the viewable emission for bandwidth limited observation in the range of 1175–1525 MHz. The green and orange pulses are 25 MHz sub-bands of the signal which exhibit the characteristic millisecond pulse duration.

as a time synchronized pulse: the total duration of the FRB is actually several seconds long and the observed signal duration is still dominated by cold plasma dispersion, as is demonstrated by the red/orange signal in Fig. 3.2.

The model comprises a combination of relatively standard physics phenomena: β-decay, magnetic field geometry and synchrotron emission. In composite, they generate a unique emission mechanism reminiscent of FRBs. The following sections (Sections 3.2.1 to 3.2.4) will be spent outlining each component of the model in greater detail and setting out the relevant equations necessary to generate the equations which describe the synchrotron emission spectra of the r-process material generated in the QN ejecta (see Section 3.3).

3.2.1 *R*-process Elements

The formation of heavy elements by the r-process is one of the predictions of the QN model (Jaikumar et al. 2007; Charignon et al. 2011; Kostka et al. 2014c). Due to a large number of free neutrons delivered by the ejected neutron star crust, it is possible for heavy fissile nuclei to be created during the r-process. *R*-process calculations show that superheavy ($Z > 92$) fissile elements can be produced during the neutron captures. This leads to fission recycling during the r-process (Kostka et al. 2014c). Each fission event ejects (or releases) several ($\sim 5 - 10$) neutrons back into the r-processing system. (This is due to neutron evaporation during asymmetric fission and is the same mechanism present in nuclear reactors.) Because of this, once these fissionable elements are produced, we are guaranteed to have free neutrons continually resupplied to the system which recombine into heavier elements which will undergo fission again and create a feedback loop in the r-process inside the QN ejecta. This allows for continued neutron captures and "r-processing" much longer than traditionally expected (see Fig. 3.3). These unstable isotopes are then able to supply us with the electrons from β-decay which are emitted in coherent bunches over different magnetic fields to produce the final aggregate emission spectrum.

R-process Rates

The basic r-process mechanism operates as a competition between neutron capture reactions (n, γ) and its inverse photo-dissociation (γ, n) with the much slower β-decays slowly building up each successive isotope. This picture holds true early on while the ejecta is hot and dense; however, as the gas expands and cools, the photo-dissociation rates fall off very quickly with temperature. The neutron-capture rates, on the other hand, do not have as strong a temperature dependence and are mainly a function of neutron density (see Fig. 3.4).

For an initially dense ejecta (which is of course the case for a neutron star crust $\rho \sim 10^{14}$ g cm^{-3}) this means that neutron captures can continue at low temperatures even after significant initial decompression. Instead of competing with photo-dissociations, they will begin to compete with β-decays instead as shown in Fig 3.4. At this point, simulations show that the isotopic distribution

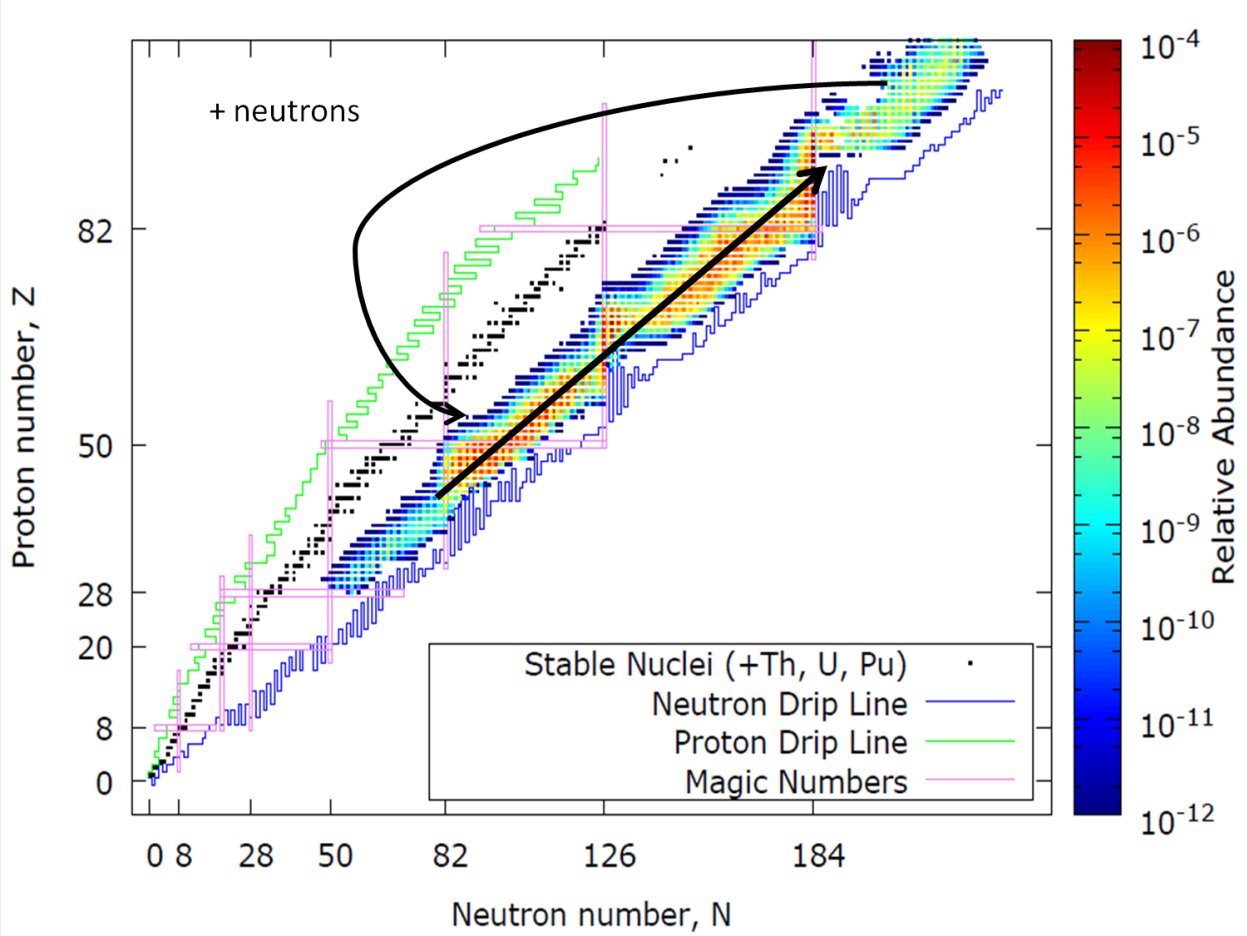

Figure 3.3: Stationary distribution of the r-process near the end of the r-process. The neutron source becomes largely depleted and no major changes to the distribution occur; however, fissionable nuclei emit neutrons and create a cyclic recycling process which can maintain a distribution of unstable nuclei for several seconds (> 10 s) in contrast to the milliseconds required for generation of r-process material. The distribution is computed using r-Java 2.0 as in Kostka et al. (2014c).

enters an approximate steady state (possible because of the fission recycling) which is maintained by the re-emitted neutrons and high density of the ejecta. The rates shown here come from Möller et al. (2003) and the BRUSLIB database (Goriely et al. 2008, 2009). These rates are all theoretical due to the difficulty of measuring them in the lab (Krücken 2011) and represent a way of observationally constraining β-decay rates by measuring synchrotron radiation from theses decay chains.

Decay Chain of Unstable Isotopes

For elements lighter than the actinides, β-decay (or electron capture) is the dominant decay mode available to them. These decay chains can be described by coupled differential equations which have a simple analytic solution known as the Bateman equations (Krane & Halliday 1988):

$$\mathscr{A}_n = N_0 \sum_{i=1}^{n} c_i e^{-\lambda_i t}, \tag{3.2}$$

$$c_m = \frac{\prod_{i=1}^{n} \lambda_i}{\prod_{i=1}^{n} {}' (\lambda_i - \lambda_m)}, \tag{3.3}$$

where the prime indicates that the lower product excludes the term where $i = m$. This equation gives the activity (number of events per unit time) of a decay chain. For a purely β-decay chain this gives the rate at which free electrons are produced by nuclei. As can be seen in Fig. 3.5, once β-decay dominates, the unstable nuclei will decay roughly exponentially and have a short burst of activity that will emit synchrotron radiation if subject to an external magnetic field. This naturally gives us an exponential fall-off time once neutron captures stop, which as discussed above, can be much later in the expansion than traditionally expected in the r-process due to the high density of the ejected material (which is abruptly triggered by decompression across the LC). Once emitted, the electrons will recombine with the surrounding weakly ionized plasma which should prompty emit in the keV range and could be visible if the plasma is diffuse enough; however, at much lower total emission power than the FRB burst itself (likely making it undetectable).

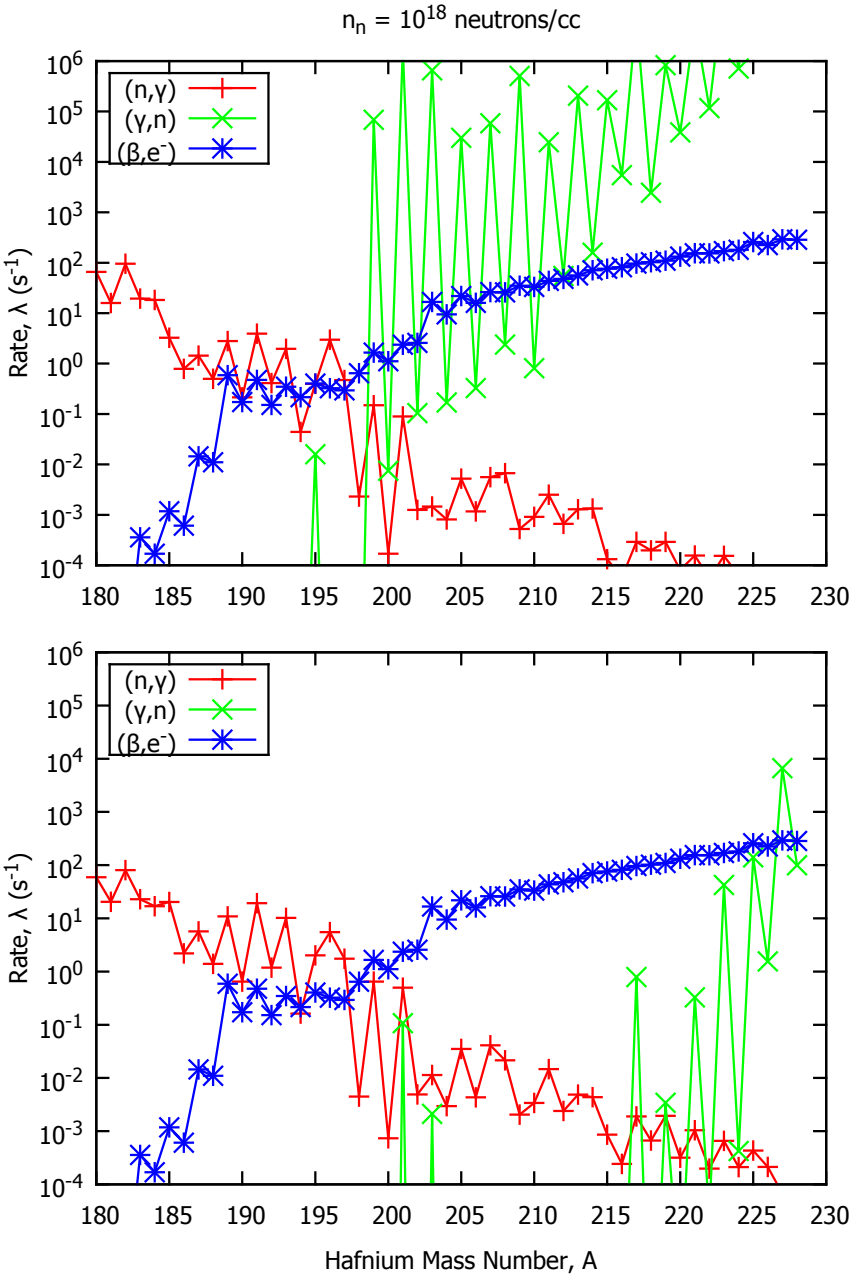

Figure 3.4: Relevant temperature dependent rates for hafnium show different regimes in the r-process. The neutron density is 10^{18}cm^{-3} and the temperatures are 1.0×10^9K (top) and 0.5×10^9K (bottom).

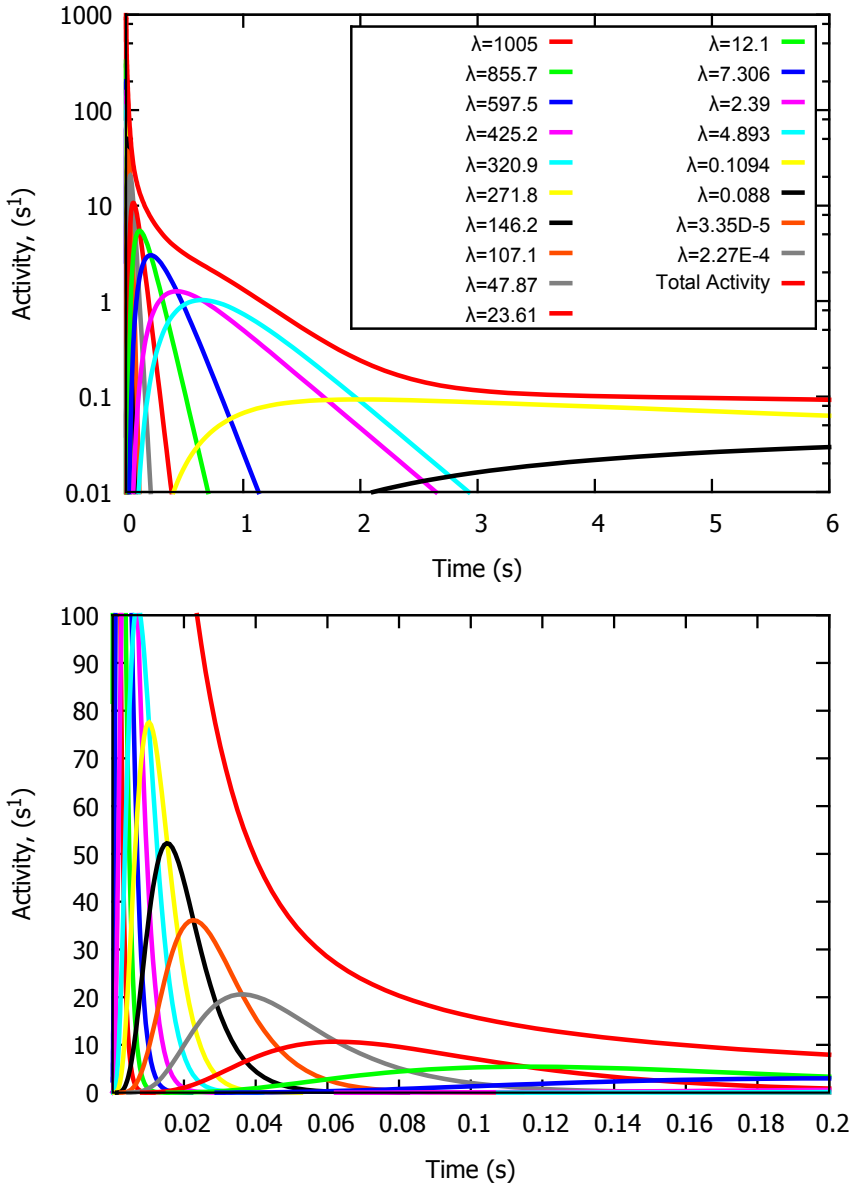

Figure 3.5: Solution of the Bateman equation for the A=156 β-decay chain beginning near the neutron drip-line. Once the neutron decays stop competing with β-decays at the end of the r-process (when the density falls sufficiently), the activity of the material will β-decay with this characteristic exponential behavior. The top panel is logarithmic in the activity (y-axis) and the bottom panel is the very early portion of the above panel without the logarithmic y-axis.

3.2.2 Geometry and Field Configuration

Assuming that the emission is triggered at the LC, we need to define a coordinate system with which to describe emission time and magnetic field strength (see Fig. 3.6). The LC is simply defined as the point where a co-rotating magnetic field would be rotating at the speed of light. The magnetic field configuration has a breakpoint in it where the magnetic field lines no longer reconnect and fall off as a mono-polar magnetic field. For an LC radius defined by: $r_{LC} = \frac{cP}{2\pi}$, where c is the speed of light and P is the period, the magnetic field strength at the LC at latitude ϕ is given by

$$B = B_0 \left(\frac{r_0 \cos\phi}{r_{LC}} \right)^a, \begin{cases} a = 3 & 0^\circ \leq \phi < 30^\circ \\ a = 2 & 30^\circ \leq \phi < 90^\circ. \end{cases} \tag{3.4}$$

This will cause radiation in the equatorial plane, where the dipolar field configuration exists, to be a factor of c weaker (c^2 for power).

For a relativistic, spherical shell this also provides a straightforward description for the arrival time of the material at the LC:

$$t_{\rm arr} = t - \frac{P}{2\pi\beta} \sec\phi, \tag{3.5}$$

which provides a time delay between emission at different latitude angles.

3.2.3 LC Details and Magnetic Field

The magnetic field configuration outside due to the LC will transition to a monopolar magnetic field for an aligned rotator (Michel 1973; Contopoulos et al. 1999) or will have a more complicated shape for an unaligned rotator (Spitkovsky 2006). As the QN ejecta passes through this region, the magnetic field will be disrupted and the details of the dynamics would be complicated to simulate; however, the disruption of the currents and the change of the magnetic field are assumed to cause a disruption of the QN ejecta. The details of the expansion across the LC are beyond the scope of this paper; however, as the ejecta passes through the boundary, there will be decompression of the material as the magnetic field distribution changes and the currents at the LC will interact with the

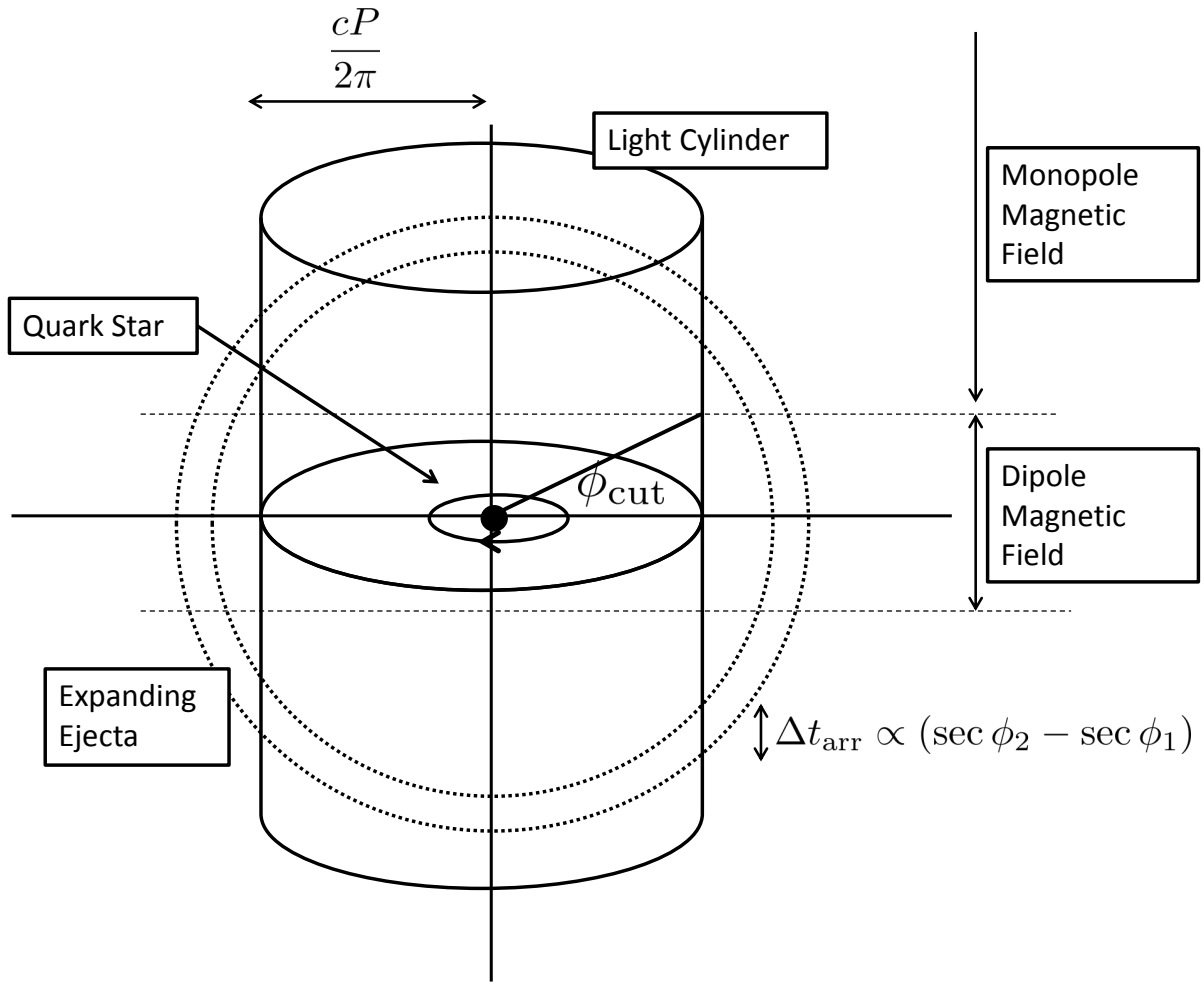

Figure 3.6: Diagram outlining geometry of the model. The latitude angle is specified relative to the quark star location and depicts the angle at which the spherical QN ejecta intersects the LC. The figure depicts two intersections of the ejecta with the cylinder at two different latitude angles separated by the arrival time of the two latitude angles.

matter and be disrupted. Since the LC inhibits emission of electromagnetic radiation across the LC (Jessner et al. 2000), this physical disruption can help to explain the sudden rise in the emission of the FRBs.

Both the neutron star and quark star will have a LC and so there is some possible ambiguity in what magnetic field will be present at the LC when the ejecta crosses it. Since QN ejecta is highly relativistic ($v \sim 0.99c$) we expect it to reach the LC of the parent neutron star before there is time for the quark star to fully rearrange the magnetic field around it which occurs much more slowly (Ouyed et al. 2006). This can allow inference of properties of the neutron star population which undergo a QN and emit these FRBs.

3.2.4 Synchrotron Emission

The emitted electrons are assumed to have a constant γ across all decaying elements. This is done both to simplify the model and also due to a lack of nuclear data of β-decay electron energy distributions. If we look at the flux density, this factor is suppressed and so the assumption ends up not factoring into comparisons for flux density (see Equations 3.15 and 3.16 for expanded form of the equations).

The synchrotron frequency and power per electron are given by

$$\nu_{\text{sync}} = \kappa_\nu \gamma^2 B, \tag{3.6}$$

$$P_e = \kappa_p \gamma_\perp^2 B^2, \tag{3.7}$$

where $\kappa_p = 1.6 \times 10^{-15}$ ergs s^{-1} G^{-2} and $\kappa_\nu = 1.2 \times 10^6$ Hz G^{-1} are constants (Lang 1999). For simplicity, we have used the synchrotron peak frequency in place of the sharply peaked complete distribution.

If we assume the electrons only emit for a short time (either due to recombination or dissipative processes) then the number of synchrotron electrons is the same as the activity, $\mathscr{A}$. The activity is,

of course, related to the decay constants of the unstable neutron-rich r-process nuclei

$$N_{\text{total}}(t) = \sum_{i}^{chain} \frac{\mathscr{A}_i}{\lambda_i}. \tag{3.8}$$

We write this explicitly to emphasize that there are many nuclear species present at the end of the r-process and there are many decay rates simultaneously contributing. This makes it difficult to constrain individual β-decay rates, but can help to constrain nuclear theory models (not unlike the *r*-process).

3.2.5 Summary of Model Components

Our model involves many individual components as outlined above in sections 3.2.1-3.2.4 and so we will shortly summarize how each qualitatively affects the emitted spectra. The *r*-process and fission recycling generate the electrons required for synchrotron emission and the LC provides a valve-like disruption and a monopolar magnetic field. The spectrum is affected by the characteristics of the geometry and nuclear decay that exists in a QN. The exponential decay generates an exponential pulse at each particular emission frequency; whereas, the period of the neutron star affects magnetic field strength that the nuclei see as they cross the LC. In this simple model, the QN ejecta emits at decreasing energies and frequencies as the latitude of intersection increases and the exact bandwidth of the emission is determined by the parent neutron star's period and LC field. In Equations 3.15 and 3.16 we show a complete expressions for the emitted spectrum.

3.3 Total Power and Spectrum

The total number of nuclei and by extension electron emitters at a particular latitude is expressed as:

$$N_e = \sum_i \left(\frac{\mathscr{A}_i}{\lambda_i}\right) \int_{\phi_1}^{\phi} \cos\phi' d\phi' = \sum_i \left(\frac{\mathscr{A}_i}{\lambda_i}\right) (\sin\phi - \sin\phi_1). \tag{3.9}$$

The number of emitting electrons is then conveniently defined as a fraction of the total activity of the ejecta which is related to the total number of initial radioactive isotopes as defined in Eq. 3.2.

This is simply the total number of isotopes in the QN ejecta and is given by:

$$N_0 = \frac{m_{\text{QN,ejecta}}}{A_{avg} m_H}. \tag{3.10}$$

The power then decays exponentially in time according to the activity of the nuclear species in the ejecta as it passes through the LC.

In order to determine the total power over the entire area we integrate the polar angle and latitude while keeping in mind that there is a time delay associated with the arrival of each latitude angle, ϕ due to the intersection of the spherical shock wave with the LC (giving us the Heaviside theta function, Θ).

We can then construct expressions for both the instantaneous power and spectral flux density as follows

$$\mathscr{P} = \Theta(t) P_e N_e, \tag{3.11}$$

$$\mathscr{S} = \frac{\Theta(t) P_e N_e}{\nu}, \tag{3.12}$$

which are all evaluated at the arrival time (Eq. 3.5) which has an angular dependence. These expressions can then can be integrated to get the total power or spectral flux density

$$P(t) = \oiint_{S(\theta,\phi)} dP = \oiint_{S(\theta,\phi)} \left[\frac{\partial \mathscr{P}}{\partial \phi}\right] d\Omega, \tag{3.13}$$

$$S(t) = \oiint_{S(\theta,\phi)} dS = \oiint_{S(\theta,\phi)} \left[\frac{\partial \mathscr{S}}{\partial \phi}\right] d\Omega, \tag{3.14}$$

which are both very unfriendly looking integrands; however, they both only have functional dependence on latitude angle, ϕ.

It is worth noting here that these integrals are evaluated at the source (in a frame near the LC). This means that cosmological redshift and dispersion are not accounted for in these expressions. While redshift is not included in this paper, new smaller dispersion measures are computed using the intrinsic time delay between emitted frequencies given by our model which traces out the magnetic field strength of the LC. These power and flux equations can of course both be integrated

with respect to time to compute the total energy and the fluence respectively. The full integral equations for the power and flux density are the

$$P(t=t_{arr},\theta,\phi)=\oiint_{S(\theta,\phi)}\frac{\partial}{\partial\phi}\left[\Theta(t)\kappa_p\gamma_\perp^2B_0^2\left(\frac{2\pi r_{NS}\cos(\phi)}{cP}\right)^{2a\ chain}\sum_i\left(\frac{\mathscr{A}_n(t)}{\lambda_n}\right)(\sin\phi-\sin\phi_1)\right]d\Omega \tag{3.15}$$

$$S(t=t_{arr},\theta,\phi)=\oiint_{S(\theta,\phi)}\frac{\partial}{\partial\phi}\left[\Theta(t)\frac{\kappa_p}{\kappa_\nu}B_0\left(\frac{2\pi r_0\cos(\phi)}{cP}\right)^{a\ chain}\sum_i\left(\frac{\mathscr{A}_n(t)}{\lambda_n}\right)(\sin\phi-\sin\phi_1)\right]d\Omega. \tag{3.16}$$

The expression are left unevaluated as derivatives because they become lengthy and do not add any insight to the problem.

Parameter	**Value used**
B_0	10^{12} G
ϕ_{cut}	30°
P	10 s
$\{\lambda_i\}$	$\{1004, 855, 597, 425, 320\}$ s^{-1}
β	0.99
γ	2
r_0	10 km
$m_{\rm QN,ejecta}$	10^{-3}M$_\odot$
$A_{\rm avg}$	180

Table 3.1: Summary of parameter values used in Fig. 3.7 and Fig. 3.9.

3.3.1 Model Assumptions and Limitations

The model has two major assumptions: 1) the high density ejecta from the QN maintains a distribution of unstable nuclei for far longer than is normally thought possible and 2) the interaction at the LC causes a disruption of the r-process distribution. The r-process stationary distribution and its lifetime have been simulated using the nucleosynthesis code r-Java 2.0[2]. While it is a surprising result, we have theoretical background and simulation results to show that it is theoretically

[2]r-Java 2.0 is an open use nucleosynthesis code developed at the University of Calgary at quarknova.ca (Kostka et al. 2014c).

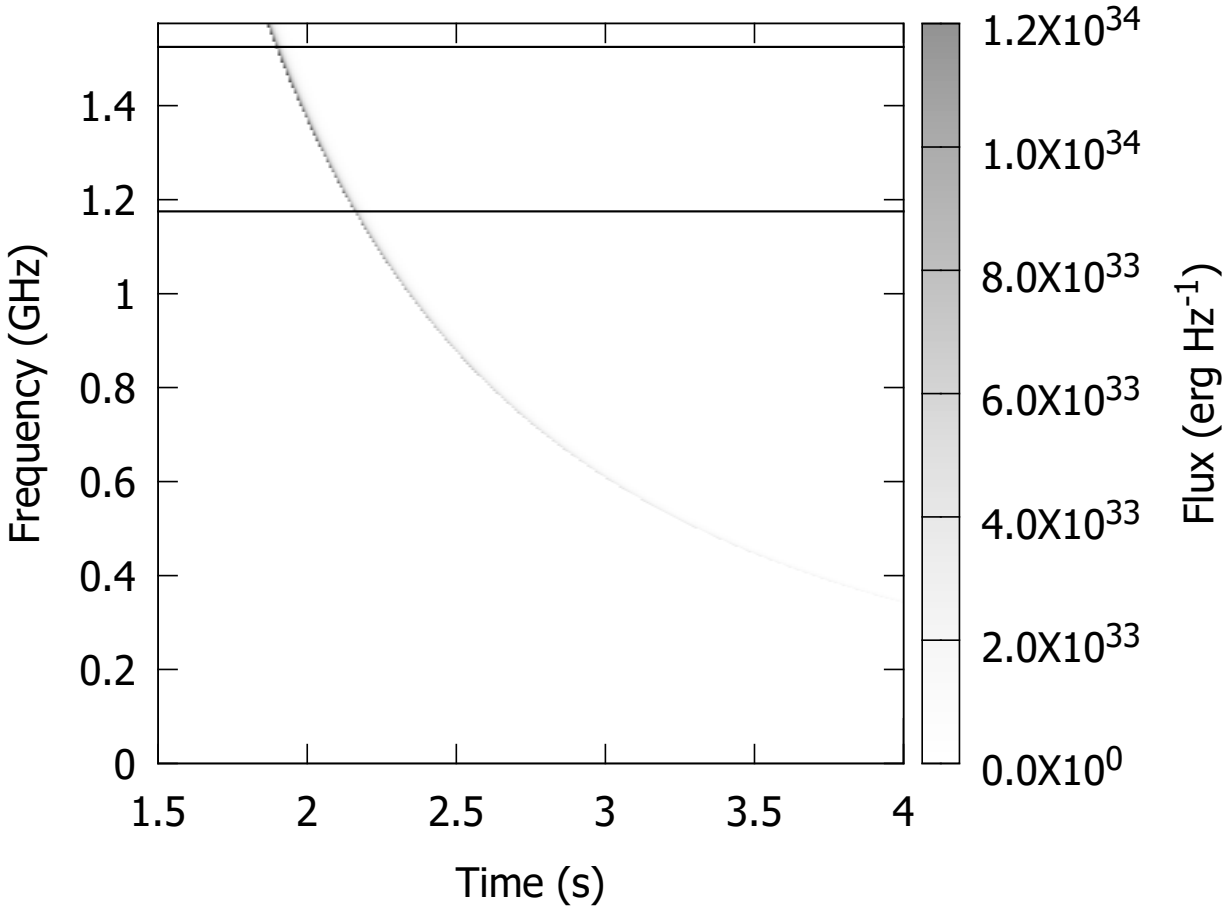

Figure 3.7: A spectrum of the flux density at the emission location. The upper edge of the spectrum is a cut-off frequency determined by the transition angle of the magnetic field where the magnetic field becomes mono-polar ($\phi = 30^\circ$). The two horizontal lines indicate the bandwidth which has been measured by (Thornton et al. 2013). This plot is a fit to data using the parameters outlined in Table 3.1 (no statistical fitting was performed to find best fits to the data).

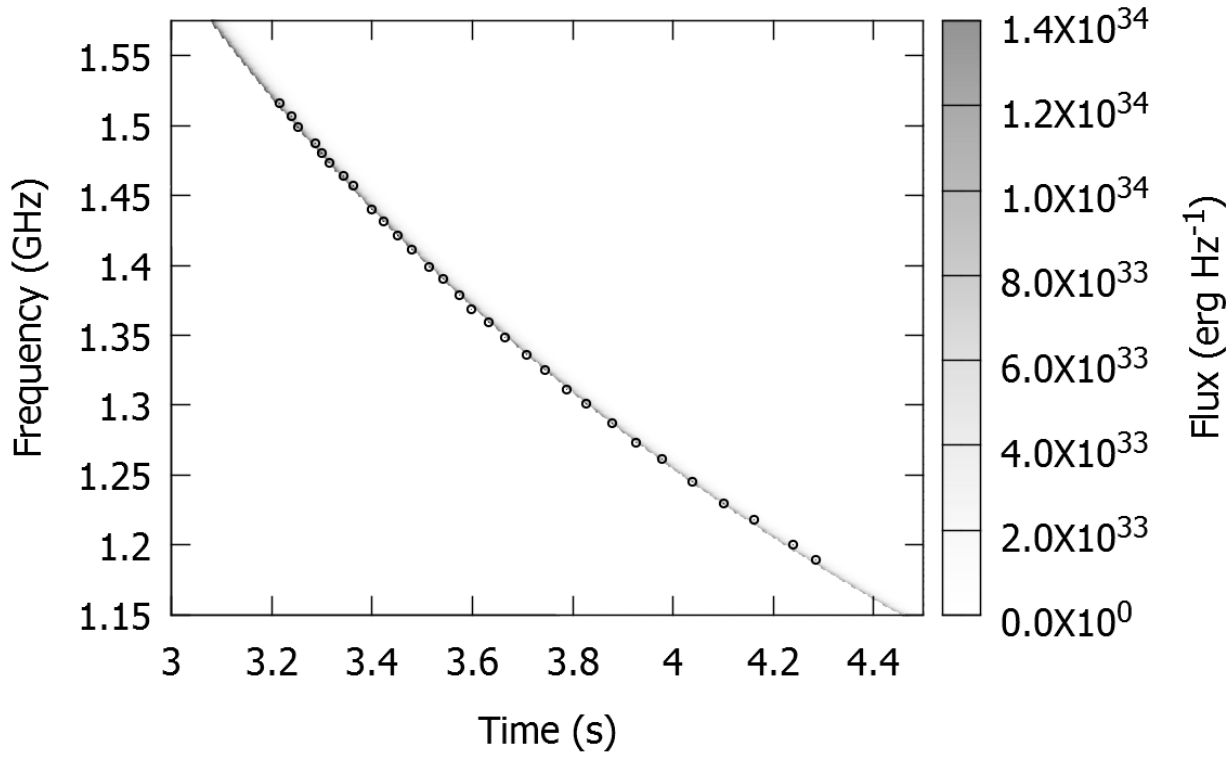

Figure 3.8: A spectrum of the measured data (green points) with our theoretical model predictions. A DM of 725 cm^{-3} pc has been applied to account for the time delay discrepancy between the emission at source and measurement. The green circles on the plot show where the observational data peaks in the spectrum.

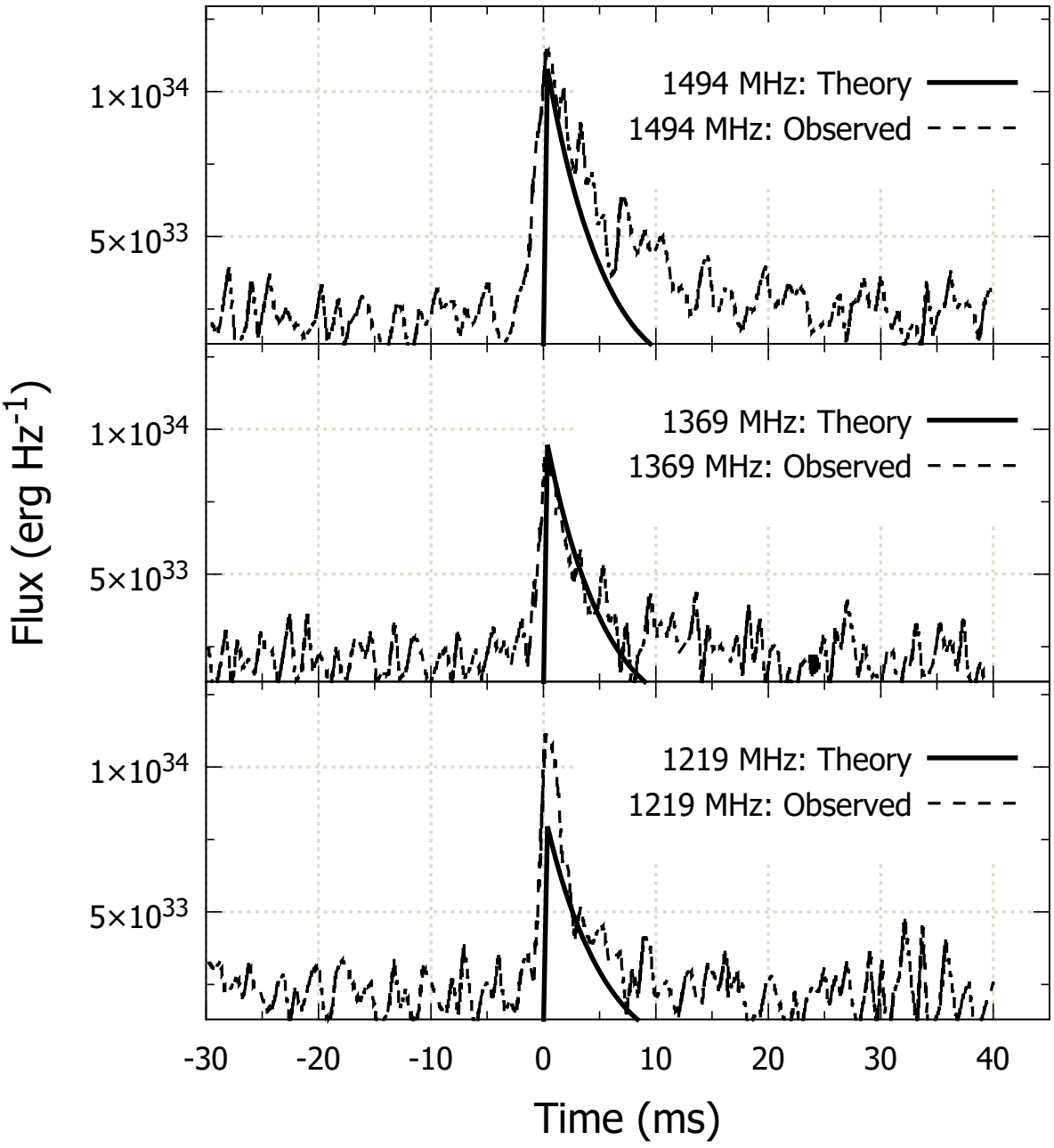

Figure 3.9: Slices into the spectrum of Fig. 3.7 at 1.494, 1.369 and 1.219 GHz (from top to bottom). The relative height (or flatness) of the flux at these frequencies across the observing band provides a constraint on the period of the neutron star progenitor. This plot is a fit to data using the parameters outlined in Table 3.1 (no statistical fitting was performed to find best fits to the data).

possible. The second assumption is much more difficult to quantify. To our knowledge, there has been no theoretical work done on the behaviour of dense nuclear material as it passes at relativistic velocities across a LC. This would require complex magneto-hydrodynamic modelling of material near what is already a difficult numerical problem. In order for the model to work, we require a disruption of the r-process distribution at the LC. The most straightforward way to accomplish this is with rapid decompression of the material as shown quantitatively by the following equation:

$$r_{(n,\gamma)} = n_n \langle \sigma \rangle Y_i, \tag{3.17}$$

where $r_{(n,\gamma)}$ is the neutron capture rate of isotope i, n_n is the neutron number density, $\langle \sigma \rangle$ is the average cross section and Y_i is the number of isotopes in the system. If the ejecta is rapidly decompressed at the LC, this would lead to a rapid decay of all isotopes to stable isotopes.

Other approximations include: a symmetric spherical thin shell expansion of the ejecta, simplified electron energy distributions and use of theoretical decay rates, simplification of the synchrotron radiation spectrum of an electron, and a simplified selection for β-decay rates. These are each worth exploring in detail to provide a more accurate model; however, the agreement with observations leads us to conclude that these assumptions are all appropriate and physically valid.

3.4 Results

Application of the model to the radio burst FRB 110220–the most spectroscopically complete FRB in Thornton et al. (2013)–is presented in Figs. 3.7, 3.8, and 3.9 using model parameters summarized in Table 3.1. The total spectrum emitted using these parameters is presented in Fig. 3.7. The emission has a maximum frequency and decays for the lower frequencies over time. A comparison to the measured data of FRB 110220 (after a newly inferred DM is applied) is shown in Figs. 3.8 and 3.9.

3.4.1 DM, Burst Profile and Distance

The geometry and fields provide inherent cut-off ranges and characteristic emission timescales for our emitted spectra. The sudden turn-on (as represented by our Heaviside function) at the LC provides us with a frequency leading edge which depends on magnetic field strength, period and – to a lesser extent – magnetic field configuration. The leading edge of the pulse for each frequency (as seen in a spectrum) is a direct consequence of the geometry. The curve traced out in frequency over time is given by:

$$\nu_{\rm edge} = \kappa_\nu \gamma^2 B_0 \left(\frac{r_0}{\beta c}\right)^a \frac{1}{t^a}, \tag{3.18}$$

where parameter a is the magnetic field configuration power. Using this, we get a time delay *at the source* between two frequencies. This can be combined with observations to calculate a DM of the pulse which will be smaller than that calculated assuming synchronous emission. For FRB 110220, this leads to a DM of 725 $\rm cm^{-3}$ pc as fit in Fig. 3.8 which is a reduction from 944 $\rm cm^{-3}$ pc as measured in Thornton et al. (2013).

There is an ambiguity in fitting a DM from the pulse time which is resolved by the magnetic field strength and the breakpoint between dipolar and monopolar field lines. Since the radiation emitted at the equatorial region is so much fainter, the maximum frequency of the measured spectra is given by:

$$\nu_{max} = \kappa_\nu \gamma^2 B_0 \left(\frac{2\pi r_0 \cos\phi_{cut}}{cP}\right)^2. \tag{3.19}$$

This can be used to help infer the correct DM of the measured radio burst. This, in combination with the spectral flux at each frequency, can be used to calculate a more accurate DM and distance. The $\rm P^{-2}$ dependence in Eq. 3.19 leads to a wide range of possible frequencies. For example, given a millisecond period neutron star (P = 1 ms, B = 10^{14} G) the peak frequency would be 16×10^{18} Hz putting it in the X-ray regime. This extreme case is unlikely to be realized, as discussed in Section 3.1. More realistic parameters suggest that FRB-like spectra are present in the optical and infrared bands, which depend on the period and magnetic field strength of FRB progenitors. Determination of the likelihood of emission at different frequencies from this mechanism would

require detailed neutron star population studies aimed specifically at determining FRB-QN rates.

In tandem with the new DM, we can estimate the distance to these QNe-FRBs by integrating the flux density or power spectra and comparing this to the measured energy or fluence. This is possible even for bandwidth limited measurements provided there is an estimate from the above quantities of the period and magnetic field by only integrating over the same range of frequencies present in the measurement. If these bursts are in fact cosmological, the cosmological redshift will have to be incorporated into the above equations.

3.4.2 FRB Rates

Assuming that FRB progenitors are old neutron stars, we can estimate their rate based on a simplified population model. We give a rough estimate of the FRB rate by making use of the following assumptions: a constant core-collapse supernova rate (0.02 yr^{-1} galaxy^{-1}), a lognormal magnetic field distribution ($\chi(\log \mathrm{B}) = 13.43 \pm 0.76$) and a normal distribution for the initial period ($\pi(\mathrm{P}_0) = 290 \pm 100$ ms), where the values for the initial period and magnetic field are taken from Regimbau & de Freitas Pacheco (2001) (the magnetic field distribution is from the "unseen" population of Model A). In order to decide the lifetime of the neutron stars when they go FRB we have made two choices: 1) they go QN-FRB after a common timescale (or age), or 2) they go QN-FRB once they reach a certain location in the $\mathrm{P}\dot{\mathrm{P}}$ diagram. For the second case, we consider neutron stars reaching critical density near the observed death line and employ the death line of Zhang et al. (2000):

$$\log\left(\frac{\dot{P}}{\mathrm{s\ s^{-1}}}\right) = 2\log\left(\frac{P}{\mathrm{s}}\right) - 16.52. \tag{3.20}$$

After modelling the neutron star population of a Milky-Way-like galaxy, the last step is to estimate the fraction of neutron stars which are QN candidates. Since only slowly rotating, massive neutron stars are FRB candidates, we only count the neutron stars with periods greater than 100 ms and whose stellar progenitors had masses between 20–40 $\mathrm{M}_\odot$. Integration of the initial mass function (Kroupa 2001) and the initial period distribution (assuming the period and magnetic field are in-

dependent) identifies approximately 14% of neutron stars as QN candidates. This approach does not take into account any possible viewing selection effects (e.g. threshold observing brightness, viewing angle, beaming, etc.), which may affect the detectability of these events. Both the period and death line estimates of the rate give consistent results of approximately 3 per thousand year per galaxy, as summarized in Table 3.2, which is consistent with the observed FRB rate, assuming that the observed FRBs are extragalactic.

Critical Period (s)	**Rate ($\mathbf{yr}^{-1}$ $\mathbf{galaxy}^{-1}$)**
1	0.0028
10	0.0027
Death Line	0.0028

Table 3.2: Summary of FRB rates calculated using a simplistic population synthesis of neutron star population.

3.5 Model consequences and predictions

While we can generate excellent fits to currently available FRB data, there are other important observables and consequences that come along with the scenario we have put forth to explain these radio transients. As mentioned earlier, we can use this model to constrain certain physical and astronomical phenomena. The relation to nuclear properties is somewhat complex due to the number of nuclear species present and is best left for more detailed analysis and higher resolution measurements. There are, however, two astronomical puzzles that we believe can be explained assuming this model is in fact correct.

3.5.1 Neutron Star Population

Assuming the model is correct, FRBs provide measurements of the period and magnetic field strength of isolated NS before they undergo a QN. Based on the agreement of the model with FRB 110220 and the spectral consistency of the FRB measurements, it appears that these are NS that undergo QN. These neutron stars have periods of around 10 seconds and magnetic fields of

10^{12} Gauss (as determined by our parameter selection and its fit to observational data). This is perhaps puzzling if we look at the so-called P$\dot{\text{P}}$ diagram: there are no observed neutron stars in this region (Lorimer & Kramer 2012). This empty region of the P$\dot{\text{P}}$ diagram is beyond what is referred to as the "death line" and we propose an explanation for this: once an isolated neutron star spins down to the 1 to 10 second period and enters the neutron star graveyard, it reaches deconfinement densities at its core and dies via a QN explosion. This instantaneously moves the neutron star into the 10^{15} Gauss regime of the diagram as quark stars generate these high magnetic fields after birth (Iwazaki 2005). Instead of magnetars, we then populate this anomalous region of the P$\dot{\text{P}}$ diagram with quark stars whose magnetic fields decay not through spin down, but through magnetic field expulsion from the color superconducting core (Niebergal et al. 2010, 2006). This drives the quark star from its new position straight downwards as the star ages and provides an explanation for the observed high magnetic field population in the P$\dot{\text{P}}$ diagram.

3.5.2 511 keV Line and Super-heavy Fissionable Elements

The production of super-heavy ($A > 240, Z > 92$) elements is responsible for the fission recycling in the QN ejecta. While these calculations are based on theoretical predictions of mass models, fission recycling from these elements is theoretically expected. Some of these super-heavy nuclei are also thought to be quasi-stable and long-lived. While they are (currently) impossible to make in the lab, these neutron-rich super-heavy nuclei may outlive the β-decaying nuclei and undergo fission much later. If this is correct, these super-heavy nuclei would undergo fission and emit photons over a long period of time and produce extended emission of MeV photons. These emitted photons then have the appropriate energy for efficient production of electron-positron pairs (via γ-γ annihilation). The annihilation events would produce 511 keV photons when the produced positrons find an electron and provide a potential explanation for the positron emission which is an observed phenomenon that still has no definitive explanation for its Galactic origin (Weidenspointner et al. 2008).

This radiation would of course not be as energetic as the original FRB and is likely not measurable from an extragalactic source; however, this does provide a possible explanation for the

511 keV photons observed in our own Galaxy. The current observed annihilation rate of positrons inferred from the 511 keV positronium line is $\sim 10^{43}$ s^{-1} (Knödlseder et al. 2005). Based on our model, we can then constrain the lifetime of super-heavy neutron rich nuclei to be on the order of 1000 years using the following logic.

Given a Galactic QN rate of 1 per thousand years, if we assume the following parameters: $M_{\rm QN,ejected}$ = 10^{-2} M$_\odot$, average nuclei mass A$\sim$ 100 and 10% of nuclei (by number) are super-heavy fissionable elements, we can expect about 10^{-5} $M_\odot$ nuclei to be produced in the QN ejecta which gives about 10^{51} fissionable nuclei per QN event. Given the expected QN rate of 0.001 year^{-1} this produces an average of 10^{48} super-heavy nuclei per year. If we compare this to the current event rate this implies a characteristic lifetime of about 1000 years for the fission events (see Petroff et al. (2015) for further discussion of observational qualities and proposed astrophysical theories).

While these calculations are an order of magnitude approximation, they have several promising features. QNe come from massive (20-40 $M_\odot$) stars and are expected to operate (like the r-process) continually over the entire history of the Galaxy. This leads naturally to a concentration of 511 keV lines near the active portions of the Galaxy (the bulge and the disk) where most of this emission is observed. This matches the observed clustering of the 511 positron emission that has been measured (Weidenspointner et al. 2008). Additionally, because a quark star is an aligned rotator, we expect no radio pulsations to be observed alongside this emission which, again, seems to agree with observation and is one of the difficult aspects in explaining these positronium annihilation events. Finally, the Galactic center and plane have many high energy photons which would allow for efficient conversion of the MeV photons from fission to electron-positron pairs (because the pair production requires a γ-γ interaction). This emission should then carry a P Cygni profile as well as a net exponential decay which could be detected from observations.

It is also possible that the heavy nuclei do not spontaneously experience fission, but instead undergo photo-fission triggered by the high energy photons present in large numbers especially

near the Galactic center. This would lead to a slightly different observable: instead of half-lives we could infer photo-fission cross sections which would give indirect measurements of the level density and fission barrier heights of these nuclei. Instead of a plain exponential, we would instead observe rates proportional to the photon density.

3.6 Conclusion

QNe are capable of generating fast radio pulses using electrons generated by r-process nuclei. Assuming decompression or any other disruption of the r-process at the neutron star's LC, we have shown how the emission spectrum has an intrinsic time delay across its frequency band and has a predictable bandwidth (cut-off frequency) which can be used to measure magnetic field strength and period of otherwise undetectable neutron stars. If correct, FRBs can be used to probe and measure properties of unstable nuclear matter and measure properties of old neutron star populations. Our model predicts that these explosions are indeed one of the most energetic explosions in radio astronomy (with energies on the order of 10^{41} ergs); however, they need not necessarily be cosmological as was inferred from previous analysis of the data. The model naturally provides explanations for the timescales and energies of the FRB emissions using synchrotron emission in the strong magnetic field of a newly-formed QN.

Chapter 4

Critical assessment of nuclear sensitivity metrics for the *r*-process

Forward to Paper II

The following paper has been written in part as a response to a series of papers published on the topic of nuclear sensitivity studies. The earliest of which appears to have been a paper published in 2009 focused on the $A = 130$ r-process peak (Surman et al. 2009). In this paper the typical exercise of running an r-process simulation with different mass models was augmented with small variations on a per isotope basis to the neutron capture rates. Each isotope was then given a rating based on a globally calculated value $F = \sum_A |X(A)_{A,\mathrm{baseline}} - X_A|$ (Eq. 2 in (Surman et al. 2009)). This, for perhaps the first time in published literature, provided a clear method for determining quantitatively how simulations were affected by individual isotopic properties. The traditional idea that isotopes in the r-process path are of importance can be more accurately quantified through this type of calculation and it provides an understandable roadmap for predicting the best isotopes for more accurate study. This is especially important for nuclear experiments where a single measurement can be expensive and time consuming.

The r-process abundances, however, currently have no formal or tractable mechanism for estimating the errors in simulations data. In many cases, the abundance predictions are only qualitatively good and are off from the solar r-residuals by several orders of magnitude. Coupled with the logarithmic variation in the abundances, metrics that examine differences like this are unsurprisingly biased towards the peaks. This seems like an philosophically unattractive quality to a statistical method aimed at providing estimates on global abundance variations and the impact of nuclear inputs. This triggered the search for what I hoped would be a formal statistical method for

determining the biggest change in the r-process. In the end a new metric was "invented" and tested on sample data and compared to some previously used (in the literature) variations of the original F metric. The results led to the suggestion that, for now, conclusions based on what are effectively arbitrary metrics can be used to assist in identification of key isotopes, but user discretion is advised when interpreting the results.

The work in this paper in terms of data generation, collection and analysis was done exclusively by me. Assistance in programming the sensitivity module was provided by Nico Koning. All co-authors were involved in the discussion of the results and in determining their relevance and assistance in production of the final manuscript.

Critical assessment of nuclear sensitivity metrics for the *r*-process

Zachary Shand, Nico Koning and Rachid Ouyed

Department of Physics and Astronomy, University of Calgary, 2500 University Drive NW, Calgary AB T2N 1N4, Canada

Iris Dillmann and Reiner Krücken

TRIUMF, 4004 Wesbrook Mall, Vancouver, BC V6T 2A3, Canada

Prashanth Jaikumar

Department of Physics & Astronomy, California State University Long Beach, 1250 Belfower Blvd., Long Beach CA 90840 USA

Abstract: Any simulation of the *r*-process is affected by uncertainties in our present knowledge of nuclear physics quantities and astrophysical conditions. It is common to quantify the impact of these uncertainties through a global sensitivity metric, which is then used to identify specific nuclides that would be most worthwhile to measure experimentally. Using descriptive statistics, we assess a set of metrics used in previous sensitivity studies, as well as a new logarithmic measure. For certain neutron-rich nuclides lying near the r-process path for the typical hot-wind scenario, we find opposing conclusions on their relative sensitivity implied by different metrics, although they all generally agree which ones are the most sensitive nuclei. The underlying reason is that sensitivity metrics which simply sum over variations in the *r*-process distribution depend on the scaling used in the baseline, which often varies between simulations. We show that normalization of the abundances causes changes in the reported sensitivity factors and recommend reporting a minimized F statistic in addition to a scale estimation for rough calibration to be used when comparing tables of sensitivity factors from different studies.

4.1 Introduction

About half of all the stable nuclei heavier than iron are produced by the mechanism of rapid neutron capture, or the *r*-process Burbidge et al. (1957); Cameron (1957), which occurs in explosive neutron-rich astrophysical environments. Obtaining a better fit to the solar system's isotopic abundances of heavy elements (within astrophysical uncertainties) gives confidence that we have identified the primary site of *r*-process nucleosynthesis. Parameterized studies of neutron-rich flows and a growing set of observations from metal-poor stars suggest that no proposed site can produce the entire *r*-process from the first peak around A=80 to the third peak at A=195 Qian & Wasserburg (2003); Sneden et al. (2008). For a complete understanding of the origin of heavy elements, theoretical simulations of the *r*-process are essential in discriminating between the several proposed astrophysical sites, but are faced with modeling uncertainties in the nuclear physics inputs for neutron-rich nuclei. Rare-isotope measurements at existing and upcoming experimental facilities can help reduce these uncertainties in *r*-process simulations. This requires that key isotopes for the *r*-process in experimentally accessible regions of the nuclide chart be identified for measurements. To accomplish this, quantitative metrics, called "sensitivity factors," have been developed (Mumpower et al. 2015; Brett et al. 2012; Mumpower et al. 2012).

Nuclear mass models are crucial to the *r*-process, since they affect neutron separation energies (S_n), β-decay Q-values (Q_β), β-decay half-lives ($T_{1/2}$), neutron-capture cross sections (σ) etc., which are all important nuclear input parameters to a full network calculation. Even in the classical waiting-point approximation, the use of different nuclear mass models with variations in the predicted shell structure near the magic numbers alters the neutron separation energy (i.e. the *r*-process path) and the final calculated abundance Mumpower et al. (2015). Although we will not achieve a complete measured range up to the drip line, as the number of experimentally measured masses increases we can hope that the predictive power of the nuclear mass models will improve Sobiczewski & Litvinov (2014).

To quantify how the uncertainty in nuclear properties propagates to the *r*-process abundance

pattern, a global sensitivity measure (or "impact parameter") F is utilized in some studies, which is examined in detail in this paper (see (Mumpower et al. 2015; Brett et al. 2012; Mumpower et al. 2012) for various definitions of F). Based on this metric, key pieces of data are identified near the neutron closed shells and the precursors of the rare-earth peak which are most influential in generating the overall abundance pattern Surman et al. (2014). While this metric, and its variations in the series of papers on sensitivity studies (see Ref. Mumpower et al. (2016) for a review), is a simple way to capture the impact of variations in the nuclear parameters (locally or globally), distilling the sensitivity to a single number is fraught with erroneous conclusions on the relative importance of some isotopes, as we demonstrate in this paper. The freedom to scale or normalize the simulated r-process pattern in an arbitrary way leads to opposing conclusions on the sensitivity depending on the metric used.

The purpose of this work is two-fold: (i) to show that application of the currently existing metrics lead to varying conclusions on the relative importance of certain nuclides in producing the best fit to the r-process abundance pattern; (ii) introduce a statistical significance to the F-metric that takes the arbitrariness in baseline normalization into account, so that conclusions on the sensitivity are more refined and specific to the particular metric used.

This is the first step towards a more universal definition of sensitivity for r-process studies. The paper is organized as follows: In Sec. 4.2, we set up our r-process waiting-point simulation with the SiRop code and calculate the variations in the abundance using different measures due to changes in the nuclear mass model. In Sec. 4.3, we compare the performance of four different metrics (two absolute, one relative and one log-difference) and highlight differing conclusions on the sensitivity of the r-process pattern to nuclear masses around the A=130 peak. In Sec. 4.4.1, we describe the effect of scaling and normalization, followed by our conclusions in Sec. 4.5.

4.2 Simulation Parameters

We generate our *r*-process simulation data using an extension of the *r*-Java 2.0 code Kostka et al. (2014c,b) that now includes a graphical-user interface (GUI) module for sensitivity runs. This first-of-its-kind code, "SiRop", allows users to run the *r*-process simulation and output sensitivity metrics in a single Java-based application in order to represent and analyze changes in the abundance curves. The data used to compare the sensitivity studies was computed in the waiting point approximation for fast computation of data to test and compare each metric. The results of the baseline and varied simulations is shown in Fig. 4.2. For the baseline, we used a parametric trajectory for the density of $\rho = \frac{\rho_0}{(1+t/2\tau)^2}$ where $\rho_0 = 10^{11}$ g cm^{-3} and τ=0.001 sec, and with an initial temperature T=3 $\times$ 10^{9}K. The trajectory ensures validity of the waiting point approximation and production of *r*-process elements including the third peak at A=195.

The initial isotopic composition of the environment was set to 50% ^{70}Fe by mass (i.e. $X_{70\mathrm{Fe}}$=0.5) corresponding to an initial neutron-to-seed ratio of 62. The code was run until the neutron-to-seed ratio dropped below one at which point the temperature and neutron number density of the simulation were 2.7×10^9 K and 4.64×10^{28} cm^{-3}. These values were used to calculate the waiting point population coefficients displayed in Fig. 4.1 as circles. The varied simulations consisted of changes in masses of a single isotope in a grid spanning from ^{128}Cd to ^{139}Te. These isotopes were chosen as they are in the predicted r-process path and match the isotopes selected in Surman et al. (2009). For each isotope, the simulation was run twice corresponding to a decrease and increase in the isotopes mass by 0.0005% which corresponds to a change of approximately $\pm$0.6 MeV, where this value corresponds to the average deviation of mass models from experimental values.

4.3 Metric Performance Comparison

Both global and local sensitivity metrics have been used in other works (e.g. (Mumpower et al. 2015; Brett et al. 2012; Mumpower et al. 2012)), with global sensitivity metrics (sums of variations over mass numbers) providing a convenient and digestible value which can be used to estimate

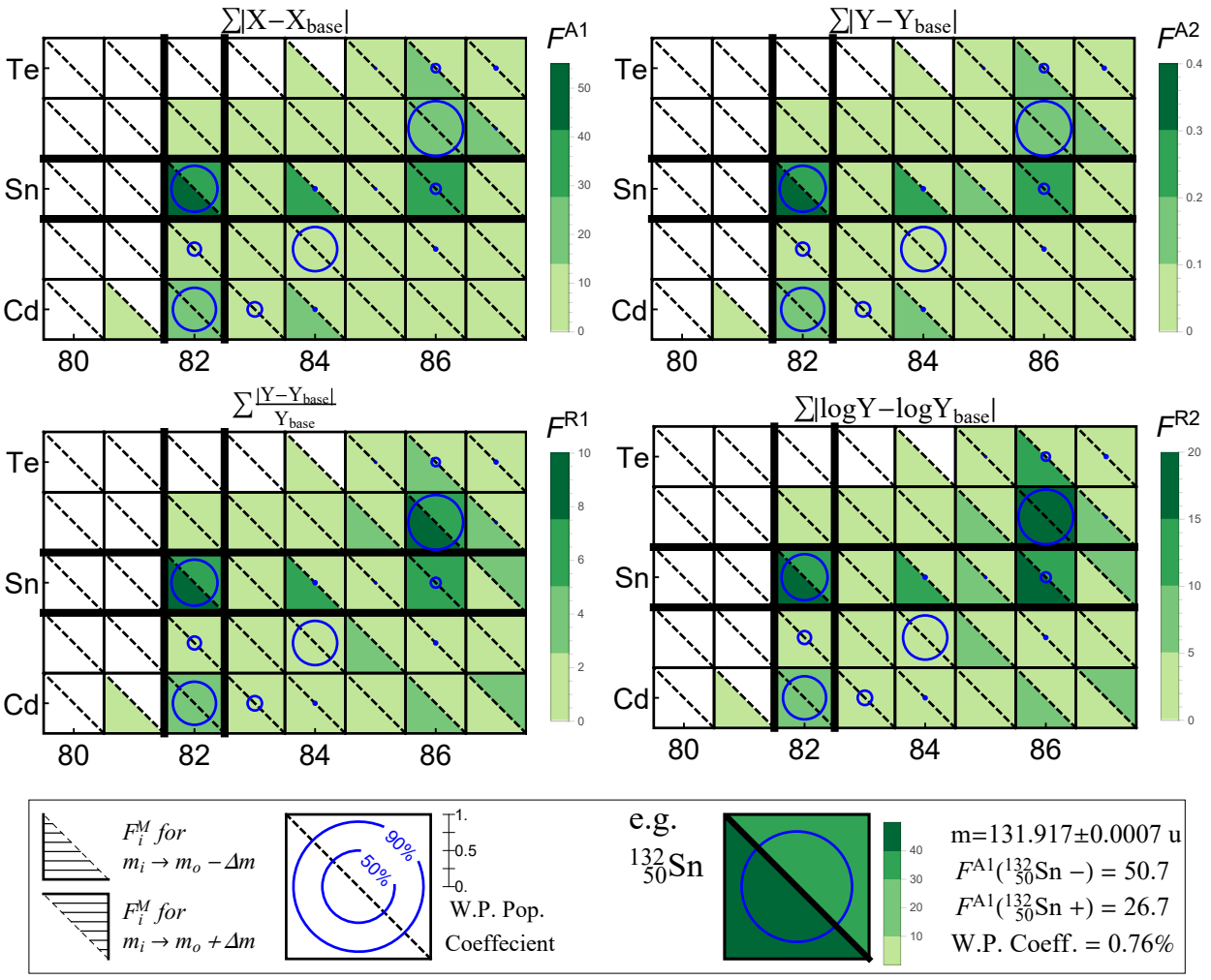

Figure 4.1: The calculated sensitivity factors (F_i^M) for each metric is color coded as shown in the legend. The sensitivity factor calculated after decreasing the mass of one isotope is plotted in the bottom left of the isotope in the chart. Similarly the increase in mass is plotted on the top right triangle. The circles indicate the *r*-process waiting points population coefficients (WPPC) as determined by the nuclear Saha equation, where the diameter is proportional to the population coefficient where the full height of each square corresponds to 100%. The sensitivity over the mass range $120 \leq A \leq 200$ is calculated using mass fraction normalized abundances. Even for our the small test study we see that the metrics disagree both qualitatively and quantitatively.

the total variation induced by a changing nuclear parameter (or set of parameter changes). This number alone, however, provides no description of how the abundances changed. For example, large overproduction of a single isotope is indistinguishable from many equivalent differences distributed over many isotopes. We test four different definitions of the metric (the first three have previously been used, the fourth is newly introduced in this work):

- A1: absolute mass fraction difference $|\text{X-X}_{\text{base}}| = |\text{A (Y-Y}_{\text{base}})|$
- A2: an abundance difference $|\text{ Y-Y}_{\text{base}}|$
- R1: a relative difference $|\frac{\text{Y}-\text{Y}_{\text{base}}}{\text{Y}_{\text{base}}}|$
- R2: a log-ratio $|\log_{10}\frac{\text{Y}}{\text{Y}_{\text{base}}}| = |\log_{10}\text{Y} - \log_{10}\text{Y}_{\text{base}}|$.

For metrics R1 and R2 the use of mass fractions or abundances is interchangeable as the factor of A ($X = A \cdot Y$) cancels out in the ratio. Metrics A1 and A2 overweight changes at or near the peaks in the *r*-process distribution due to the order of magnitude differences between isotope abundances. They are also more sensitive to an overproduction of isotopes. In contrast, R1 and R2 do not overemphasize the more abundant isotopes which is a useful feature when examining the details of the abundance distribution. Both R1 and R2 produce similar results when the changes in ratio or percentages are small, because the series expansion to first order of the log-ratio is identical (within a constant) to the relative difference.

Application of these metrics to the simulated data shows that each metric has varying sensitivity to the mass variations in our study. It is apparent from Fig. 4.1 that the four metrics have very different numerical values as expected, but significantly, they do not necessarily agree on the relative sensitivities of different isotopes. A1 and A2 favor the most abundant isotope ^{132}Sn as expected,[1] and indicate higher sensitivity to the mass of ^{132}Sn being decreased rather than increased by the same amount. In contrast, R1 and R2 assess ^{137}Sb as the most sensitive isotope and indicate

[1]Normally ^{130}Cd is expected as the most abundance isotope in our region of interest as the precursor to the $A = 130$ peak; however, in our test data set of the waiting point strongly favoured ^{132}Sn at freeze-out conditions.

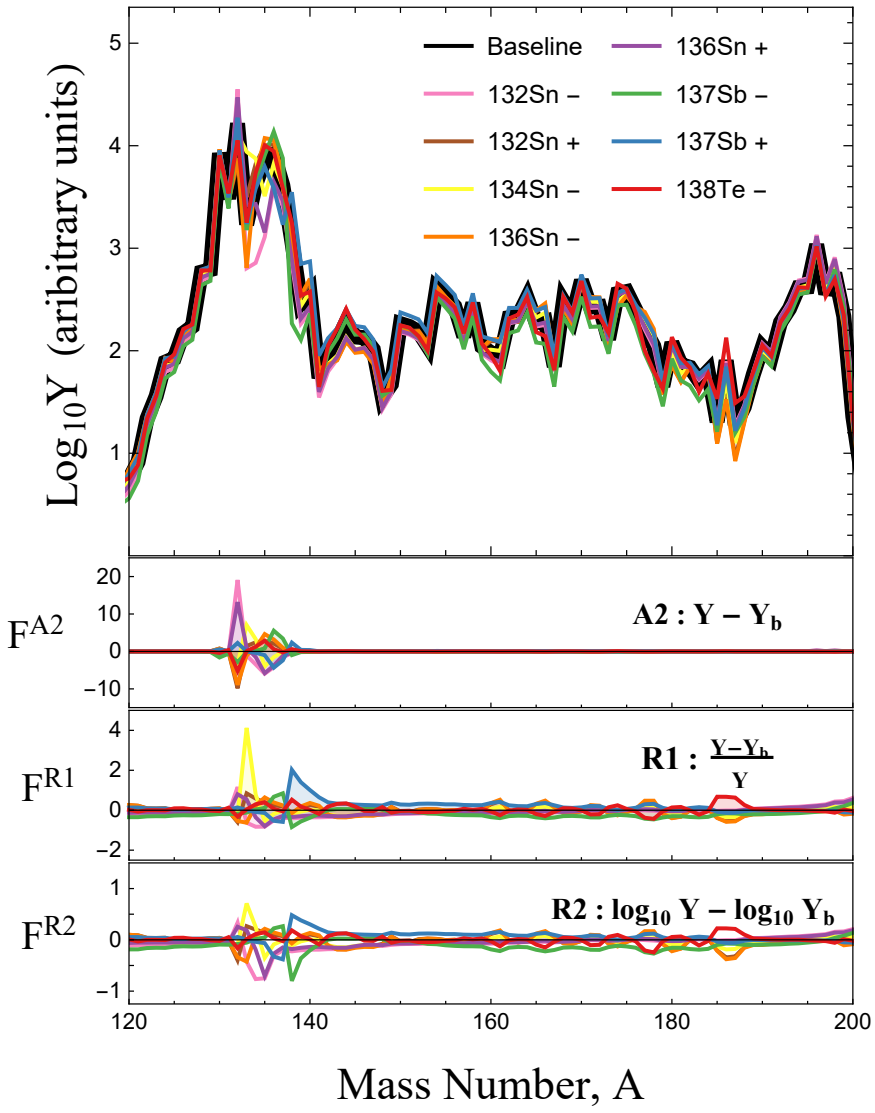

Figure 4.2: Abundance pattern in the *r*-process simulation showing baseline vs eight most sensitive mass changes (labels indicate isotope's mass was changed by $\pm 0.0005\%$). The lower three panels show the deviation from the baseline as defined by the metrics listed in sec. 4.3, where the top shows metric A2 (units of mass normalized abundance multiplied by 10^4), the middle shows metric R1 (unitless) and the bottom shows metric R2 (unitless).

nearly identical sensitivities for the increase and decrease in the mass of ^{132}Sn. Metrics A1 and A2 are identical except for a weighting by mass number present in A1 which will cause the two to perform differently when comparing changes near the first, second, and third abundance peaks. For our test data, R1 and R2 perform almost identically; however, R1 emphasizes overproduction of isotopes which had smaller abundances in the baseline (see ^{134}Sn and ^{137}Te in Fig. 4.2 and Fig. 4.1) while R2 responds equally to under- and over-production by a constant factor (e.g. twice the abundance vs. half the abundance).

In Fig. 4.2 we see that the exponential sensitivity of the waiting point to the one-neutron separation energies (S_{1n}) leads to rather large changes to the abundances. While metric A2 (Y-Y_b) seems to imply that large changes only occur in the neighborhood of the changed nuclide, the relative metrics (R1,R2) (bottom two panels in Fig. 4.2) magnify changes in low-abundance nuclides, showing that there are large effects also on heavier nuclides. As can be seen in Fig. 4.2, changes to some isotopic masses (like ^{134}Sn) cause strong local variation in the simulated abundances, while others (like ^{137}Sb) produce changes to the abundance of several isobars. In calculating a global sensitivity factor we lose information about the details of the differences in the data, but greatly simplify the interpretation and presentation of the calculated sensitivity.

Due to the differences between the metrics the best choice of metric seems unclear and depends on what type of changes in the *r*-process distribution are of interest. For large scale variations like the type shown in the test data here, it seems like the log-ratio R2 performs best; however, different changes in the nuclear parameters do not necessarily provoke such strong variations. Changes in the β-delayed branching ratios, for example, are likely to only cause small local changes during "freeze-out," and in this instance A2 could be the best metric for studying these nuclear parameters. Due to these potential disagreements and differences in sensitivity of the metrics, we caution against placing too much weight on any single global sensitivity metric for assessing sensitivity to nuclear input parameters.

	F_{default}	F_{min}	ΔF (%)	a/b	
$F^{(A1)}$	^{132}Sn−	53.6	50.7	-5.4	0.70
	^{136}Sn+	40.2	39.3	-2.2	0.85
	^{134}Sn−	29.0	28.6	-1.5	1.03
	^{136}Sn−	31.1	28.1	-9.6	0.81
	^{137}Sb−	26.9	26.9	-0.0	0.97
$F^{(A2)}$	^{132}Sn−	0.396	0.366	-7.5	0.46
	^{136}Sn+	0.296	0.289	-2.3	0.82
	^{134}Sn−	0.214	0.210	-1.6	1.03
	^{136}Sn−	0.228	0.203	-11.0	0.81
	^{132}Sn+	0.223	0.194	-12.8	0.84
$F^{(R1)}$	^{136}Sn−	16.0	16.0	-0.0	1.00
	^{132}Sn+	14.9	14.9	-0.2	0.98
	^{137}Sb−	20.0	14.7	-26.5	1.24
	^{132}Sn−	15.7	14.7	-6.7	1.09
	^{134}Sn−	14.0	13.5	-3.5	1.04
$F^{(R2)}$	^{136}Sn−	7.43	7.27	-2.3	1.05
	^{132}Sn−	8.15	6.99	-14.2	1.15
	^{132}Sn+	6.73	6.61	-1.7	1.05
	^{137}Sb−	10.3	6.32	-38.8	1.31
	^{137}Sb+	6.74	5.57	-17.4	0.89

Table 4.1: Sensitivity factors reported using default scaling/normalization factor ($a/b = 1.0$) compared to those minimized sensitivity factors calculated. The blocks consist of the top five rated isotopic changes (after minimization). The columns list from left to right: the isotope whose mass was changed, the default sensitivity value, the minimal sensitivity factor, the percent difference, and the scaling constant which provided the F value.

4.4 Normalization and Calibration

4.4.1 Normalization

The *r*-process is a set of abundance values which are important in aggregate as a relative distribution and, without an astrophysical context, the absolute abundances are arbitrary up to a positive multiplicative constant. When observationally available, these relative abundances are consistent with the solar *r*-process residuals ($\mathrm{N}_r = \mathrm{N}_\odot - \mathrm{N}_s - \mathrm{N}_p$) Sneden et al. (2008). In principle, a good agreement of a single simulation does not say anything: one has to run hundreds of simulations with varying astrophysical input parameters (metallicity, stellar masses, sites, etc.) and then see the solar r-process abundances as a superposition of these values. Observations are normalized to

Ba for (s-process) or Eu (r-process), but simulated data from a single calculation is typically normalized by mass fraction. For this reason, comparing theoretical calculations to observational data or other simulation data is not so straightforward. In order then to assign calculate the sensitivity value we need to somehow normalize our simulated abundances before we can calculate how sensitive the *r*-process is to the underpinning nuclear parameter we have varied. If we had information about an underlying probability distribution for the *r*-process abundances it would be more obvious how to compare the two sets of data (e.g. χ^2 or other maximum likelihood methods); however, the sparsity of observational data, long simulation times, and large variability in abundances from simulations preclude many standard statistical methods. For these reasons, we are forced to rely on these simple tests to estimate which inputs caused the largest or most significant variation. This is possible only if we can meaningfully interpret the numerical values computed for our sensitivity factors and ensure that the methods for determining relative sensitivity are properly normalized and consistent.

In order to understand what we mean by this, we first re-write the sensitivity metrics with two arbitrary scaling constants a and b as follows:

$$F_i^{(A1)} = \sum_A |aX_i - bX_b| = \sum_A b \left| \frac{a}{b} X_i - X_b \right| \tag{4.1}$$

$$F_i^{(A2)} = \sum_A |aY_i - bY_b| = \sum_A b \left| \frac{a}{b} Y_i - Y_b \right| \tag{4.2}$$

$$F_i^{(R1)} = \sum_A \left| \frac{aY_i - bY_b}{bY_b} \right| = \sum_A \left| \frac{\frac{a}{b} Y_i - Y_b}{Y_b} \right| \tag{4.3}$$

$$F_i^{(R2)} = \sum_A \left| \log_{10} \frac{aY_i}{bY_b} \right| = |\sum_A \left| \log_{10} \frac{a}{b} Y_i - \log_{10} Y_b \right|, \tag{4.4}$$

where Y_{base} is the baseline abundances and Y_i is the abundance data with our i$^{\text{th}}$ varied set of nuclear parameters. In each metric we can identify the term $\frac{a}{b} Y_i$ which indicates that when comparing Y_i to Y_b we can find constants a, b which minimize F. We refer to solving for the constant a/b which minimizes the computed sensitivity factor as normalization. For our test data, we show the change to the final reported value for the most sensitive values (after normalization) for each metric in Table 4.1. The normalization procedure does not vary most values by more than a few

	$F^{(A1)}$	$F^{(A2)}$	$F^{(R1)}$	$F^{(R2)}$
^{130}Cd−	18.4	0.137	7.3	3.23
^{130}Cd+	17.5	0.130	7.2	3.13
^{131}Cd−	10.7	0.081	3.2	1.38
^{132}Cd+	11.9	0.089	3.2	1.52
^{135}Cd+	10.9	0.080	6.7	2.86
^{134}In−	10.3	0.075	6.2	2.66
^{132}Sn−	<u>50.7</u>	<u>0.366</u>	14.7	<u>6.99</u>
^{132}Sn+	26.7	0.194	<u>14.9</u>	<u>6.61</u>
^{134}Sn−	<u>28.6</u>	<u>0.210</u>	13.5	4.73
^{135}Sn−	12.4	0.091	3.9	1.50
^{136}Sn−	28.1	0.203	<u>15.9</u>	<u>7.27</u>
^{136}Sn+	<u>39.3</u>	<u>0.289</u>	11.4	5.11
^{137}Sn+	11.6	0.085	7.1	3.04
^{136}Sb−	11.0	0.080	6.4	2.73
^{137}Sb−	26.9	0.193	<u>14.7</u>	6.32
^{137}Sb+	20.6	0.147	13.3	5.57
^{138}Sb−	13.6	0.099	9.4	3.91
^{138}Te−	17.4	0.127	10.6	4.51
Range: $120 \leq A \leq 200$				
$Y_{\max} = 0.165$ at $A = 132$				

Table 4.2: Summary of global sensitivity factors computed based on different statistical metrics. The isotopes and sensitivity factors reported in are a combination of the top 15 most sensitive isotopes according to each metric. The top three most sensitive isotope mass changes are underlined in each column. These sensitivity values have been computed after normalization (i.e. $F^a_{\min}$) according to each respective metric.

percent for any of the metrics, but in the test data here the variation can be as much as 39%. However, we do see differences which have the potential to become more pronounced when applied to either more comprehensive or more complex studies. In cases where there is significant non-local change, normalization is expected to show more significant corrections to the sensitivity factors and will allow for more robust measures of these changes. The computational simplicity makes it a reasonable and prudent improvement to the existing method for computing sensitivity factors.

4.4.2 Calibration

When writing the sensitivity factors with normalization constants, we have also explicitly exposed another potential ambiguity in interpreting and comparing metrics defined using simple differences of abundances (or mass fractions). In equations 4.1 and 4.2 the factoring process exposed a scale parameter b which pre-multiplies the metric. (Equations 4.3 and 4.4 in contrast are purely relative or scale-free.) Given our arbitrary magnitude relative abundance data, differences in implicit scale (b) will cause these type of metrics to report different absolute magnitudes for sensitivity depending on how they happen to have been scaled. If the data is reported by an r-process code which relies on mass fraction normalization (e.g. r-Java 2.0) then we would expect the 2$^{\text{nd}}$ r-process peak to have an abundance of Y$\sim 10^{-3}$. Local changes in the peak will (for these difference type metrics) swamp out any non-local changes and the sensitivity factor will be close to 10^{-3}. The values we have reported in Table 4.2 were computed after multiplying our abundances by a factor of 100 (this has the effect of making our definition of F^{A1} in Eq. 4.1 consistent with the definition in Mumpower et al. (2015)) and as expected, the reported values for $F^{(A1)}$ and $F^{(A2)}$ are the same order of magnitude as the maximum abundance ($F^{(A1)} \sim A_{\max} \cdot Y_{\max} = 21.8$ and $F^{(A2)} \sim Y_{\max} = 0.165$) as indicated at the bottom of Table 4.2. For this reason, we recommend that sensitivity factors be reported with the peak abundance as we have done at the bottom of Table 4.2. The maximum abundance in the baseline, while not a perfect indicator, can assist in comparison of studies. We refer to this technique as "calibration" and it will allow comparison of sensitivity values from different studies with different baselines.

4.5 Conclusion

In summary, we have performed sensitivity studies of the r-process using a waiting-point simulation to assess a few different global sensitivity metrics that have been proposed in recent work. While some of the biases and limitations of the metrics have been mentioned before, this is the first work that compares its various definitions by applying them on a single simulation. Besides show-

ing that metrics of the form presented in this work give different results on the relative sensitivity of certain nuclides that lie on or near the *r*-process path, we also demonstrate that normalization of the abundances can affect the computed sensitivity. Computations done in the rare earth element region were also performed (but not presented in this manuscript) which confirm the preferential bias of metrics A1 and A2 for higher sensitivity near the abundance peaks. In addition, we presented a technique for calibrating sensitivity values from different studies.

Based on our findings of variations from one metric to another, we recommend against their use as the only analysis tool for sensitivity. Ideally, one should understand the particular response of each metric definition, but computation of all metrics simultaneously (and any others that seem reasonable) seems prudent. We also recommend that the abundance distributions should be normalized in some fashion and recommend reporting a minimized F. When reporting metrics $F^{(A1)}$ or $F^{(A2)}$, maximum abundance information should be provided to assist in calibration and comparison of different sensitivity studies. These recommendations are aimed at improving the strength of sensitivity studies using global sensitivity factors and are designed to allow for more robust statistical inference from *r*-process simulations.

4.6 Addendum to Paper II

The preceding paper manuscript was prepared and submitted to Physical Revue C Rapid Communications which maintains a page limit. At this point, however, it seems appropriate to include an expanded discussion of the reasoning for the recommendations made in the paper. The two main ideas in the manuscript are understanding the statistical calculation and its potential implications or biases. The second is a discussion of how we normalize the data and compare it to other sets of simulated (or observed) data.

During the development phase of SiRop, one of the things I noted about about the first metric $F^(A1)$ was that it was prone to biases near the peaks. This was noted in some of the existing sensitivity studies, but the implications were not explored further. The effect is more noticeable if we compare Fig. 4.2 in the paper above to an additional set of data in Fig. 4.3 which expanded the set of isotopes whose abundances are much lower than those in Fig. 4.2. The variation in the mass range 150 to 180 that can be visually identified in the abundances (top panel) are not identified by the $F^{(A1)}$ or $F^{(A2)}$, but seems much more significant to metrics $F^{(R1)}$ and $F^{(R2)}$ as shown in the bottom three sub-panels of Fig. 4.3. This quantitatively illustrates the potential bias introduced by the peaks when computing global statistics.

Normalizing data in r-process simulations relies on decoupling the density of the environment from the individual masses of the isotopes and normalizes the abundances in simulations by mass or mass fraction. In order to calculate the actual number of isotopes produced in an r-process environment, these normalized mass fractions can be multiplied by the expected r-process mass ejected by the environment. These values can be compared to observations only through models for GCE and introduces an extra layer of models before we can compare simulated r-process abundances to observed abundance data. When comparing to the solar abundance data (which is the most complete r-process abundance data) the superposition of many sites for nucleosynthesis must be considered. As a result, the observational data which is normally normalized to Ba or Eu abundances must be somehow compared to the simulated abundances which are normalized by

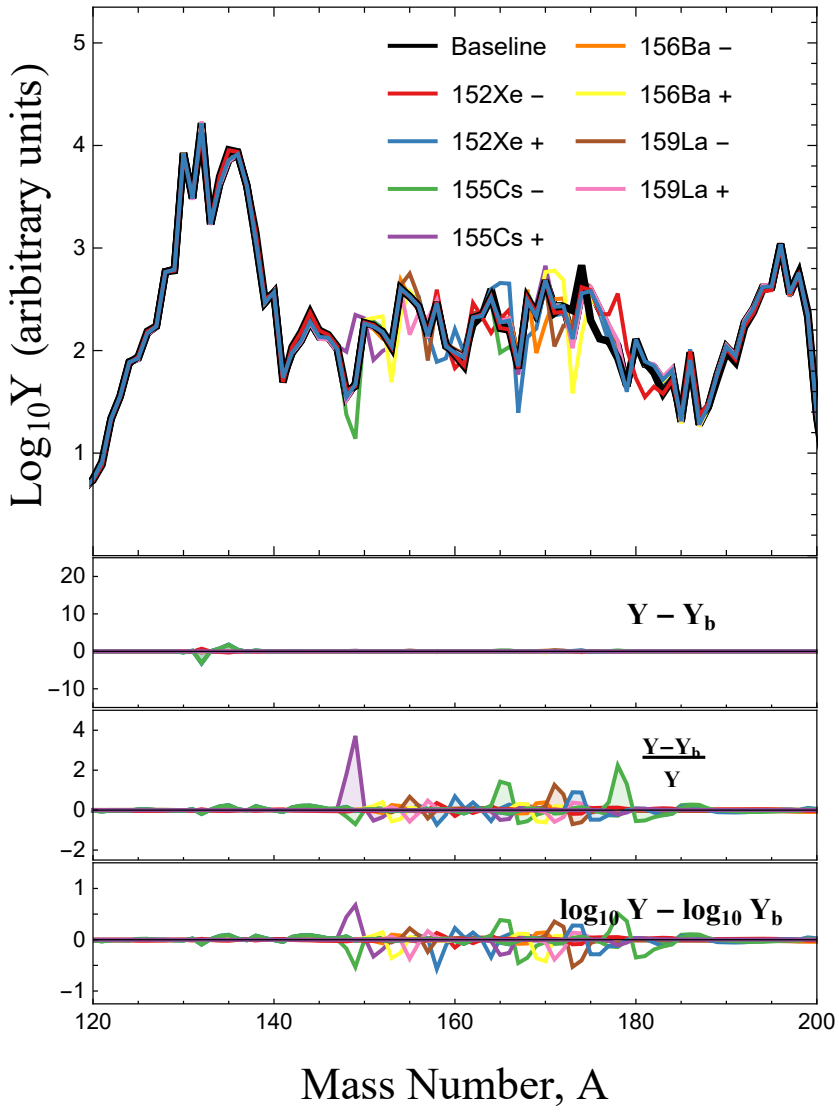

Figure 4.3: Sensitivity study results with variation of nuclear masses for isotopes between the second and third r-process peaks. The variation picked up by the relative metrics as shown in the lower portion of the graph shows the bias towards the peaks when compared to Fig. 4.2.

mass fractions through a model.

When calculating statistics as we have in the paper above, the global sensitivity factor F^X is only computed over a range of masses (120 to 200) and so the range of isotopes being considered no longer normalized with an indeterminate mass fraction being excluded. This could be accounted for and renormalized and all sensitivity data could be analysed using re-normalized abundances; however, just like the metric choice the effect of the re-normalizing the abundances has never been studied. Since the observed abundances in other stars seems to match the solar r-process residuals in a robust (at least for Z¿56) I proposed that we compare simulated data in a sensitivity not by normalizing it to mass fractions, but instead to first fit the secondary simulation to the baseline by minimizing the difference between the baseline and the second simulation. In this way, we are reporting something similar to a minimized ^{2} and in our case is a sum of the residuals between the ”best fit” and the baseline. This is in contrast to a third ”normalizing” scheme that seems to be another option which would be to pick a reference isotope (e.g. europium) and normalize to these isotopes.

The constant which is to be chosen (a/b in the paper) is selected by minimizing the statistic F^X. In Fig. 4.4 we can see an example of the shape of the function for F which must be minimized. The points on the curve indicate the values the sensitivity factor (labelled objective function in the plot) could have based on different normalizations to the baseline based on matching abundances between the two simulations. The number of points above the default or minimized normalization factors a/b provide an indication of the number of isotopes which had large changes compared to the baseline. Further exploration of these details, like the spread of points on this graph may lead to additional methods for identifying nuclear sensitivity based on the spread and shape of the objective function, or range of possible F values, but more importantly it indicates that there is a quantitative difference generated by the way we scale our baseline and sensitivity data.

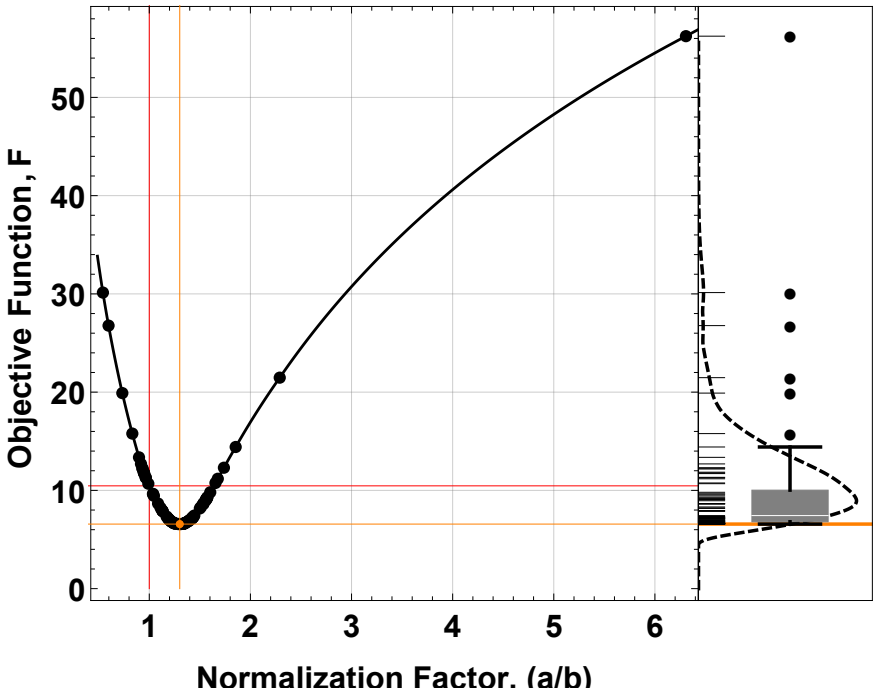

Figure 4.4: Minimization for scaling a simulation to the baseline values in a senstivity study. The red crossed lines indicates the value computed using default scaling factor (i.e. a/b = 1) and the orange crossed lines indicate the new minimized values for the sensitivity study with a change in mass of antimony-137. The line is a smooth curve showing the continuous values for a/b and the points indicate discrete options for normalizing to all the different isobars. The right-hand panel shows a density estimation for minimizing to the different isobars or the density of black points in the graph. This minimization was done with respect to the metric $F^{(R2)}$.

Chapter 5

Summary and Conclusion

SiRop has been designed to allow for a large range of scientific study ranging from theoretical astrophysics to experimental and theoretical nuclear physics. With that in mind, a portion of my thesis project involved small projects on high-energy astrophysics. The main result was the construction of a novel model for FRBs presented, but other applications to high-energy sites capable of hosting r-process nucleosynthesis will hopefully also make profitable use of SiRop for theoretical simulations. From the nuclear perspective, the opportunities for theoretical investigation of unmeasured nuclear properties is becoming especially important as a result of the increased availability of nuclear measurements of neutron-rich unstable isotopes which has increased in the last decade and will continue to increase as newer experimental facilities finish construction.

What is perhaps of particular importance going forward, is understanding how to analyse the data generated by SiRop. Current methods for determining global sensitivity estimates are currently an exciting new technique which has improved on the traditional r-process path identification, but they nevertheless have demonstrated some limitations which may need to be overcome for future investigation. The increased availability of theoretical data will be invaluable for generating high-quality statistics and will hopefully allow for more sophisticated statistical methods to be discovered and applied. Moving forward, however, the method for normalizing these global sensitivity I recommended should allow these types of statistical metrics to be more easily interpreted and compared across various studies from different simulations.

The proposed model for FRBs seems like an extraordinary opportunity for a new set of astronomical observational constraints in addition to the traditional r-process abundances derived from the solar abundance measurements. If the model can be shown to be the source for FRBs then we have not only provided a direct solution to an interesting new astrophysical phenomena, but also

provided a method for directly observing an astronomical due to the decay of elements from the r-process in other galaxies. Even if the model does not hold against further observational data, it provides an interesting example of how SiRop and the r-process in general can be used to expand astrophysical models in a non-traditional way. The r-process isotopes may be observable in other high-energy environments which could power some sort of observable light-curve. If any such observable decay of the r-process is ever detected, it would provide a means to directly measure or constrain isotope half-lives which might otherwise be impossible to generate and measure in a lab.

Regardless of the specialized area of interest, with regards to r-process simulations, SiRop has significantly enhanced from r-Java 2.0. The rich capabilities of the program provide an excellent tool for learning about and gaining a more complete understanding of the r-process and allows researchers a flexible r-process code. The program allows the r-process abundances measured in our solar system and the Galaxy as a method to be used a to validate and compare nuclear and astrophysical data and theory.

Bibliography

Aoki, W., Honda, S., Beers, T. C., & Sneden, C. 2003, ApJ, 586, 506

Arcones, A., & Bliss, J. 2014, Journal of Physics G Nuclear Physics, 41, 044005

Arcones, A., & Thielemann, F.-K. 2013, Journal of Physics G Nuclear Physics, 40, 013201

Audi, G., M., W., A. H., W., et al. 2012, Chinese Physics C, 36, 002

Brett, S., Bentley, I., Paul, N., Surman, R., & Aprahamian, A. 2012, European Physical Journal A, 48, 184

Burbidge, E. M., Burbidge, G. R., Fowler, W. A., & Hoyle, F. 1957, Reviews of Modern Physics, 29, 547

Caballero, O. L., McLaughlin, G. C., & Surman, R. 2012, The Astrophysical Journal, 745, 170

Cameron, A. G. W. 1957, AJ, 62, 9

Cescutti, G., François, P., & Matteucci, F. 2005, in IAU Symposium, Vol. 228, From Lithium to Uranium: Elemental Tracers of Early Cosmic Evolution, ed. V. Hill, P. Francois, & F. Primas, 445

Charignon, C., Kostka, M., Koning, N., Jaikumar, P., & Ouyed, R. 2011, A&A, 531, A79

Contopoulos, I., Kazanas, D., & Fendt, C. 1999, ApJ, 511, 351

Drago, A., Lavagno, A., Pagliara, G., & Pigato, D. 2015, arXiv:1509.02131

Falcke, H., & Rezzolla, L. 2014, A&A, 562, A137

Farouqi, K., Kratz, K.-L., Pfeiffer, B., et al. 2010, ApJ, 712, 1359

Flores, C. V., & Lugones, G. 2014, Classical and Quantum Gravity, 31, 155002

Fuller, J., & Ott, C. D. 2015, MNRAS, 450, L71

Geng, J. J., & Huang, Y. F. 2015, ApJ, 809, 24

Geng, J. J., Huang, Y. F., & Lu, T. 2015, ApJ, 804, 21

Gondek-Rosińska, D., Gourgoulhon, E., & Haensel, P. 2003, A&A, 412, 777

Goriely, S., Hilaire, S., & Koning, A. J. 2008, A&A, 487, 767

Goriely, S., Hilaire, S., & Koning, A. J. 2009, in American Institute of Physics Conference Series, Vol. 1090, American Institute of Physics Conference Series, ed. J. Jolie, A. Zilges, N. Warr, & A. Blazhev, 629

Iwazaki, A. 2005, Phys. Rev. D, 72, 114003

Jaikumar, P., Meyer, B. S., Otsuki, K., & Ouyed, R. 2007, A&A, 471, 227

Jessner, A., Lesch, H., & Kunzl, T. 2000, in Astronomical Society of the Pacific Conference Series, Vol. 202, IAU Colloq. 177: Pulsar Astronomy - 2000 and Beyond, ed. M. Kramer, N. Wex, & R. Wielebinski, 463

Keränen, P., Ouyed, R., & Jaikumar, P. 2005, ApJ, 618, 485

Knödlseder, J., Jean, P., Lonjou, V., et al. 2005, A&A, 441, 513

Kostka, M., Koning, N., Leahy, D., Ouyed, R., & Steffen, W. 2014a, Revista Mexicana de Astronoma y Astrofsica, 50, 167

Kostka, M., Koning, N., Shand, Z., Ouyed, R., & Jaikumar, P. 2014b, arXiv:1402.3824

Kostka, M., Koning, N., Shand, Z., Ouyed, R., & Jaikumar, P. 2014c, A&A, 568, A97

Krane, K. S., & Halliday, D. 1988, Introductory nuclear physics (Wiley)

Kroupa, P. 2001, MNRAS, 322, 231

Krücken, R. 2011, Contemporary Physics, 52, 101

Lang, K. R. 1999, Astrophysical formulae (Springer)

Lodders, K. 2003, ApJ, 591, 1220

Lorimer, D. R., Bailes, M., McLaughlin, M. A., Narkevic, D. J., & Crawford, F. 2007, Science, 318, 777

Lorimer, D. R., & Kramer, M. 2012, Handbook of Pulsar Astronomy (Cambridge University Press)

Lyubarsky, Y. 2014, MNRAS, 442, L9

Manchester, R. N., Hobbs, G. B., Teoh, A., & Hobbs, M. 2005, AJ, 129, 1993

Meyer, B. S., Mathews, G. J., Howard, W. M., Woosley, S. E., & Hoffman, R. D. 1992, ApJ, 399, 656

Michel, F. C. 1973, ApJ, 180, 207

Möller, P., Pfeiffer, B., & Kratz, K.-L. 2003, Phys. Rev. C, 67, 055802

Mumpower, M. R., McLaughlin, G. C., & Surman, R. 2012, Phys. Rev. C, 86, 035803

Mumpower, M. R., Surman, R., Fang, D.-L., et al. 2015, Phys. Rev. C, 92, 035807

Mumpower, M., Surman, R., McLaughlin, G., & Aprahamian, A. 2016, Progress in Particle and Nuclear Physics, 86, 86

Niebergal, B., Ouyed, R., & Leahy, D. 2006, ApJ, 646, L17

Niebergal, B., Ouyed, R., Negreiros, R., & Weber, F. 2010, Phys. Rev. D, 81, 043005

Olausen, S. A., & Kaspi, V. M. 2014, ApJS, 212, 6

Ouyed, R., Dey, J., & Dey, M. 2002, A&A, 390, L39

Ouyed, R., Koning, N., & Leahy, D. 2013, Research in Astronomy and Astrophysics, 13, 1463

Ouyed, R., & Leahy, D. 2009, ApJ, 696, 562

Ouyed, R., Niebergal, B., Dobler, W., & Leahy, D. 2006, ApJ, 653, 558

Ouyed, R., Niebergal, B., & Jaikumar, P. 2013, arXiv:1304.8048

Ouyed, R., Staff, J., & Jaikumar, P. 2011, The Astrophysical Journal, 729, 60

Pen, U.-L., & Connor, L. 2015, ApJ, 807, 179

Perego, A., Rosswog, S., Cabezón, R. M., et al. 2014, MNRAS, 443, 3134

Petroff, E., Bailes, M., Barr, E. D., et al. 2015, MNRAS, 447, 246

Popov, S. B., & Postnov, K. A. 2007, arXiv:0710.2006

Popov, S. B., & Postnov, K. A. 2013, arXiv:1307.4924

Qian, Y.-Z., & Wasserburg, G. J. 2003, ApJ, 588, 1099

Rauscher, T., & Thielemann, F.-K. 2001, Atomic Data and Nuclear Data Tables, 79, 47

Regimbau, T., & de Freitas Pacheco, J. A. 2001, A&A, 374, 182

Shand, Z., Ouyed, A., Koning, N., & Ouyed, R. 2016, Research in Astronomy and Astrophysics, 16, 011

Sneden, C., Cowan, J. J., & Gallino, R. 2008, Annual Review of Astronomy and Astrophysics, 46, 241

Sobiczewski, A., & Litvinov, Y. A. 2014, Phys. Rev. C, 90, 017302

Spitkovsky, A. 2006, ApJ, 648, L51

Staff, J. E., Ouyed, R., & Jaikumar, P. 2006, ApJ, 645, L145

Surman, R., Beun, J., McLaughlin, G. C., & Hix, W. R. 2009, Phys. Rev. C, 79, 045809

Surman, R., Mumpower, M., Cass, J., et al. 2014, in European Physical Journal Web of Conferences, Vol. 66, European Physical Journal Web of Conferences, 07024

Thornton, D., Stappers, B., Bailes, M., et al. 2013, Science, 341, 53

Totani, T. 2013, PASJ, 65, L12

Weidenspointner, G., Skinner, G. K., Jean, P., et al. 2008, New A Rev., 52, 454

Woosley, S. E., & Hoffman, R. D. 1992, ApJ, 395, 202

Zhang, B., Harding, A. K., & Muslimov, A. G. 2000, ApJ, 531, L135

Appendix A

Numerical Background and Prospects for Future Numerical Improvements

This historical development of SiRop and its predecessors has left an imprint in the numerical method used for solving the system of ODEs which is relevant for users and future developers of the code alike. In the first code, r-Java, the dynamical r-process simulation code used the WPA to determine the isotopic distribution on a per element basis and coupled these elemental isotopic chains together with the slow β-decays. This is numerically advantageous for two reasons: 1) the size of the system is much reduced by tracking only the hundred or so elements instead of the thousands of isotopes, and 2) the system is insulated from some of the stiffness of the problem by avoiding use of the neutron capture rates directly. The evolution of the code from this earliest version has lead to a porting over of the numerical integration scheme and the method for accounting for available neutrons.

The code makes use of implicit tracking of neutrons through baryon conservation. Since the mass fraction is normalized, the number of free neutrons in the system can be calculated by subtracting the mass fractions of all other species from 1. This method for computing neutron mass fraction was inherited in the following version, r-Java 2.0. By excluding neutrons from explicitly being represented as a species in the reactions we maintain a high level of sparsity and low bandwidth in the reaction matrix used to evolve the system in time. Computationally this allows for the use of much faster sparse matrix algorithms and eliminates a large potential for rounding errors to creep into the system. As a result the current version has been optimized to run quickly, with hopefully small numerical errors, and is required, by design, to always conserve baryons. As a result of the neutron capture centric design of the code, it has become resistant to large-scale addition of more complex interactions (e.g. charged particle reactions) without significant code

modifications and redesign of the stabilization scheme for the newly added non-linearities in the differential equations.

Due to the stiffness and non-linearity of the coupled system of ODEs, numerical schemes for solving or evolving the system in time requires careful selection and testing. Explicit methods, like the famous RK4 scheme, are generally inappropriate and we are forced to make use of implicit schemes to integrate between time steps. As a result, we are immediately saddled with a class of methods which are less-precise due to the need for accurate, stabilized methods. The methods available to solve stiff problems come with the added burden of the slowness inherent to numerical matrix arithmetic. A large class of co-called "A-stable methods" are available for stiff problems. r-Java has made effective use of the a linearisation of the ODE integrated using the semi-implicit trapezoidal method (i.e. Crank-Nicholson applied to an ODE) which is the highest order and highest precision implicit linear multi-step method possible (see Second Dalquist barrier (Dalquist 1963)). Without making use of an embedded higher order technique, which would be capable of providing a formal estimate of its own truncation error, implicit ODE solvers must include some form of adaptive step-size control (e.g. see Fig. 6 in Kostka et al. 2014 nuclear) which ensures accuracy of the solution.

In our case, it is likely that we have an over-conservative step controller; however, it is very difficult to generate more efficient schemes given the possibility for different nuclear model inputs. Due to the early adoption of Crank-Nicholson integration scheme any further extensions to the code's repertoire of nuclear reactions using this method will require creation and testing of a new step-size controller able to monitor the linearisation of additional reactions. This does, however, offer the potential for a more efficient choice of either step-size controller or implementation of a more sophisticated higher-order embedded ODE solver. Higher-order L-stable or B-stable methods which contain embedded strategies for time step selection (or even order selection) seem to present the best hope for improvements. Preliminary work on the subject suggests that any new integrator must be carefully tested and compared to the current version of the code to en-

sure any new method remains stable and is not overcome by numerical errors. Future work to optimize or extend the code is far from a trivial task, but it may be required if auxiliary reactions (e.g. charged particle reactions) become a critical component of simulating r-process abundances or if large numbers of simulations are required to produce high-quality statistics (e.g. Monte-Carlo parameter estimation).

Evaluation of the ODE in time produces the following time discretisation scheme for the ODE (for more details see)):

$$\frac{d\vec{Y}}{dt} = \frac{\vec{Y}^{n+1} - \vec{Y}^{n}}{\Delta t} = \frac{1}{2}\left[\overleftrightarrow{R}^{n+1} \cdot \vec{Y}^{n+1} + \overleftrightarrow{R}^{n} \cdot \vec{Y}^{n}\right] \tag{A.1}$$

where Y is the isotopic abundance at the nth discrete time point and $\overleftrightarrow{R}$ is rate matrix. Strictly speaking the decomposition of the time derivative into a matrix-vector makes no mathematical assumptions about the linearity and the rate matrix, in general, depends on the isotopic abundances. The linearisation occurs when we re-write the update formula in the common $Ax = b$ form as:

$$\left[\overleftrightarrow{I} - \frac{\Delta t}{2}\overleftrightarrow{R}^{n}\right] \cdot \vec{Y}^{n+1} = \vec{Y}^{n} + \frac{\Delta t}{2}\overleftrightarrow{R}^{n} \cdot \vec{Y}^{n} \tag{A.2}$$

where we exclude neutrons as an explicitly evolved species and assume the rate matrix does not change between time steps (implicitly requiring the neutron number density and temperature to remain roughly constant). Written in this form, the problem is reduced to solving for $\vec{Y}^{n+1}$ each at each time step, followed by verification that the new state has not evolved too much for our linearisation to be valid (e.g. make sure the neutron density has remained roughly constant). We compare this method to the explicit Euler and implicit Euler with linearisation which give the following update methods:

$$\vec{Y}^{n+1} = \vec{Y}^{n} + \Delta t \frac{d\vec{Y}}{dt} \tag{A.3}$$

$$\vec{Y}^{n+1} = \vec{Y}^{n} + \Delta t \left[I - \Delta t J\right]^{-1} \cdot \frac{d\vec{Y}}{dt} \tag{A.4}$$

$$\vec{Y}^{n+1} = \vec{Y}^{n} + \Delta t \left[I - \frac{\Delta t}{2} J\right]^{-1} \cdot \frac{d\vec{Y}}{dt} \tag{A.5}$$

which are the forward Euler, backward Euler and semi-implicit Euler method respectively, where J is the Jacobian matrix. The forward Euler method is typically considered a poor method due to its low order and the ease of constructing stable and accurate higher order methods. In contrast, the use of low-order implicit methods is common due to the fact that higher order implicit methods are much more difficult to formulate due to the strict stability requirements. These methods are usually difficult to code and are typically computationally expensive when executed. This makes their application to non-linear problems somewhat problematic for the pragmatic reason that the effort involved in writing and testing these methods is very time consuming and not guaranteed to be suitable for the nuances involved in a particular non-linear ODE.

Appendix B

SiRop Manual

The following included document is a copy of the user's manual written for SiRop. It is designed to list the program features and explain how to execute the program for r-process simulations and sensitivity studies.

UNIVERSITY OF CALGARY

SiRop Manual

A User's Guide to Using the r-process code SiRop

Zachary Shand

2016-09-01

SIROP MANUAL

A USER'S GUIDE FOR USING THE R-PROCESS CODE SIROP

CONTENTS

PREFACE

This document is meant to provide a starting place for those interested in using SiRop for running r-process simulations. SiRop is an evolution of an earlier r-process code which was developed specifically to perform sensitivity studies. In other words, we wanted a program that we could use to run automated or "script-like" execution of code. This involved a complete re-work of the user interface an addition of code to perform automated queueing, execution and analysis of r-process simulations. This manual will, as a result, be focused on the modules for sensitivity studies, but will also include a description of how to use the code for r-process simulations in general. Supplementary descriptions for the behavior of this program can be found in the two papers Kostka et al. 2014a and Kostka et al. 2014b along with the r-Java 2.0 manual available at www.quarknova.ca/rJava since it and SiRop are built on the same underlying code base.

INTRODUCTION

The r-process, or rapid neutron capture process, is the astrophysical process which is responsible for producing some of the elements we see in the Galaxy today. Due to the shape of the nuclear binding energy curve and the high coulomb repulsion of heavy nuclei elements heavier than iron or nickel cannot be produced through regular burning phases inside of a star. Elements beyond the iron group are then assumed to be mainly produced by neutron capture processes. The r-process is one such nucleosynthesis mechanism which involves nuclear reactions in some sort of neutron rich environment where isotopes are converted into heavier and heavier isotopes through a sequence of neutron captures and beta-decays. This means the isotopes involved in simulating the r-process are frequently unmeasured and in many instances theoretical calculations must be used to supplement the existing nuclear (see Figure 1). For this reason it is of interest both on purely theoretical grounds and for planning of nuclear experiments to understand what isotopes are most important to the r-process.

Nuclear sensitivity studies are a way of understanding the role of individual isotopes and their physical characteristics like mass or half-live. When we perform a sensitivity study what we're doing is taking a set of nuclear inputs, running a simulation with these parameters and then comparing these base results to the results of simulations where we have changed a small number of inputs. Statistical analysis of this can then provide a quantitative value to the changes to the final results of a simulation of an r-process site. We could, for example, vary the masses of all unmeasured isotopes that are accessible to an experimental facility to identify more important candidates for measurement (at least most important to the r-process). Alternatively, currently measured properties of isotopes could be varied within their experimental uncertainty to test whether current measurement uncertainties are low enough to provide no measureable change to the r-process simulated results. SiRop is designed to assist in answering these questions and has a flexible design and user interface which allows for a large range studies to be performed.

Simulating this process in various different astrophysical environments requires solving differential equations numerically and this is the heart of what an r-process code like SiRop does. The details are beyond the scope of this manual and is beyond what a user needs to know, but there are a couple main features to keep in mind when running SiRop. The ordinary differential equation (ODE) SiRop solves can be written simply by listing all of the nuclear processes which transmute an isotope as follows

$$\frac{dY_i}{dt} = \sum processes\ which\ create\ Y_i - \sum processes\ which\ destroy\ Y_i\,,$$

where Y_i is the abundance (or total number) of a single isotopic species. For example, a neutron capture process of iron-56 "destroys" iron-56 and creates iron-57 and so the reaction rate is

added to two pairs of coupled isotopic rate of change. So if we were only considering neutron capture, neutron photo-dissociation and beta-decay reactions the ODE for a single isotope, say tin-132 would look like the following

$$\frac{dY_{132Sn}}{dt} = n_n\langle\sigma v\rangle Y_{131Sn} + \lambda_\gamma Y_{133Sn} + \frac{\ln 2}{T_{1/2}} Y_{132In} - n_n\langle\sigma v\rangle Y_{132Sn} - \lambda_\gamma Y_{132Sn} - \frac{\ln 2}{T_{1/2}} Y_{132Sn}$$

where n_n is the neutron number density, $\langle\sigma v\rangle$ is the thermally averaged cross-section, λ_γ is the neutron photo-dissociation rate, $T_{1/2}$ is the beta-decay half-life and Y_X is the abundance of isotope X as indicated. Each nuclear property is that of the multiplied isotope abundance, so, for example, in the term $n_n\langle\sigma v\rangle Y_{131Sn}$, $\langle\sigma v\rangle$ is the thermally averaged cross-section of tin-131. (For a more thorough discussion see, for example, the overview provided in Hix and Thielemann 1999.) The reason for writing this out explicitly is to highlight a critical assumption used in SiRop where each nuclear quantity is assumed to be a true constant taken from a lookup table. In reality, for any parameter which has been determined theoretically using some form of nuclear model the reality is that these values are functions of the parameters used in the nuclear model. So for example, if we computed the half-lives using Fermi's Golden rule, we could right the decay rate as a function of the matrix elements, nuclear charge, and nuclear decay energy $\lambda_\beta(W_{np}, Z, Q_\beta)$ but any modification to the underlying parameters (e.g. mass) in a sensitivity study would not capture the change to the decay rate which should, in principle, be accounted for. Ideally, a code would encapsulate a model for all aspects of the r-process and include a full astrophysical explosion model and a full quantum mechanical model for nuclear parameters. Such a code would be an enormous undertaking, to say the least.

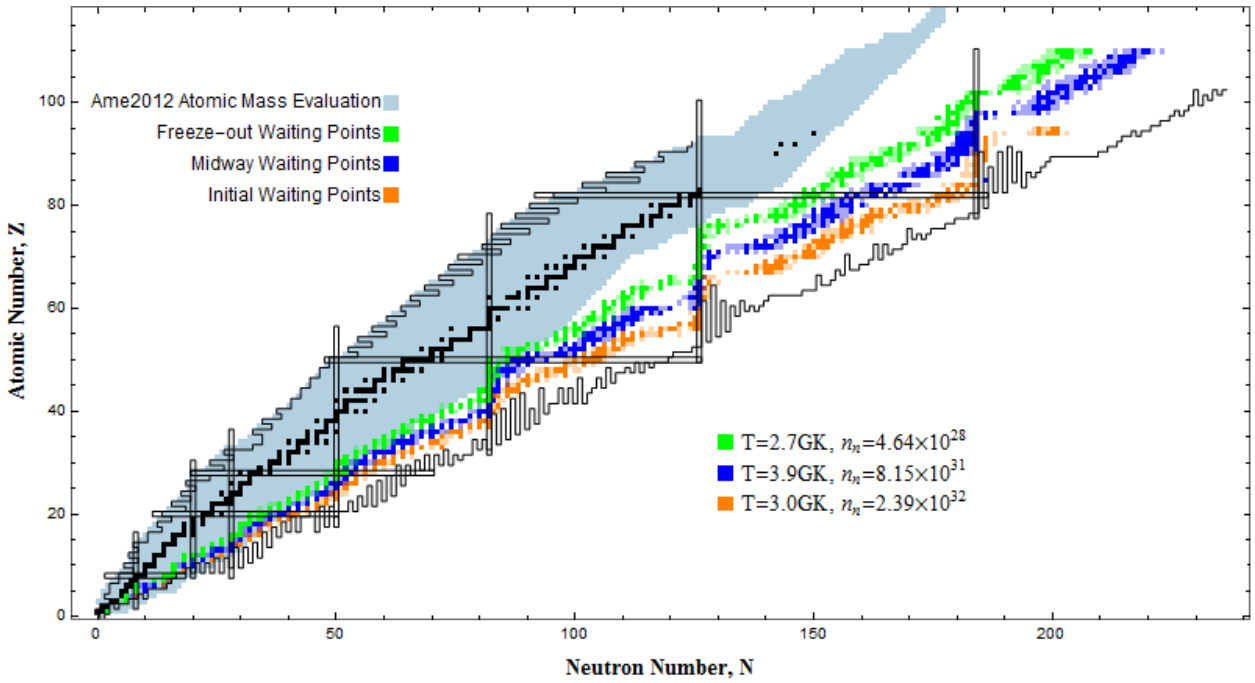

Figure 1 Chart of nuclides displaying (in blue) the isotopes with measured masses as indicated in the 2012 Atomic Mass Evaluation along with theoretical r-process paths (in green, blue and orange). The black squares indicate stable isotopes and the naturally occurring actinides. The jagged black lines are the proton drip line (experimental) and the neutron drip (HFB21 theoretical) and the black rectangles indicate the nuclear magic numbers.

SIROP BASICS

SiRop provides the user with a Graphical User Interface (GUI) as opposed to a command line interface. In addition to providing a more user-friendly experience, this allows the code to provide immediate graphical feedback during execution of the code. The program groups different functionality into different modules available as different tabs or pages in the program (each can be opened as its own window which is useful in multi-monitor environments). The modules available are as follows:

Desktop: Home page, provides access to other modules.
Code: Holds parameters for running the code (e.g. initial density and temperature).
Data: Table of all nuclear inputs. Allows for importing and single cell editing.
Chart: Allows user to create useful graphs which are updated as code runs.
Sensitivity: Allows for setting up complex sensitivity studies.
3D: Presents a 3D real-time graph of the abundances on a chart of nuclides like visualization.
Messages: Displays messages during code execution and other information.
R-Path: Uses input nuclear parameters to explore the r-process path.

In addition to the modules, the program has a top and bottom ribbon which offers quick access to the different modules at the top of the window, includes a button for un-docking the individual modules into their own windows (top right) and in the bottom left provides a progress bar which indicates the execution state of the program along with an “x” icon which can be used to terminate in-progress dynamic r-process simulations.

DESKTOP

The Desktop page is displayed after the program has finished loading after being opened. The Desktop lists all modules which can be opened from the Desktop page or from the top bar of the program. These icons can be attached (by dragging and dropping individual icons from the desktop page) to the top hot-bar for easy access from other pages in the application (see Figure 2 for a screenshot). In order to execute an r-process simulation (after setting up all the initial conditions) the Calculate command (orange maple leaf) can be pressed. Additionally, the state of the program can be saved as projects. This can be done by pressing the Save or Save As icons. This allows you to setup a complex set of parameters and perhaps defer execution until later or save results in the program for re-opening later. Any saved projects should appear in the Recent Projects section of the desktop, but can also be found at the location you saved the project to using the Open button. (The program cannot be saved mid-execution and any running calculations must be terminated before saving).

Figure 2 SiRop Desktop screen where from which the different program modules can be accessed.

CODE

The Code module exposes different methods for computing nuclear abundances and all of the relevant parameters (with the exception of the values for the nuclear inputs). The left hand panel contains a queue of Operations or calculations to be chained during execution of the code. (This is mainly to allow for nuclear statistical equilibrium (NSE) to be used as an initial condition.) See Figure 3 for a screenshot. The options here are:

r-Process: Sets up the initial conditions for a dynamic r-process calculation.
NSE: Runs a (static) calculation to determine the abundances using the equations for nuclear statistical equilibrium. This can be executed on its own as a stand-alone calculation or it can be used as initial conditions for an r-process calculation by listing it immediately before an r-process calculation in the Operations sub-panel.
Fission: Calculates the fission yields as they are calculated in the code when full fission is selected. Uses fission barrier widths and heights along with a neutron energy to calculate the probability distribution following fission. See the r-Java 2.0 manual for more details (available at www.quarknova.ca) or the Kostka et al. 2014b paper on r-Java 2.0.
Reset: This is executed once at the beginning of the Calculate command by default and copies the initial mass fractions listed in the data table to the active mass fractions to be

used as initial conditions (i.e. set the initial seed nuclei). Normal usage of the code won't normally require this to be added manually.

Waiting Point Rates: Calculates and displays to the message module calculated results for the r-process path calculated based on the rates instead of the classical waiting point approximation (see later section for more details).

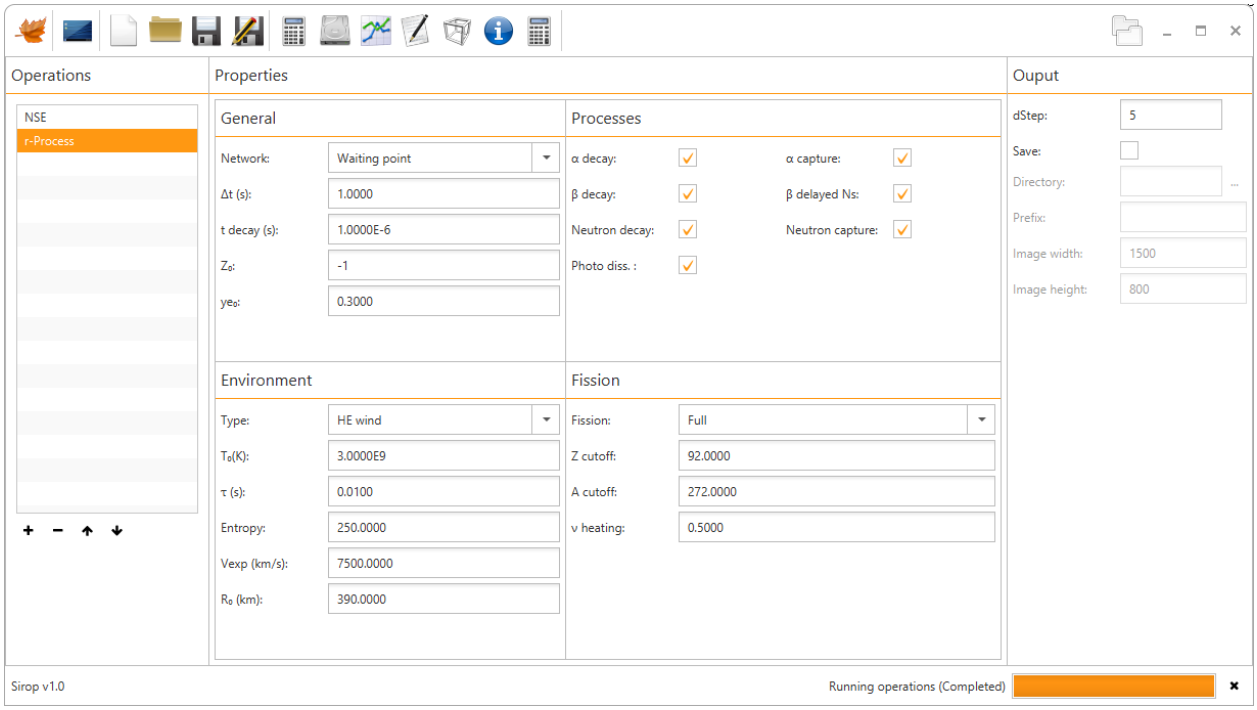

Figure 3 Code module where the different parameters can be set for running the different calculations and simulations available in SiRop.

These different calculations can be added to the Operations queue by clicking on the plus icon at the bottom of the window on the left. Similarly, operations added can be removed by selecting them (by clicking on them with the cursor) and pressing the minus button. The order of operations can be changed by selecting an added operation and pressing the up or down arrows.

The main (central) portion of the window presents different options based on the selected Operation. The r-Process operation options include temperature and density evolution parameters, lists of nuclear reactions to include, fission parameters and the option to be run using the full rate equation or using the Waiting Point Approximation (WPA). For NSE operation the options are density, temperature and electron fraction. The Fission operation lists standard channel I and II barrier heights and widths in addition to incident neutron energy. The Reset operation has no options. The Waiting Point Rates operation requires temperature, neutron number density and elemental bounds (minimum and maximum Z). In most cases the default

values are what you might want to try and start with until you're more familiar with the program.

The right hand panel has a few options relevant to dynamic calculations. The dStep option controls the number of steps in between GUI update events which refresh the charts with current data from the simulation. The save checkbox indicates whether the data should be saved to a directory in files to catalogue the evolution of the simulation data. When enabled, the data will be output to the specified directory with the supplied prefix and images will be generated at the specified size. The program will output these files (if enabled) at every update step.

DATA

All nuclear inputs are summarized in this (large) table of values. By default, no data exists and all relevant data must be imported. By default, however, some preset values can be imported. These values include the masses, neutron cross sections and photo-dissociation rates from the HFB21 mass model in addition to the neutron induced fission rates calculated using the HFB14 mass model (available at www.astro.ulb.ac.be/bruslib) and the beta-decay half-lives and beta-delayed neutron emission probabilities calculated using the FRDM mass model (see Möller et al. 2003). If custom data is to be imported, each category must be imported from a file individually starting with a file containing all isotopes to be listed in the network. Each category can be imported by right clicking the table header (grouped by color) and clicking import in the context menu which appears. A wizard with a preview of the results of the importer will appear.

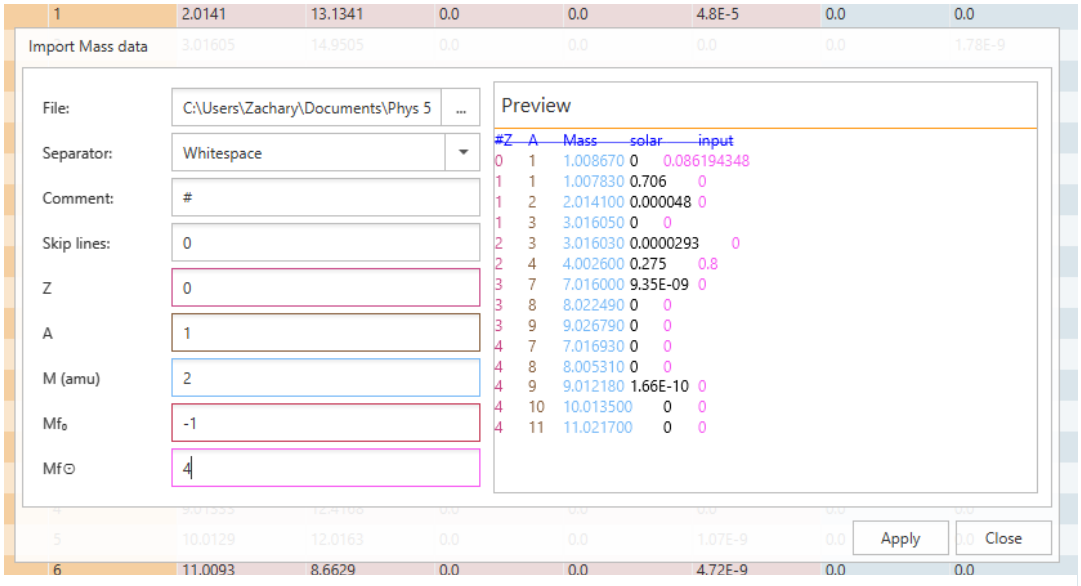

Figure 4 Import wizard which opens a file and has partially selected columns of a sample data file shown.

The importer (and data file in turn) requires text based tabular data organized in rows. In each category, the atomic number (Z) and atomic mass (A) must be included. Each category requires the user to specify a file to parse, the separating characters (spaces, tabs, commas, or generic whitespace), any comment characters (which must be at the beginning of a line) and any number of lines to skip. After these options, the columns of the required data must be specified (the column indexing scheme is zero based so 0 is column 1) where a value of -1 indicates that the column will be skipped during this import (except Z and A MUST be provided). This allows for data in one category in the code could be imported from multiple files. After entering a column number the preview pane should highlight the column in the same colour outlining column input box. A screenshot of a partially complete mass import can be seen in Figure 4.

The temperature dependent cross-sections and rates follow a similar import process, but due to the requirement for indicating the temperature grid points where the values were calculated the import process is slightly more complicated. The file these values are being imported from needs a row which indicates the temperatures which begins with “T9” and has all the temperatures (these temperatures must be given in units of GK). This row must be indicated to the importer and the first column of rate/cross-section data must be listed. An example of a valid text file format is in Table 1. If you are only interested in importing a single property (for e.g. half-lives) then the default values can be exported and re-imported or the default values can be simply overwritten by importing the values after a “Reset” to the default values.

T9	0.1	1	10	
#Z	A			
56	70	Value at T=0.1	Value at T=1	Value at T=10
56	71	Value at T=0.1	Value at T=1	Value at T=10

Table 1 Schematic example of a file structure for importing temperature dependent cross sections or rates.

CHART

The charting module is rather simple and automatically sets some appropriate defaults. The graphs which SiRop can generate are and abundance vs mass number graph, a color coded Z vs A vs Abundance graph, and a [density, temperature, electron fraction, neutron number density] vs. time graph (where any or all of these values may be plotted on a graph vs time). These are the Isotope Graph, Chart of Nuclides and Time Dependent Graphs which are available to add by

clicking the plus sign in the top left corner next to the tab names. Several graphs can be generated and are available in different tabs. An important thing to note about the X vs time graphs is that they only plot points during update steps (as set in the code panel) and so if these quantities are of interest the graph must be added before running the code as this data cannot be plotted retroactively. A sample graph from midway through an r-process calculation is shown in Figure 5.

The values in these graphs are updated at each update step so the state of the program can be monitored. This is especially useful for those new to running r-process simulations or for trying to setup initial conditions with a specific goal in mind. At any time during the program (although updates will interrupt this if they are set to rapid intervals) a right click on the graphs will bring up a context menu which allows the user to change plotting options or save the data points which are plotted.

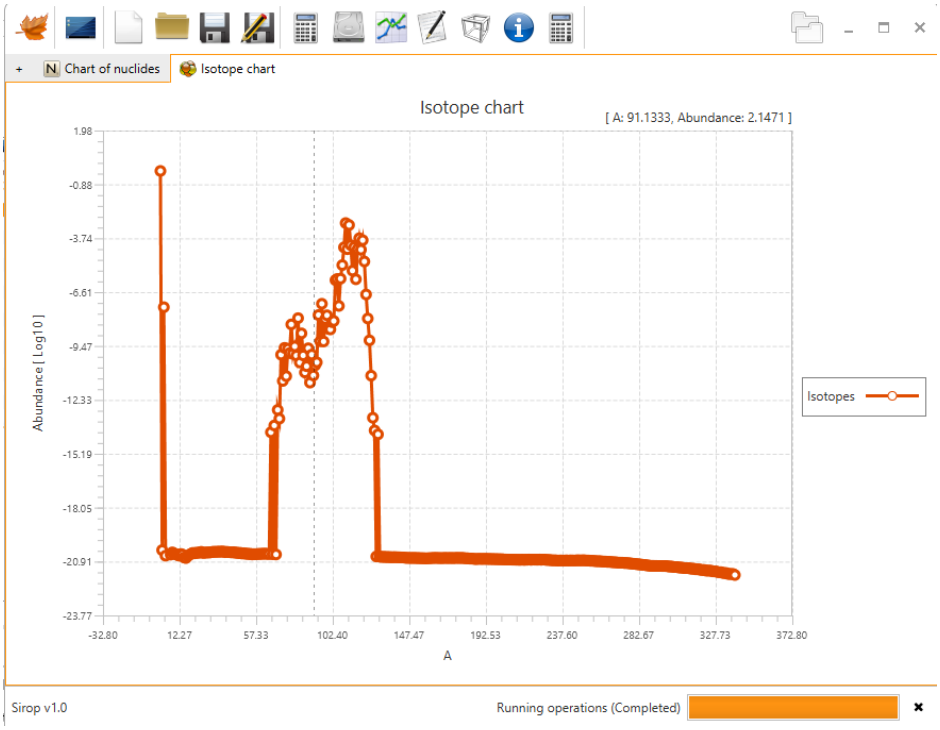

Figure 5 Abundance vs Mass graph partway through a NS merger r-process simulation.

SENSITIVITY

This module contains a Setup and Results page. This module allows for setting up complex sensitivity study parameters before executing a sequence of simulations in batch followed by statistical analysis of the data. This module mainly consists of a user interface designed to set up many Operations which are groups of changes to the nuclear parameters which will be used

during the batch execution of the code. For more details see the section below “Running a Sensitivity Study.”

3D

Displays a 3D chart of nuclides-like graph. The plot shows a color coded graph of the abundances on a log-scale which is updated along with the charts in the Chart module during update steps as set in the Code module.

MESSAGES

The messages module displays text based output from the code during its execution. The data here is typically available in graphical form through the various charts available or through the automatic file output created through the code module. Nevertheless, this can be a good place to find information about the code. In addition, if any errors do occur during the execution of the code they will be pushed to this module. Under normal execution this should not be a problem, however, should this occur this can offer the development team information which can assist in troubleshooting and correction of the problem.

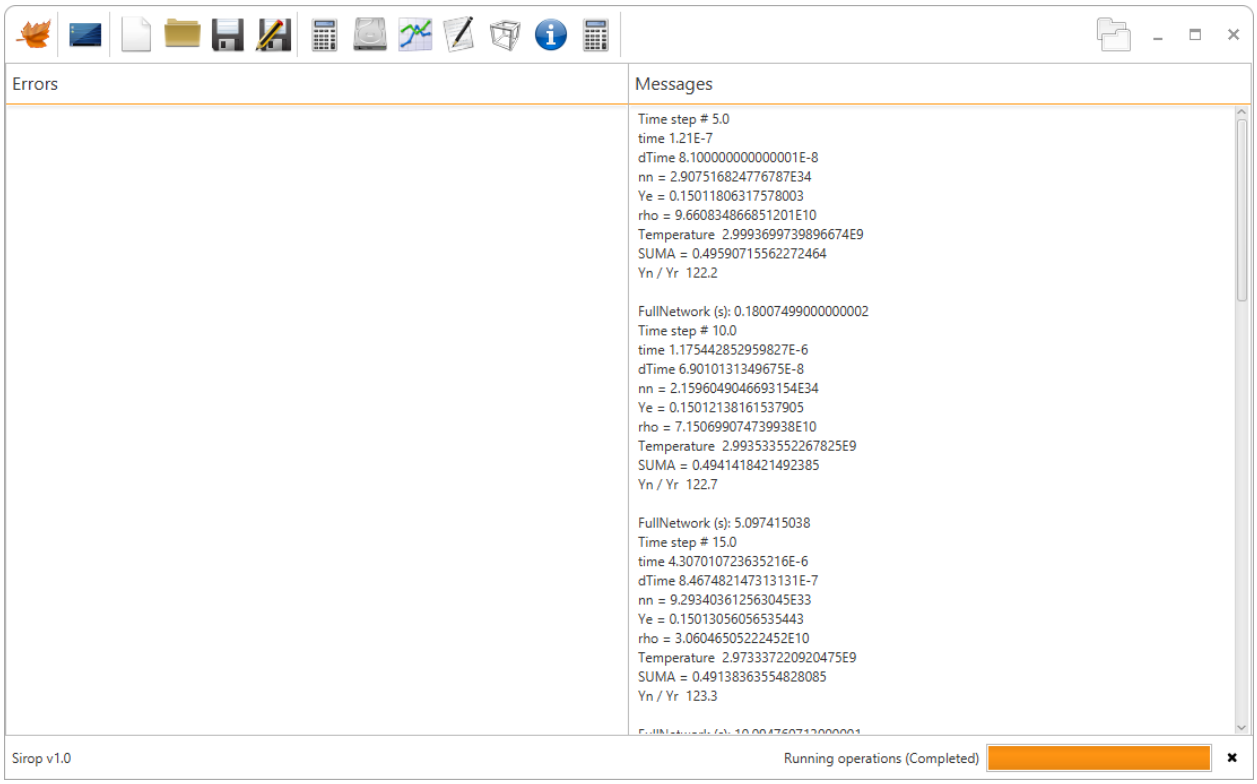

Figure 6 Screen capture of the output in the Messages module during an r-process simulation.

R-PATH

This module is an entirely new addition to SiRop and has been added to assist in understanding the r-process using computationally cheap methods to estimate the isotopes of importance by calculating and plotting the r-process path. This is done using three different methods and all three are plotted together. Each method requires temperature and neutron number density as inputs and so require knowledge of these parameters during a particular r-process environment (which could be found using the data from an execution of the code which lists these values during the simulation).

The first is calculated using the classical WPA which produces population coefficients. Isotopes with population coefficients above 10% are plotted and outline the r-process path which is relevant at high temperatures (above about 1GK). The second is a bracketing method of sorts which identifies the transition regimes where the rates switch from being dominated by neutron capture rates, to beta-decay dominated to photo-dissociation dominated. These boundaries are calculated using the explicit rates and cross sections provided to the program in the Data module. Instances where the classical WPA and this method do not overlap indicate regimes where the WPA fails. The third method is a random walk computed with the cross sections and rates in the Data module. This method is not quite as cheap as the first two, but provides a “dynamic” method for determining the isotopes which will be involved in the r-process. An example of the graph from the Rates module is shown in Figure 7Figure 6.

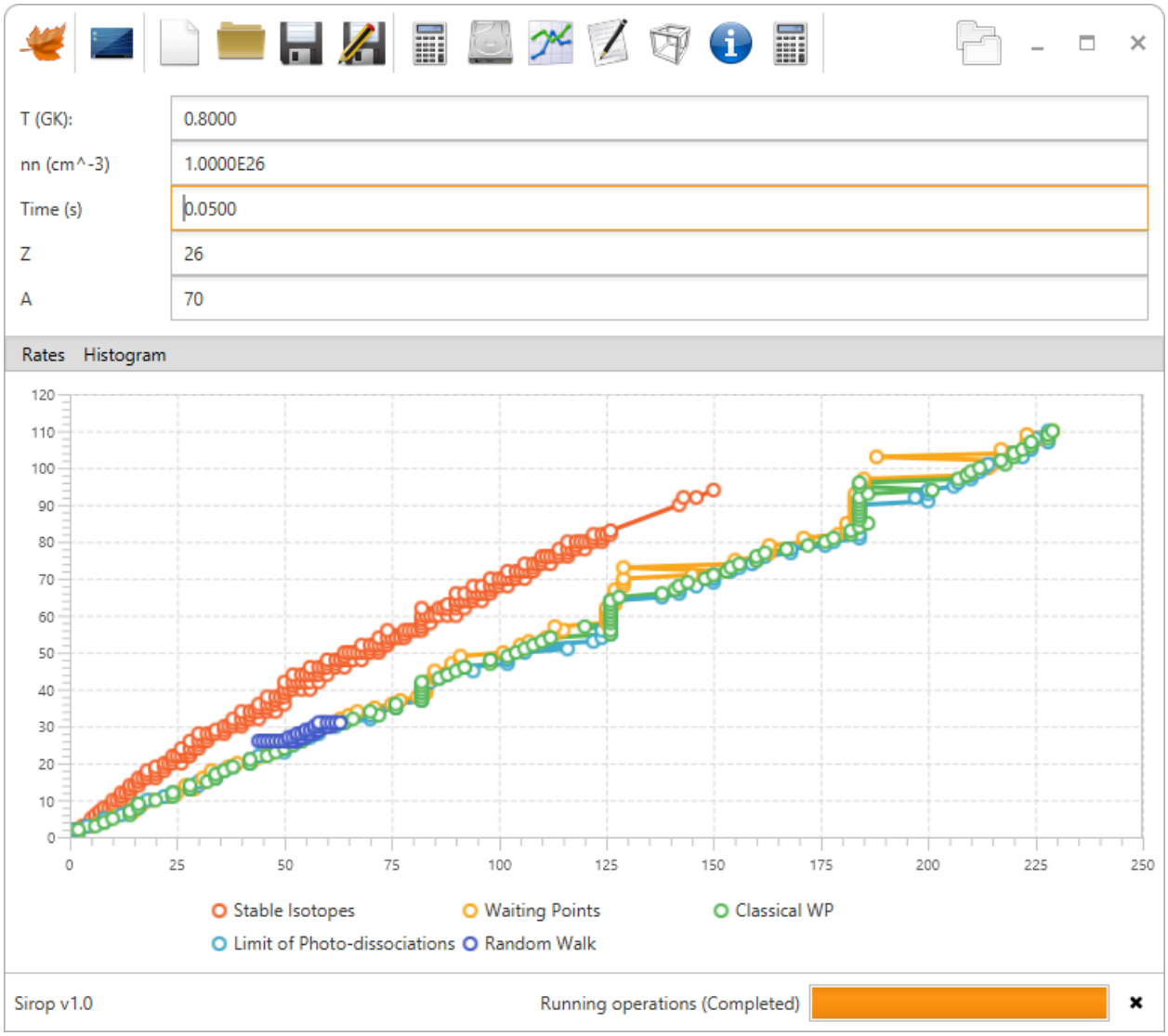

Figure 7 Graphs showing a sample of the calculated r-process paths in the Rates module using iron-70 as a test isotope. The graphs shows the average path such an isotope would spend over 0.05 seconds.

PROGRAM USAGE: R-PROCESS SIMULATIONS

SiRop was built on r-Java 2.0 so can continue to be used as an r-process code in the same fashion. It is recommended that a user interested in using SiRop for sensitivity studies be familiar with running the program for non-batch execution to because the sensitivity module simply runs the program in serial with varied parameters as indicated by the setup in the Sensitivity module. When beginning an r-process simulation it is important to identify the initial conditions for the astrophysical site to be used. This includes identifying the initial temperature and density, the parametric evolution for the density to be used during the evolution of the r-process, and the initial nuclear composition and neutron richness. All these quantities should be based on reference material indicating the conditions using some sort of astrophysical model. As a reference we will outline some salient features of a few popular r-process models.

OVERVIEW OF POPULAR R-PROCESS SITES

SiRop comes with some built-in models for the density and temperature evolution of come r-process sites. A screen-shot of the selection menu is available in Figure 8 and each option is discussed in detail below. Some order or magnitude estimates for these values are also presented to assist those less familiar with these parameters and r-process codes.

HIGH-ENTROPY WINDS OF CORE-COLLAPSE SUPERNOVAE

Supernovae are arguable the oldest and most extensively studies r-process site and it continues as an active are of research to determine the nucleosynthetic yield of these environments. The nucleosynthesis occurs in a low density environment between the proto-neutron star and the outer supernova ejecta. Here, the predicted high temperatures lead to complete dissociation of elements from the iron core into constituent neutrons and protons. The high-entropy descriptor or requirement comes was introduced when original hydrodynamic parameters failed to lead to r-process elements being formed. It was found that an increase in the predicted entropy could lead to successful fusion of the free protons and neutrons into heavy seed nuclei while still retaining a high number of free neutrons for the remainder of the main r-process in the supernova model. These seed nuclei are formed by helium or alpha particle fusion into heavier and heavier isotopes where a large majority of the material is converted into inert (with respect to neutron capture) helium-4. Consequently this environment is sometimes referred to as an alpha-rich freeze-out (e.g. Woosley and Hoffman 1992). Additionally, the assumption of high-entropy provides a simplifying assumption about the density and temperature evolutions which is attractively simple as it is a simple polynomial function (or almost polynomial in the HEW model of Farouqi et al. 2010 provided in SiRop).

Some rough order of magnitude estimates for the physical initial conditions (at the onset of the r-process) for this scenario put the density at around 10^5 g cm^{-3}, temperatures around 3 GK, and neutron number densities with a large range from about 10^{22} cm^{-3} to 10^{26} cm^{-3} depending on physical parameters (e.g. entropy) employed in the charged particle reaction phase of the model. Because SiRop is purely an r-process code, initial seed compositions and neutron richness or neutron to seed ratios must be taken from sources which have computed these values (see Woosley and Hoffman 1992 for an example of suitable tabulated data).

NEUTRON STAR MERGERS

Neutron star (NS) mergers provide an obvious mechanism for providing free neutrons and seed nuclei through the ejection of the outer crust of a neutron star. The surface crust of a neutron star is expected to be composed of heavy neutron rich isotopes in NSE which provides the seed isotopes which can capture the neutrons ejected along with this outer crust. The merger types can be between two NS (NS-NS) or a NS and a black hole (BH) (NS-BH). The expansion of the ejected material can be modelled in SiRop as an expanding polytope whose details can be found in the paper “r-Java 2.0: the Astrophysics” (Kostka et al. 2014). The initial densities and temperatures should be around 10^{11} g cm^{-3} to 10^{14} g cm^{-3} and around 1 GK to 3 GK. The corresponding neutron number densities are also quite high at around 10^{34} cm^{-3}. The initial nuclear composition are frequently found using NSE which for low electron fraction parameters predicts a very strong r-process.

QUARK NOVAE

The third site which has pre-set hydrodynamic properties included in SiRop is a Quark Nova (QN). A QN is the explosion of a NS due to a phase transition from hadronic to free quark matter. The phase change and resulting quark deconfinement is theoretically expected to release an enormous amount of energy which can eject an outer layer of the neutron star at relativistic speeds. This scenario has similar initial conditions as a NS merger scenario in terms of initial temperatures, densities and nuclear composition, but has a different evolution in time. The presets in the code list physical parameters of the parent NS in addition to a parameter, zeta, which determines the predicted fraction (In percent) of the energy transferred to the QN ejecta (around 1% is typical).

GENERIC ASTROPHYSICAL ENVIRONMENT

In addition to pre-canned astrophysical models above, there is an option to simply model a generic site’s density as a simple function (usually a polynomial in time). This is Custom environment and it can be used with initial conditions similar to the above sites (in terms of

temperature, density and implied neutron number density) for expansions which do not fit exactly with the other available defaults.

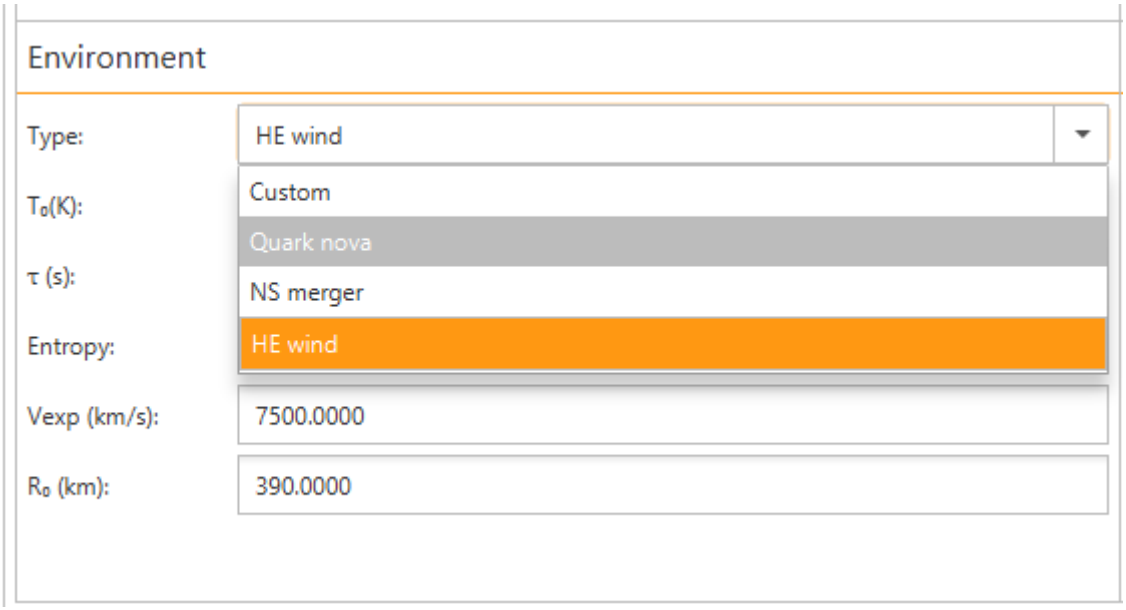

Figure 8 A screen capture of the area in the Code module with an r-process calculation selected in the Operations queue which shows the different astrophysical models available.

EXECUTING THE CODE

Once the initial conditions have been set for the site and the desired nuclear parameters have been loaded into the program the settings for the r-process need to be chosen. There are two modes for running dynamic simulations: Full or Waiting Point. The Waiting Point option evolves the r-process in the WPA and is generally an outdated method. It is nevertheless an option and can be useful when you want to run a fast simulations (as the WPA is much faster as an analytic approximation to the full set of rate equations) to understand the initial conditions used or when only masses have been changed without correlations to other nuclear inputs.

The Full options runs the simulation using the full set coupled ODEs which includes only the nuclear processes available and selected in the code. SiRop includes the following nuclear reactions: neutron capture, neutron photo-dissociation, beta-decay, beta-delayed neutron emission, alpha decay, fission (spontaneous, beta-delayed and neutron induced) in addition to a rudimentary alpha capture chain (He-C-O-Ne). Any or all of these options can be turned off in the panel shown in Figure 9 (although turning off neutron capture or beta-decay don't normally make sense to disable). There are some additional options for fission which allow for fission to be turned off (None), to use a fully symmetric fission model which fission isotopes which exceed a mass and charge cutoff (Cutoff), or a non-symmetric fission model which produces a

distribution of isotopes following fission events. Unless the role of a particular reaction is under study, it is generally advised to leave all nuclear processes on.

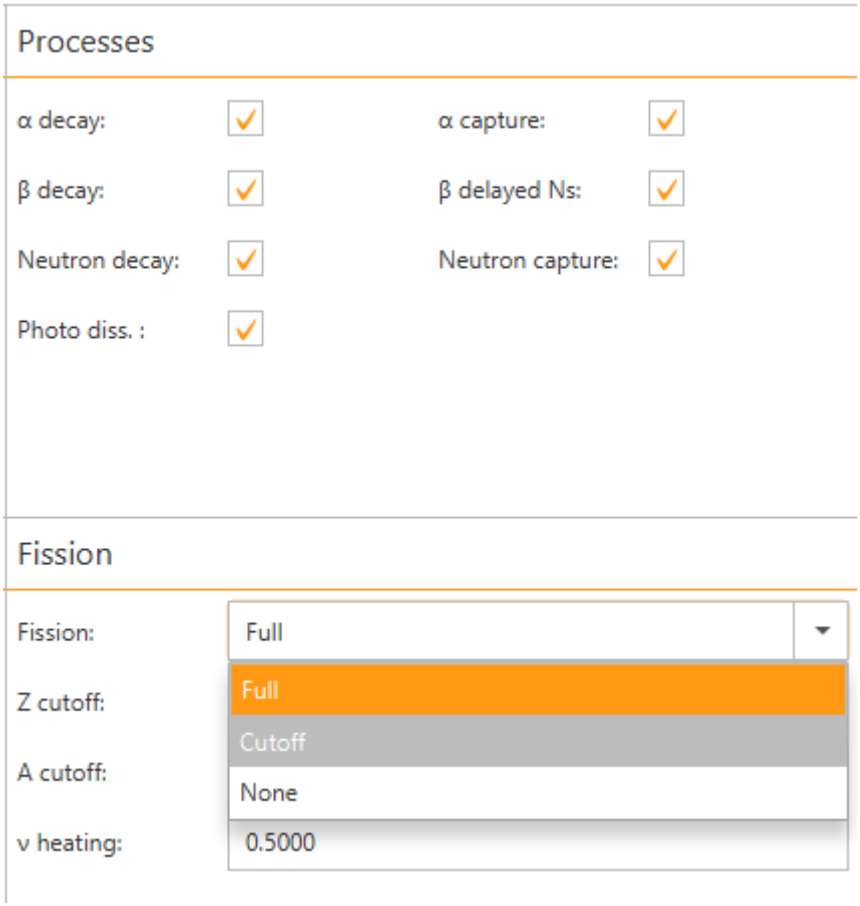

Figure 9 Panel available after selecting an r-process calculation in the Code module. The different nuclear reactions can be turned off by clicking the checkboxes.

Regardless of the mode selected (Full or Waiting Point) the program, upon execution, will run until the simulated time has exceeded the listed time (Δt) or the available neutrons have dropped below a threshold. The internal cutoff occurs when the neutron to seed ratio drops below 1.0 at which point the program will terminate the r-process simulation. Once the r-process is complete, the program will run the nuclear decay reactions for the specified amount of in simulation time (t decay) or until the program determines that stable isotopes have been reached. In general the defaults for the in simulation time are appropriate, but some slow expanding or very neutron rich environments may require simulations to track the r-process for more than 1 second.

Once all these settings have been selected, the program can be executed by pressing the maple leaf SiRop logo button (the Calculate button) available from the Desktop or the top left of the

top toolbar. The program takes a variable amount of time to execute depending on the site and initial conditions, but in practice can take between 30 minutes to over 24 hours. The progress of the simulation can be monitored using the Chart module and the Messages module. The final results can be saved in a number of ways including: right clicking on any of the graphs and exporting the data, copying data from the Data module, or by having selected the Save option in the Code module before executing the code.

RUNNING A SENSITIVITY STUDY

Once a simulation setup has been chosen and initialized (as indicated above), the code is ready to run a nuclear sensitivity study. The Sensitivity module has two tabbed pages which can be accessed by selecting (mouse click) either the Setup or Results tab from the top left corner of the module page. As implied, the Setup page contains options for setting up the study and the results tab lists some textual and graphical output about the state of the batch execution and the computed statistics.

The Setup page has six different areas: Operations, Sensitivity Factors, two Properties, Output and Options. The Operations section and its Properties (to the right of Operations) contains a list of simulations to be run in sequence. The Sensitivity Factors and its Properties (to the right of Sensitivity Factors) contains a list of simple statistical metrics to be computed. The Output section allows for automatic logging of the results to a directory during the execution of the sensitivity study (similar to the Code module). The Options section contains the range of mass numbers upon which the sensitivity metrics will be calculated.

The Results page contains a Console section which prints out textural information, a Graphs section which provides graphical summary of the completed simulations from the sensitivity study being run (or completed) and a Sensitivity Results section which lists the computed statistics for each simulation queued up in the Operations section from the Setup page. This page is mainly for displaying statistics and each section has a context menu available when right-clicking which allows for manual updating and saving the sensitivity data presented.

The Sensitivity module has been designed to allow arbitrary modifications to the underlying nuclear data. To SiRop a single set of changes to nuclear parameters is referred to as an Operation. Each Operation has a name to identify it (listed under Options) and contains a list of changes in a set of Groups. Each Group contains a list of Isotopes and Values which indicate the isotopic values to change and by what amount (Add, Relative, or Percent). The setup for a particular Operation makes most sense with some examples below. Once all sensitivity Operations have been setup, they can be run by pressing the cog button located in the bottom left of the Operations panel.

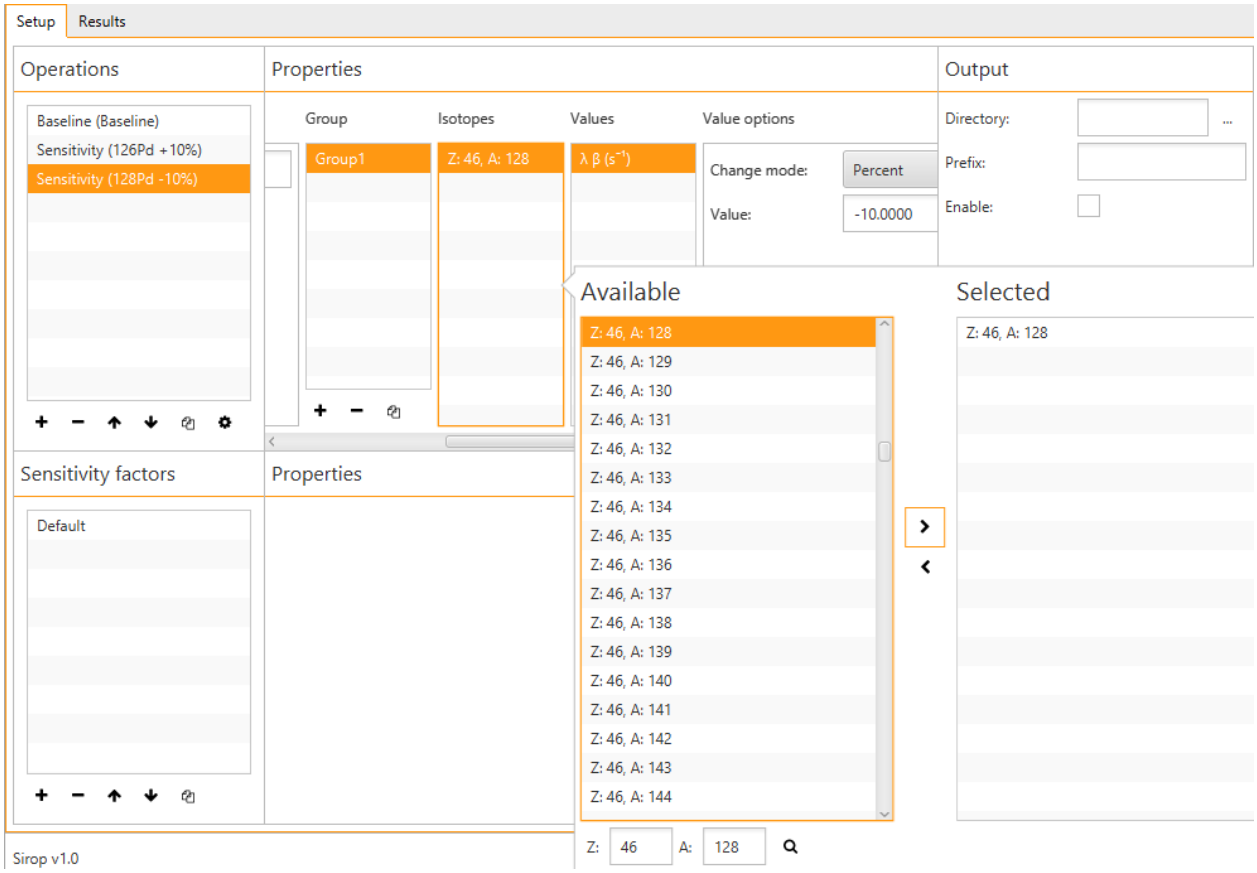

Figure 10 Screen capture midway through setting up the sensitivity study suggested in Example 1.

EXAMPLE 1: CHANGES IN SINGLE ISOTOPE HALF-LIVES

Suppose we wish to identify the N=82 isotope whose half-life is most impactful to the r-process. For simplicity's sake we will only list a few of these isotopes. For this study we're going to multiply the half-lives (or the rates) by ±10% for each isotope. For 128Pd, 129Ag, 130Cd, 131In and 132Sn this means 10 different Operations. The values in each Operation will be almost identical, so we'll list the details for one. In the Options section in the Operations Properties section we'll add the name "*128Pd +10%",* in Group we'll add a group by clicking the plus button. Now that there exists a group, we ensure it is selected (click on it if it isn't highlighted in orange) and in the Isotopes section we'll right-click to bring up a context menu with the isotopes imported listed. In the search bar at the bottom I've typed in Z: 46 and A: 128 for 128Pd and after hitting enter that isotope has been selected. The right arrow in the context panel adds this isotope to the group and the context menu can be navigated away from by clicking outside of it or hitting the escape (Esc) key. Similarly, the λ β (beta-decay rate) can be added to values. Once added, the change can be specified in the Value Options: in our example, we click the drop-down menu to select percent then change the value to 10 and hitting the

enter key to confirm the entry. Now we have one operation set. For the decrease by 10% we can easily make that operation by copying the "*128Pd +10%*" operation in the Operation list and click on the copy icon at the bottom to the right of the down arrow. Once the operation is copied, we can name it "*128Pd -10%*", select the value in the only group and change the listed 10.0000 to -10 and hitting enter. An example of a partial setup and the right-click context menu is shown in Figure 10. This procedure is mimicked for the remaining isotopes and once we have set up all our operations, the sensitivity study can be run.

EXAMPLE 2: CORRELATED NEUTRON CAPTURES AND PHOTO-DISSOCIATIONS

The principle of detailed balance implies that a change to a neutron capture cross section should correspond to the same (multiplicative) change to the reverse reaction (the neutron photo-dissociation). This can be accomplished by setting up two groups in the Group tab. If we want to change just one isotope's (e.g. 128Pd) cross section in this Operation, we can add 128Pd to the isotope list in the first Group, set the Value to "Neutron Capture Cross Sections" to be multiplied by a factor (e.g. 10). Then the second group needs to have 129Pd added with the "Photo-dissociation Rates" Value also multiplied by the same factor of 10. For each isotope in each operation this procedure must be reproduced for each Operation of interest.

EXAMPLE 3: GROUPS CHANGES

For our last example, we won't go into as much detail, but outline an additional type of sensitivity study which is possible using SiRop. In the previous examples, only one isotope was changed per Operation (two for easily correlated values like cross-section and photo-dissociation); however, it is possible to create more complex operations. If there were evidence for shell quenching or large systematic changes to many isotopes that we were interested in, we could create this as an Operation and compare the sensitivity to the baseline and any number of additional sensitivity Operations. For the shell structure example, we could take the N=82 isotopes from "Example 1: Changes in Single Isotope Half-Lives" above, we could put 128Pd, 129Ag, 130Cd and 131In into a group together and set a multiplicative factor to the cross-sections and add a small (perhaps +0.05 MeV) the mass excess. Then in a second group, we would add 129Pd, 131Ag, 132Cd and 132In and multiply their cross sections by the same amount and subtract a small (maybe -0.05 MeV) to the mas excess. Or this change could be split into several different sub-groups for more granular control of the changes along the magic number. The flexibility to create rather complex changes in a single operation was designed into the interface to allow for arbitrary sequences of modifications.

SUGGESTED RANGES FOR SENSITIVITY FACTORS

SiRop has been designed to allow rather large user flexibility with inputs. While this allows for numerous different possibilities for how to use the program, it comes with the programmatic difficulty of verifying that the inputs into the program make sense. While some effort has been made to programmatically detect some obvious invalid input, there is some responsibility deferred to a user to understand some of these limitations. With respect to sensitivity studies, there are some suggested ranges of modifications to the nuclear inputs which are based on nuclear theory and measurements and shouldn't be exceeded without some experience with the code and the nuclear theory.

Measured Nuclear Masses: See the measurement uncertainty (<100 keV in many cases)
Unmeasured Nuclear Masses: ~0.5 MeV near measured masses
Beta-Decay Half-Lives: Factor of a few (times or divided by factors of 1-5 or 10 at the extreme range)
Beta-Delayed Neutron Probabilities: Probabilities must be normalized (and are automatically by the program during execution)
Cross-Sections: Multiplicative factors of 10-1000 are normal and strongly depend on the predictive theory used
Beta-Decay Q Values: See range for masses (not more than about 1 MeV even in extreme cases)

These are meant as a starting point for testing some values and better values for acceptable variation should be based on existing nuclear measurement errors, errors in model fits to existing measurements and comparisons of competing nuclear mass models.

R-PROCESS PATH TESTING

The R-Path module is an addition to SiRop which has been designed to assist in designing sensitivity studies and help prevent some pitfalls that can be run into when using any r-process code. The idea of the r-process path is as old as the theory and is the collection of isotopes which are produced during the r-process in a particular site. The r-process path is determined by the r-process waiting points which are the isotopes which beta-decay. Historically there are two main avenues for determining these waiting points: either by equating predicted cross-sections to beta-decay rates for a sequence of isotopes, or by calculating the waiting point population coefficients using the WPA. While both methods are certainly informative, both has physical regimes where the assumptions they make break down. At high temperatures the first method (equating beta-decay with neutron capture) does not account for the significant competition with photo-dissociations which can prevent neutron captures from meeting at equilibrium with the beta-decays. The classical waiting points as computed in the WPA is only valid at high-temperatures which provide enough high-energy (MeV) photons to maintain equilibrium with the neutron captures and at temperatures much below 1 GK this assumption starts to break-down.

Access to computed rates for neutron captures, photo-dissociations and beta-decays allows for us to test when these two methods are applicable and provide better estimates for the r-process path. Since these nuclear processes are random we can simply execute a random walk with the rates. In principle this should lead to average paths and show variations in the paths, but test cases show very weak variation due to the large order of magnitudes between the different rates in the r-process.

Both the Rates module and the Waiting Point Rates calculation in the Code module can be used to calculate the r-process path to assist in identifying isotopes which can be expected to be impactful in a sensitivity study. The inputs required are the temperature, neutron number density and an initial isotope to begin the random walk. The Rates module requires specification of total simulated random walk time; whereas, the calculation in the Code module requires minimum and maximum values for the atomic number Z. The Rates module will plot in a Z vs N diagram the following: stable isotopes, waiting points calculated based on where the neutron capture rates equal beta-decay rates (“Waiting Points”), waiting points as calculated by the WPA (“Classical Waiting Points”) and the waiting points calculated using the random walk (“Random Walk”). The calculation in the Code module will list the results of the random walk in the Messages module after the program Calculate button has been pressed.

In order to determine the temperature and neutron number densities to be used, the program can be run once normally with the time plots added in the Charts module to track the evolution

in time of the temperature and neutron number density. This can be used to run the calculation of the r-process path at different points during the evolution of the r-process to identify key isotopes that will be produced during the simulation. These isotopes can then be identified for inclusion in a sensitivity study Operation list and significantly reduce the time spent executing the code by only modifying values of isotopes in through which the r-process falls on or near.

TECHNICAL DETAILS AND NOTES

SiRop is a desktop based program written with a GUI written in Java. For this reason, the program should be available to all operating systems for which a Java Virtual Machine (JVM) exists. In practice this means we have distributions available for Windows, Mac and UNIX based operating systems and SiRop should run on any installed system with no cross platform limitations.

There are a few minor quirks which result from this technical choice that someone using SiRop may profitably be made aware of. The first is that occasionally due to the Just In Time compilation process inherent to the JVM, some portions in the GUI may respond slowly the first time they are accessed and used. The second is that all text input forms or boxes require hitting enter after the desired text (or numeric) input has been typed. Always ensure that you hit enter after typing into a text field with parameters to ensure that the changes are forwarded to the internals of the program.

BIBLIOGRAPHICAL REFERENCES

Farouqi, K., Kratz, K.-L., Pfeiffer, B., et al. 2010, ApJ, 712, 1359

Hix, R., & Thielemann, F.-K., 1999, J. Comput. Appl. Math., 109, 321

Kostka, M., Koning, N., Shand, Z., Ouyed, R., & Jaikumar, P. 2014a, arXiv:1402.3824

Kostka, M., Koning, N., Shand, Z., Ouyed, R., & Jaikumar, P. 2014b, A&A, 568, A97

Möller, P., Pfeiffer, B., & Kratz, K.-L. 2003, Phys. Rev. C, 67, 055802

Woosley, S. E., & Hoffman, R. D. 1992, ApJ, 395, 202

Appendix C

Copyright Agreement

The following copyright agreement is for the paper ”Quark Nova Model for Fast Radio Bursts” published by Research in Astronomy and Astrophysics (RAA) and is available from their website www.raa-journal.org. The full bibliographical reference for the paper is:

Shand, Z., Ouyed, A., Koning, N., & Ouyed, R. 2016, Research in Astronomy and Astrophysics, 16, 011

COPYRIGHT AGREEMENT
Research Astronomy and Astrophysics

Manuscript Number: MS 2640

Title: Quark Nova Model for Fast Radio Bursts

Authors: Zachary Shand, Amir Ouyed, Nico Koning & Rachid Ouyed

The above original and previously unpublished article has been accepted for publication in our journal, Research Astronomy and Astrophysics (RAA), the following terms are submitted for the authors' consideration.

The author warrants that his/her contribution is original and that he/she has full power to make this grant. The author signs for and accepts responsibility for releasing this material on behalf of any and all co-authors. The copyright transfer covers the exclusive right to reproduce and distribute the article, including reprints, translations, photographic reproductions, microform, electronic form (offline, online) or any other reproductions of similar nature.

The author warrants that the paper has not been published elsewhere in whole or in part and that no agreement to publish is outstanding.

An author may self-archive an author-created version of his/her article on his/her own website and his/her institution's repository, including his/her final version; however he/ she may not use the publisher's PDF version which is posted on www.raa-journal.org. Furthermore, the author may only post his/her version provided acknowledgment is given to the original source of publication and a link is inserted to the published article on RAA's website.

If these terms are satisfactory, please sign below and return this agreement to us. We cannot publish your paper without this approval. After submission of this agreement signed by the corresponding author, changes of authorship or in the order of the authors listed will not be accepted by RAA.

Author's signature: 

Date: 2016-01-05

Please return this form to:

Editorial office
Research in Astronomy and Astrophysics
National Astronomical Observatories
Chinese Academy of Sciences
20A Datun Road, Chaoyang District
Beijing 100012, China
Phone: +86-10-64853746
Fax: +86-10-64859720
Email: raa@raa-journal.org